

AD-A128 305

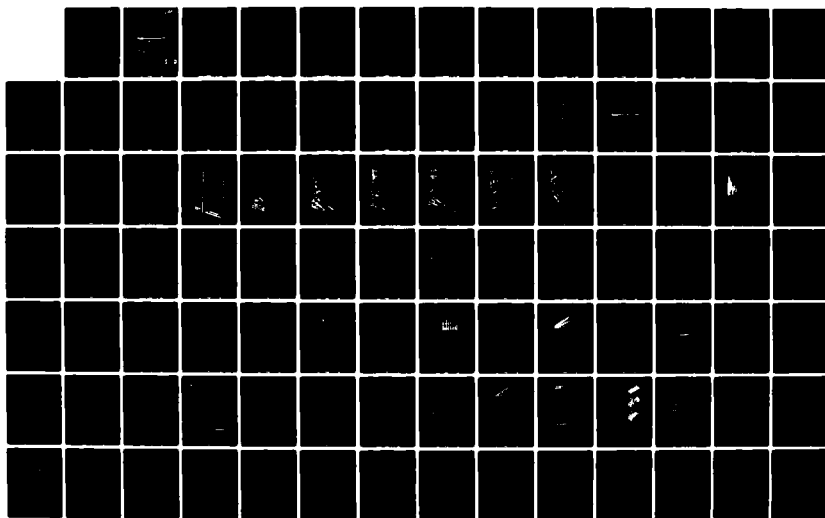
SYNTHETIC SEISMOGRAM MODELING(U) PURDUE UNIV LAFAYETTE  
IN DEPT OF GEOSCIENCES L W BRAILE 15 NOV 82  
TR-1-B2-ONR N00014-75-C-0972

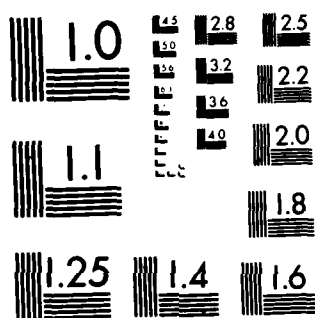
1/2

UNCLASSIFIED

F/G 8/11

NL





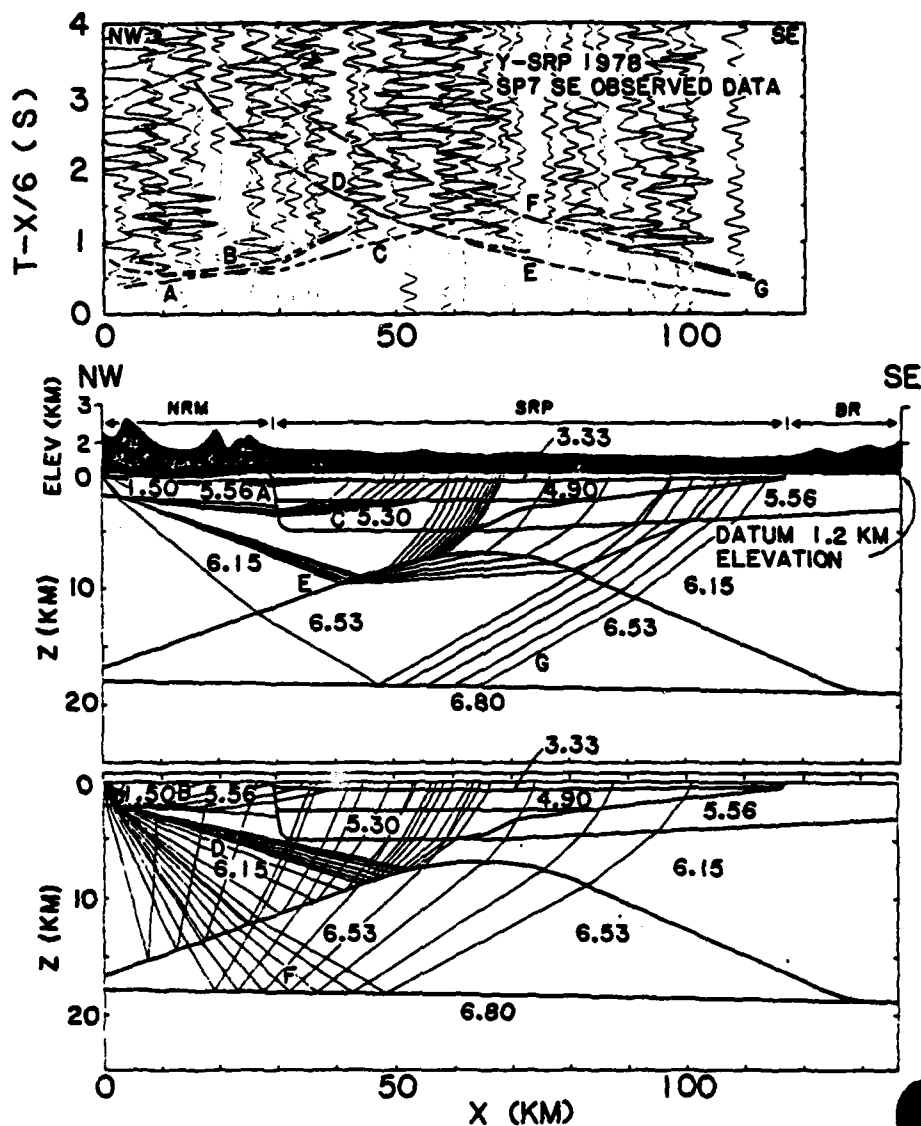
MICROCOPY RESOLUTION TEST CHART  
NATIONAL BUREAU OF STANDARDS 1963-A

AD A 128305

# SYNTHETIC SEISMOGRAM MODELING

Lawrence W. Braille  
Department of Geosciences  
Purdue University  
West Lafayette, Indiana 47907

12



DTIC FILE COPY

Final Technical Report No. ONR-1-82  
Submitted to

Earth Physics Program 83  
Office of Naval Research

Contract No. N00014-75-C-0972

Project Period 12/1/80 - 2/28/82

Report Date 11/15/82

DTIC  
ELECTE  
MAY 18 1983  
S D  
05 18 052

DISTRIBUTION STATEMENT A  
Approved for public release  
Distribution Unlimited

DEPARTMENT OF GEOSCIENCES

PURDUE UNIVERSITY

Final Technical Report

for the

EARTH PHYSICS PROGRAM

OFFICE OF NAVAL RESEARCH

Contract No. N00014-75-C-0972

SYNTHETIC SEISMOGRAM MODELING

by

Lawrence W. Braille

Technical Report No. ONR-1-82

Project Period 12/1/80 - 2/28/82

Report Date 11/15/82

**DISTRIBUTION STATEMENT A**

Approved for public release;  
Distribution Unlimited

REPORT DOCUMENTATION PAGE		READ INSTRUCTIONS BEFORE COMPLETING FORM
1. REPORT NUMBER ONR-1-82	2. GOVT ACCESSION NO. AD-A128305	3. RECIPIENT'S CATALOG NUMBER
4. TITLE (and Subtitle) Synthetic Seismogram Modeling		5. TYPE OF REPORT & PERIOD COVERED Technical 12/1/80 - 2/28/82
		6. PERFORMING ORG. REPORT NUMBER ONR-1-82
7. AUTHOR(s) Lawrence W. Braile		8. CONTRACT OR GRANT NUMBER(s) N00014-75-C-0972
9. PERFORMING ORGANIZATION NAME AND ADDRESS Department of Geosciences Purdue University West Lafayette, IN 47907		10. PROGRAM ELEMENT, PROJECT, TASK AREA & WORK UNIT NUMBERS
11. CONTROLLING OFFICE NAME AND ADDRESS ONR Resident Representative Ohio State University Research Center 1314 Kinnear Road, Columbus, OH 43212		12. REPORT DATE 11/15/82
		13. NUMBER OF PAGES
14. MONITORING AGENCY NAME & ADDRESS (if different from Controlling Office)		15. SECURITY CLASS. (of this report) Unclassified
		15a. DECLASSIFICATION/DOWNGRADING SCHEDULE N/A
16. DISTRIBUTION STATEMENT (of this Report) Unlimited		
<div style="border: 1px solid black; padding: 5px; text-align: center;"> <b>DISTRIBUTION STATEMENT A</b>            Approved for public release;            Distribution Unlimited         </div>		
17. DISTRIBUTION STATEMENT (of the abstract entered in Block 20, if different from Report) Approved for public release: distribution unlimited		
18. SUPPLEMENTARY NOTES Synthetic Seismograms, Seismic Modeling, Finite Difference, Ray Theory		
19. KEY WORDS (Continue on reverse side if necessary and identify by block number)		
20. ABSTRACT (Continue on reverse side if necessary and identify by block number) Seismic modeling techniques for one- and two-dimensional velocity models have been developed, tested and applied to analysis of observed seismic refraction and reflection data for the continental crust. The reflectivity method for one-dimensional models has proven to be an efficient and powerful method for interpretation of the amplitude and waveform of seismic record sections. The amplitude and waveform characteristics are shown to be important to interpretation of fine structure of velocity depth profiles. Applications		

20.

to modeling of a variety of seismic phases are given. Two-dimensional modeling techniques utilizing ray-trace travel-time calculations and finite-difference synthetic seismogram calculations were developed. The ray-tracing methods are capable of accurate travel-time applications but require modification for amplitude analysis. The finite-difference method is a powerful technique capable of modeling seismic data for complex geologic structures for body and surface waves. Model studies for simple one- and two-dimensional velocity structures illustrate seismic wave propagation including complex amplitude and waveform characteristics due to model complexity. The principal limitation of the finite-difference technique is the large amount of computer time and storage required.

Distribution For	
NTIS GRA&I	<input checked="" type="checkbox"/>
DTIC TAB	<input type="checkbox"/>
Unannounced	<input type="checkbox"/>
Justification	
By	
Distribution/	
Availability Codes	
Dist	Avail and/or Special
A	



## ABSTRACT

Seismic modeling techniques for one- and two-dimensional velocity models have been developed, tested and applied to analysis of observed seismic refraction and reflection data for the continental crust. The reflectivity method for one-dimensional models has proven to be an efficient and powerful method for interpretation of the amplitude and waveform of seismic record sections. The amplitude and waveform characteristics are shown to be important to interpretation of fine structure of velocity depth profiles. Applications to modeling of a variety of seismic phases are given. Two-dimensional modeling techniques utilizing ray-trace travel-time calculations and finite-difference synthetic seismogram calculations were developed. The ray-tracing methods are capable of accurate travel-time applications but require modification for amplitude analysis. The finite-difference method is a powerful technique capable of modeling seismic data for complex geologic structures for body and surface waves. Model studies for simple one- and two-dimensional velocity structures illustrate seismic wave propagation including complex amplitude and waveform characteristics due to model complexity. The principal limitation of the finite-difference technique is the large amount of computer time and storage required.

## INTRODUCTION

During the past few years our research has been aimed at developing improved methods for modeling seismograms. This effort has involved both development of new synthetic seismogram techniques and implementation and modification of existing computer programs. Our objective has been not only to provide adequate synthetic seismogram modeling techniques, which are useful for a wide variety of applications, but also to quantitatively compare these techniques, ascertain the advantages, disadvantages and range of applicability of the various methods, and to utilize the techniques to model some real seismological data. Our applications have largely been to continental crustal structure although the techniques are 'scale-independent'. The methods can be applied to a wide variety of models of geological and seismological interest including whole-earth seismograms, crustal and upper-mantle modeling the shallow seismic refraction and reflection studies including wave propagation in the ocean and ocean-bottom region which is of prime interest to the Navy. Both travel time and synthetic seismogram amplitude methods have been employed. Synthetic seismogram methods utilize both ray theory, which is approximate, but relatively fast; and wave theoretical approaches, which are more exact and include correct treatment of the various phase conversions and wave types, but may be restricted in their range of applications because of the amount of computer time required.

During the past two years, our emphasis has been on the development of two-dimensional synthetic seismogram methods. We have utilized two basic approaches in the development and application of two-dimensional synthetic seismogram modeling techniques. The first involves a ray-theoretical method utilizing ray tracing which provides primarily travel times of seismic wave arrivals. This method can be improved, however, to produce reasonably accurate synthetic seismograms for seismic wave

propagation through complicated geologic structures. Developments in these areas will be reported in a future report.

The second method that we have used involves the numerical solution of the two-dimensional heterogeneous elastic wave equation using finite-difference techniques in order to calculate complete synthetic seismograms for complex two-dimensional models. These techniques have the advantage of providing complete seismograms including effects of wave type conversion, multiples, and inclusion of body waves as well as surface waves. However, the principal disadvantage of the finite-difference techniques has been the requirement of vast amounts of computer time and storage in order to apply these techniques on a routine basis.

In this report, we summarize the status of our synthetic seismogram modeling development and application efforts. Previous reports relevant to this research effort are Department of Geosciences, Purdue University reports ONR-1-80 and ONR-1-81 prepared by Professor L.W. Braile. Additional details of some of the applications of seismic modeling performed during the research period are included in reprints of published papers which are contained in the Appendix to this report. Recent developments and improvements in finite-difference modeling techniques and in an approximate two-dimensional ray theoretical synthetic seismogram method, called Disk-Ray Theory, will be described in a subsequent report detailing research performed under contract number N00014-82-K-0034.

#### SYNTHETIC SEISMOGRAM MODELING

A summary of the travel time and synthetic seismogram modeling techniques that we have utilized and have implemented on the computers at Purdue University is shown in Table 1. This table provides a summary of the various methods and the characteristics of these methods and their associated limitations. For example, several of the techniques are restricted to

one-dimensional models - that is, models whose velocities vary only with the depth parameter. Other methods are capable of calculating synthetic seismograms for two-dimensional models in which lateral variations in velocity structure are possible.

Figure 1 is a flow chart which illustrates the interpretation procedure for combined travel-time and synthetic seismogram modeling that we apply to observed seismic data. A primary step in this procedure is the separation of observed data into one-dimensional and two-dimensional classes. Once this determination has been made, the data are subject to both travel-time and synthetic seismogram (amplitude distance) modeling procedures for which the computer programs which were described in Table 1 are available. In the remainder of this report, we describe the application of a variety of synthetic seismogram techniques which have been developed or implemented on our computers in order to illustrate the capability of these techniques. Additional details concerning applications of the synthetic seismogram methods are contained in the papers in the Appendix to this report.

#### ONE-DIMENSIONAL SYNTHETIC SEISMOGRAM METHODS

We have found the Modified Reflectivity Method (Kind, 1978) to be a very powerful technique for synthetic seismogram calculation in those cases where the velocity structure of interest is basically one-dimensional, that is where lateral variations in velocity and Q structure are not significant. A variety of real earth structures represent a close approximation to this assumption and in these cases the modified reflectivity method allows for relatively accurate and efficient modeling of observed seismic data. Some examples are contained in the papers by Olsen and Braile (1981), Olsen, Braile and Johnson (1980), Olsen, Braile and Stewart (1982), and Banda, Deichmann, Braile and Ansorge (1982) which are given in the Appendix. An additional example of the application of the synthetic

seismogram technique to observe data and the efficiency of calculation of synthetic seismograms using the modified reflectivity method is shown in Figure 2. Our experience with the modified reflectivity method indicate the importance of amplitude and waveform modeling of observed seismic data. Investigation of travel-time relationships alone provides little information as to the detailed earth model. Inclusion of amplitude distance variations and waveform characteristics, which can be treated using the synthetic seismogram technique, provide for much improved inference of the fine structure of the velocity depth curve as well as inference of Q structure (Braile, 1978).

#### TWO-DIMENSIONAL MODELING - RAY THEORY

Ray-theoretical techniques have been used for modeling of travel times of seismic waves in complex geologic structures for some time. We have implemented an efficient ray-tracing program for accurate calculation of travel times of refracted and reflected seismic waves following the method of Cerveny, Molotkov and Psencik (1978). This technique utilizes a variety of numerical schemes to approximate a two-dimensional velocity distribution with or without interfaces. The seismic ray paths are then traced using iterative Snell's Law application through the velocity structure. Reflections from various interfaces may be selected and refracted waves are also included. Refractions simulating head waves from homogeneous layers can be adequately approximated by providing for a small positive velocity gradient within the homogeneous media. The velocity gradient that we normally use to simulate the head wave is consistent with that utilized in the earth flattening transformation and corresponds to approximately 0.001 km/s/km for shallow layers. This technique provides adequate modeling of body-wave travel times in two-dimensional structures. An example of successful modeling of complex observed seismograms using

two-dimensional ray-trace modeling is shown in Figure 3. One of the limitations of this technique is that amplitudes calculated for individual ray paths are inaccurate and thus the ray tracing technique is not immediately conducive to synthetic seismogram calculation. However, we have utilized a modified ray theoretical method following the technique of Wiggins (1976) and McMechan (1974) to produce accurate synthetic seismograms from the ray trace amplitudes. Progress in this area will be described in a subsequent report.

#### FINITE-DIFFERENCE SYNTHETIC SEISMOGRAM MODELING

We have applied the finite-difference method to numerically solve the two-dimensional heterogeneous elastic wave equation for the calculation of synthetic seismograms in velocity structures with arbitrarily varying elastic properties. The idea of the finite-difference synthetic seismogram method is illustrated in Figure 4. A velocity structure is approximated by a rectangular grid of points in which the elastic properties (compressional velocity, shear velocity, and density) are tabulated. Finite-difference approximations to spatial and temporal derivatives allow solution of the two-dimensional elastic wave equation for a given instant in time as computed from displacements at previous times. Initial conditions due to an implied elastic disturbance (source) generates wave propagation which is simulated by the finite-difference calculations as a function of time for all points in the velocity grid. Displacement time histories at a variety of locations are retained in the computer and become displacement seismograms for the vertical and horizontal components of particle velocity. The theory of finite-difference synthetic seismogram calculations has been described by Boore (1972), Alford et al., 1974; Kelly et al., 1976; Mazzella, 1979; and Espindola, 1979.

The two-dimensional equations of motion for displacement in a heterogeneous isotropic elastic media are shown in Figure 5. These equations are approximated by their finite-difference approximations using an explicit finite-difference formulation as illustrated in Figure 6. Using these finite-difference approximations, the displacement at any time  $L + 1$  for any arbitrary grid location is given as a function of times  $L$  and  $L - 1$  allowing a calculation of the displacement for all grid locations at the new time. Once this calculation is complete for the entire velocity grid, it may be repeated for as many time steps as desired.

This finite-difference application is very straightforward and results in complete seismograms since it is a numerical solution of the elastic wave equation. However, there are a variety of difficulties which one encounters in attempting to apply finite-difference calculations to the calculation of synthetic seismograms. These difficulties are summarized in Figure 7. The most difficult problems are that of providing for absorbing boundary conditions at the edges of the model in which an approximate absorbing boundary condition due to Clayton and Engquist (1977) is utilized and the requirement for stability and accuracy which imply small time step and small grid spacing respectively. These requirements result in very large computer time and storage capacity. Therefore, calculation of synthetic seismograms for complicated realistic models of interest for two-dimensional geological structures may require several tens of minutes or even hours of computer time utilizing a computer with a memory capacity of a million or more storage locations.

A finite-difference synthetic seismogram computer code has been developed and is described in Mazella (1979). We have applied this synthetic seismogram method to a variety of models in order to test the accuracy, applicability, and capability of the technique. The velocity models utilized for this testing are illustrated in Figure 8. One of the useful

by-products of the synthetic seismogram calculation using the finite-difference technique is a displacement field associated with wave propagation in the elastic model at any instant in time. These displacement fields can be stored for a number of time steps during the finite-difference calculation and the displacement fields, often called 'snapshots', are illustrative of the wave propagation in the media. An example of displacement time history snapshots for one of the models shown in Figure 8 are illustrated in Figure 9.

In order to verify the accuracy of the finite-difference program, we have calculated vertical component synthetic seismograms for a one-dimensional model corresponding to a layer over a half-space for which synthetic seismograms have also been computed utilizing the modified reflectivity method. Comparison of the seismograms for these two calculations (Figure 10) illustrates the validity of the finite-difference calculations.

Calculation of synthetics for a complex two-dimensional velocity structure (model INFL 5 illustrated in Figure 8) are shown in Figure 11. The corrected seismograms (Figure 11B) for this complicated velocity structure illustrate the expected waveform characteristics of propagation through this model containing a prominent lateral velocity contrast in the form of a fault. The time delay due to the fault and diffracted and headwave arrivals from the lower interface demonstrate the capability of this technique for simulating wave propagation and complex geologic structures.

The principal difficulty with the finite-difference approach is the amount of computer time required to compute synthetic seismograms for realistic velocity structures. It is currently too expensive to compute synthetics using this technique on a routine basis for trial and error modeling of seismic refraction and reflection data. However, it is feasible to compute synthetics for a variety of characteristic

models of laterally varying geologic structures and to use the experience gained with these models as an aid to interpretation of observed seismic data. In addition, it is highly desirable to have two-dimensional synthetic seismograms calculated by the finite-difference technique for certain models in order to use for comparison with approximate techniques as verification. Furthermore, it is possible that the finite-difference techniques could be made to be somewhat more efficient, thus improving our ability to utilize the finite-difference synthetic seismogram technique on a routine basis. For example, we are currently investigating the possibilities of using an acoustic formulation of the two-dimensional finite-difference procedure as a preliminary modeling method. In addition, we are developing implicit finite-difference schemes for synthetic seismogram modeling which may be significantly faster than the explicit code that we are presently utilizing.

## REFERENCES

- Alford, R., Kelly, K., and Boore, D., Accuracy of finite-difference modeling of the acoustic wave equation, Geophysics, 39, p. 834-842, 1974.
- Banda, E., Deichmann, N., Braile, L.W., and Ansorge, J., Amplitude study of the Pg phase, J. Geophysics, (in press), 1982.
- Boore, D., Finite difference methods for seismic wave propagation in heterogeneous materials, in Methods in Computational Physics, v. 11, B. Bolt, Ed., New York, Academic Press Inc., 1972.
- Braile, L.W., The use of amplitudes in seismic refraction interpretation, (Abs), EOS, Transactions of the American Geophys. Union, 59, 1138, 1978.
- Braile, L.W., Smith, R.B., Ansorge, J., Baker, M.R., Sparlin, M.A., Prodehl, C., Schilly, M.M., Healy, J.H., Mueller, S., and Olsen, K.H., The Yellowstone-Snake River plain seismic profiling experiment: crustal structure of the eastern Snake River Plain, J. Geophys. Res., 87, p. 2597-2609, 1982.
- Cerveny, V., Molotkov, I.A., and Psencik, I., Ray Methods in Seismology, Charles University Press, Prague, 1978.
- Clayton, R., and Engquist, B., Absorbing boundary conditions for acoustic and elastic wave equations, Bull. Seism. Soc. Am., 67, p. 1529-1540, 1977.
- Espindola, J.M., Finite difference synthetic seismograms for kinematic models of the earthquake source, Ph.D. thesis, Purdue Univ., West Lafayette, IN, 151 p., 1979.
- Kelly, K.R., Ward, R.W., Treitel, S., and Alford, R.M., Synthetic seismograms: a finite difference approach, Geophysics, 41, p. 5-27, 1976.
- Kind, R., The reflectivity method for a buried source, J. Geophys., 44, p. 603-612, 1978.
- Mazzella, F.E., The generation of synthetic seismograms for laterally heterogeneous models using the finite difference technique, Ph.D. thesis, Purdue Univ., West Lafayette, IN, 225 p., 1979.
- McMechan, G.A., P-wave train synthetic seismograms calculated by quantized ray theory, Geophys. J.R. Astr. Soc., 37, p. 407-421, 1974.
- Olsen, K.H., Braile, L.W., and Johnson, P.A., Seismic velocity and Q-structure of the upper mantle lid and low velocity zone for the eastern Great Basin, Geophys. Res. Letters, 7, p. 1029-1032, 1980.
- Olsen, K.H., and Braile, L.W., Seismograms of explosions at regional distances in the western United States: Observations and reflectivity method modeling, in Identification of Seismic Sources - Earthquake or Underground Explosion, edited by E.S. Husebye and S. Mykkeltveit, 453-466, Reidel, 1981.

Olsen, K.H., Braile, L.W., and Stewart, J.N., Modeling short-period crustal phases (P, Lg) for long-range refraction profiles, Phys. of the Earth and Planet. Interiors, 31, (in press), 1982.

Sparlin, M.A., and Braile, L.W., Crustal structure of the eastern Snake River plain determined from ray trace modeling of seismic refraction data, J. Geophys. Res., 87, p. 2619-2633, 1982.

Wiggins, R.A., Body wave amplitude calculations-II, Geophys. J.R. Astr. Soc., 46, p. 1-10, 1976.

## FIGURE CAPTIONS

- Figure 1. Flow chart illustrating the interpretation procedure for combined travel-time and amplitude analysis for seismic refraction and reflection record sections for one- and two-dimensional velocity structures.
- Figure 2. Observed and synthetic seismic record sections for a seismic refraction profile recorded on the eastern Snake River Plain (Braile et al., 1982). Both record sections have been amplitude scaled with amplitudes being multiplied by distance to the 1.5 power in order to enlarge the amplitudes at large distance to make arrivals visible. Travel-time curves on both seismograms are for a plane layered velocity model which was used to calculate the synthetic seismograms illustrated in the lower record section. Good comparison is seen between the travel-time, amplitude and waveform characteristics of the primary phases for the observed and synthetic sections indicating that the velocity and Q model used for the synthetic seismogram calculation is substantially correct.
- Figure 3. Ray-trace diagram and travel times compared with observed seismic refraction data across the eastern Snake River Plain (from Sparlin et al., 1982). The ray diagrams show computer plotted ray traces for refracted (upper ray trace diagram) and reflected (lower ray trace diagram) travel times through the complex velocity structure. The numbers on the velocity structure indicate compressional wave velocity in km/s. The travel times for the various phases (designated A, B, C, etc.) are indicated on the seismic record section at the top of the diagram. The observed travel times show a good match to the theoretical travel times computed by the ray-tracing technique.
- Figure 4. Schematic diagram illustrating the velocity model for finite-difference synthetic seismogram calculations. The velocity structure in the seismic model can vary arbitrarily and is specified by elastic properties at grid points which are distributed throughout the model. The source represents initial conditions which are used to calculate displacements as a function of time throughout the velocity model. The source can be located at any position within the velocity structure. A free-surface boundary condition is applied in the finite-difference calculation and absorbing boundary conditions are utilized on the edges of the velocity structure to minimize effects of the fictitious boundaries. The seismometer locations can be arbitrarily selected, but are usually equally spaced along the surface of the model and represent locations where the displacement time histories will be stored in the computer memory to be plotted as seismograms at the end of the finite-difference calculation.
- Figure 5. Two-dimensional equations of motion for displacement for a heterogeneous isotropic elastic model.

- Figure 6. Form of the finite-difference approximations for second order spatial derivatives and cross product spatial derivatives and second order time derivatives which are approximations to the two-dimensional elastic equation of motion for displacements illustrated in Figure 5.
- Figure 7. List of factors which must be considered in explicit finite-difference synthetic seismogram calculations.
- Figure 8. Velocity depth models used for finite-difference synthetic seismogram calculations. Distance (X) and depth (Z) are given for each model. The lower boundary of each model is assumed to be an infinite half-space, but in fact, in the program it consists of a non-reflecting artificial boundary. The numbers within the model indicate the compressional wave velocity in km/s for each layer of the models. Synthetic seismogram record sections and snapshots of displacement time histories are shown for the velocity models indicated in this figure.
- Figure 9. Displacement time history snapshots for model INFL2. The Z component is shown for times 1, 2, 3, 4, 5, 6 and 7 seconds propagation time. The source is located at  $\frac{1}{2}$  km depth and 2 km distance from the origin. Distance (X) and depth (Z) directions are shown. The perspective diagram indicates the Z component of displacement at each instant of time for the 7 different times represented by the snapshots. This velocity model consists of a single layer over a half-space. The source consists of a compressional point explosive source. As the seismic waves propagate through the model, the displacement in X and Z directions can be visualized by these snapshots. Note that the moving-window process utilized in the synthetic seismogram program causes the area of the model to be shifted to the right (in the direction of increasing X) for successive time steps. This movement of the window can be seen by the shift in the X axis values shown at the bottom of each snapshot. The efficiency of the non-reflecting boundary can be seen by the snapshots, particularly at time step T=2 seconds in which a compressional wave is impinging upon the lower boundary of the window space and no prominent reflection can be seen from this non-reflecting boundary. The development of a head wave due to propagation in the 6 km/s half-space below the 4.5 km/s sedimentary layer can be seen beginning at approximately T=3 seconds and becoming more pronounced with increasing time. The head wave is clearly seen in the T=6 snapshot in which a strong compressional pulse is propagating at a sharp angle upwards and to the right through the sedimentary layer toward the surface.
- Figure 10. Synthetic seismograms calculated for model INFL3 (Figure 8) which consisted of a layer over a half-space. The Z component seismograms were sampled at a 5 km distance interval and are plotted as a reduced-time record section. The strongest arrivals are the Rayleigh waves which begin at about  $1\frac{1}{2}$  seconds reduced time on the 5 km distance seismogram but propagate at a relatively slow apparent velocity. The Rayleigh waves

are left behind by the moving-window process and thus are not prominent after the first few seismograms. The direct wave in the surface layer is visible as the 4.5 km/s apparent velocity arrival indicated on the record section. The head wave from the 6 km/s half-space is clearly seen as a first arrival from about 15 km to the maximum 50 km distance range considered. Additional arrivals consist of P-S conversions and multiple refractions and reflections. Some numerical noise exists in the later sections of several of the seismograms. However, this noise tends to be truncated by the moving window process as the window proceeds ahead of the slowly propagating noise and thus the numerical noise does not interfere with the primary phases which propagate in the early portion of the record section. Also shown for comparison is a record section calculated for the exact same model (INFL 3) by the modified reflectivity method for a similar source wavelet. The reflectivity calculation included phase velocities of 2.5 - 100 km/s and thus ignores some of the shear and surface wave arrivals. The correspondence between the two record sections is quite good demonstrating the accuracy of the finite-difference method.

Figure 11. Synthetic seismogram record sections for finite-difference calculation for model INFL 5 (Figure 8). This model consists of a two-dimensional velocity model with a prominent fault of 5 km offset which occurs 15 km from the source. The seismograms shown in the record section indicate the beginnings of a 6 km/s apparent velocity head-wave arrival in the first three seismograms and the delay due to the fault structure at 15 km distance is seen beginning at approximately 20 km on the record section. However, full visualization of the two-dimensional effect of the fault structure on the synthetic seismogram is prevented by the presence of some peculiar numerical noise which occurs in the record section. This noise is caused by an improper choice of the velocity of the moving-window which is used to speed up the calculations of the finite-difference synthetic seismogram program. In the moving-window calculation, the finite-difference equations are solved for only a portion of the velocity model, called a window, and this window is caused to move through the velocity model in such a way as to constantly include the phases of interest. The window is shifted in discrete steps to approximately move at the average horizontal velocity of the seismic waves. However, in this particular example the velocity of the window was selected slightly too slow and the wave propagation of the first arrival (compressional waves) impinged upon the leading edge of the moving window. During the next shift in the window, this resulted in truncation of the displacements at the former window position and thus this truncation effect caused the numerical noise which is seen in the seismograms from 25 to 45 km distance range. This effect can certainly be avoided by rerunning the synthetic seismogram calculations utilizing a slightly faster velocity for the moving-window. Vertical (Figure 11B) and radial (Figure 11C) component seismograms calculated by the finite-difference method for model INFL 5 (Figure 8) with a corrected window velocity. The 6.0 km/s head wave is seen to be delayed

significantly and the amplitudes affected by the fault which occurs at a distance of 15 km in the model. Much of the energy on the record sections is due to P-S conversions and Rayleigh waves which are also included in the calculation. Note the small numerical dispersion of the Rayleigh wave train at about 3 to 4 seconds reduced time on the 5 km seismogram on the vertical component record section. This dispersion is due to too large of a grid spacing in the model for the slowly propagating Rayleigh waves. The spacing is however adequate for the body waves and thus only affects the Rayleigh wave which in this case is not of primary interest.

TABLE 1. SUMMARY OF SEISMIC INTERPRETATION TECHNIQUES

	METHOD	CHARACTERISTICS	LIMITATIONS
TRAVEL-TIME ANALYSIS	Geometrical Ray theory calculation of travel-times of reflected and refracted phases (Program TXCURV).	Travel-times for head waves and reflections for plane or dipping layered models; exact.	Model geometry; travel-times only.
	Ray Tracing (Program RAY2D)	Two-dimensional Models	Travel-times only, limited number of phases, ignores P-S conversions, guided waves and surface waves.
SYNTHETIC SEISMOGRAM MODELING	Reflectivity (Program SYNCAL)	Wave-theoretical solution to response of a layered half space. Includes P, SV, guided phases and surface waves. Exact. Includes Q.	Restricted to 1-D models.
	Disk Ray Theory (modified RAY2D program)	2-D models, approximate solution for P waves, can include reflection coefficients and Q. Computationally efficient.	Inexact amplitudes for head waves and near-critical arrivals; ignores guided phases, P-S conversions and surface waves.
	Finite Difference Acoustic (Program FDWVAC)	2-D models, <u>exact</u> solution for <u>all</u> wave types in an <u>acoustic</u> media. Significantly faster than FDWVEQ, but slower than RAY2D synthetics.	Acoustic rather than elastic. Large computer time.
	Finite Difference Elastic (Program FDWVEQ)	2-D models, <u>exact</u> solution for <u>all</u> wave types in <u>elastic</u> media. Can be modified to include Q.	Extensive computer time and storage.

INTERPRETATION PROCEDURE FOR COMBINED  
TRAVEL - TIME AND AMPLITUDE ANALYSIS OF SEISMIC  
REFRACTION RECORD SECTIONS

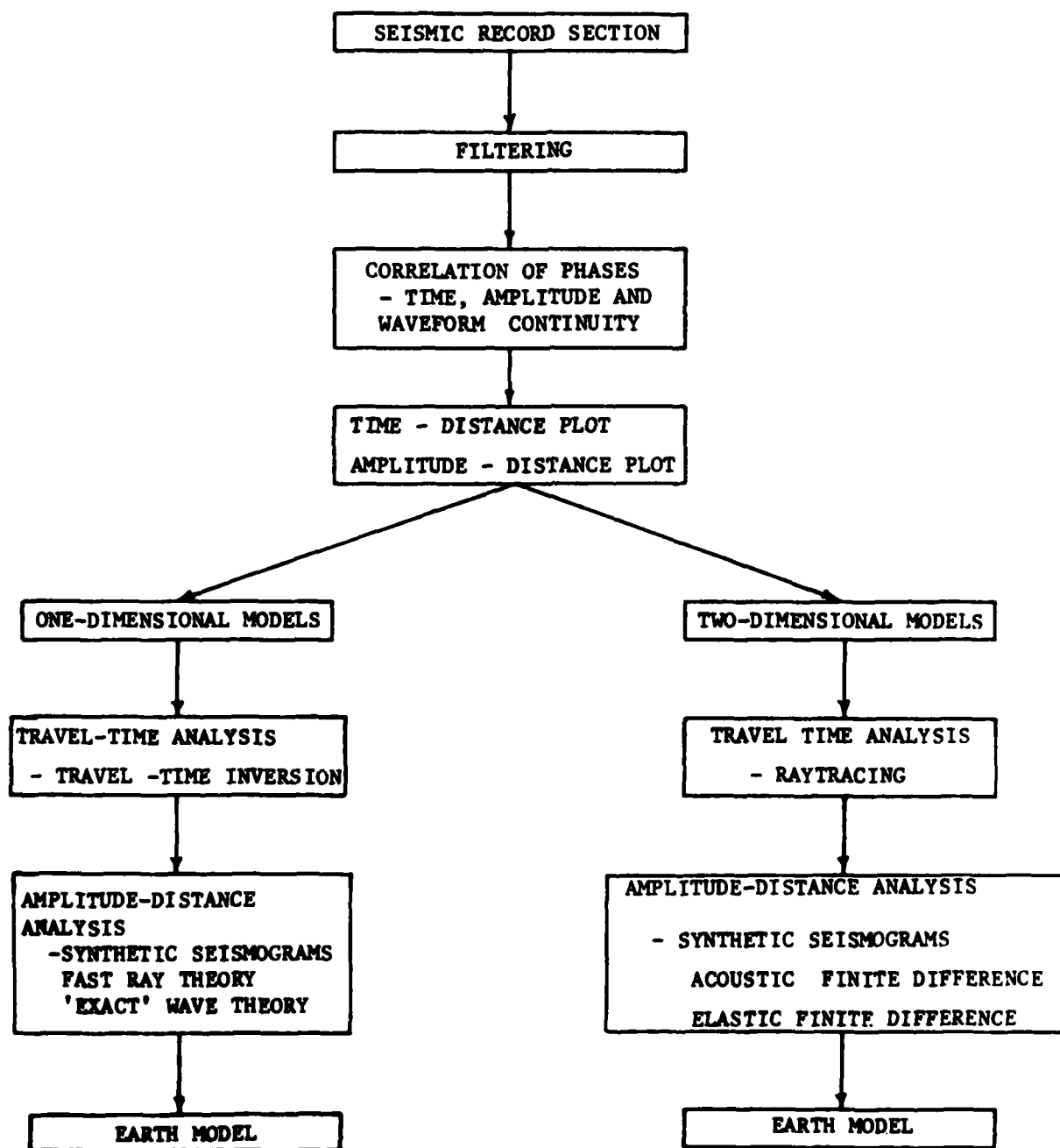


Figure 1.

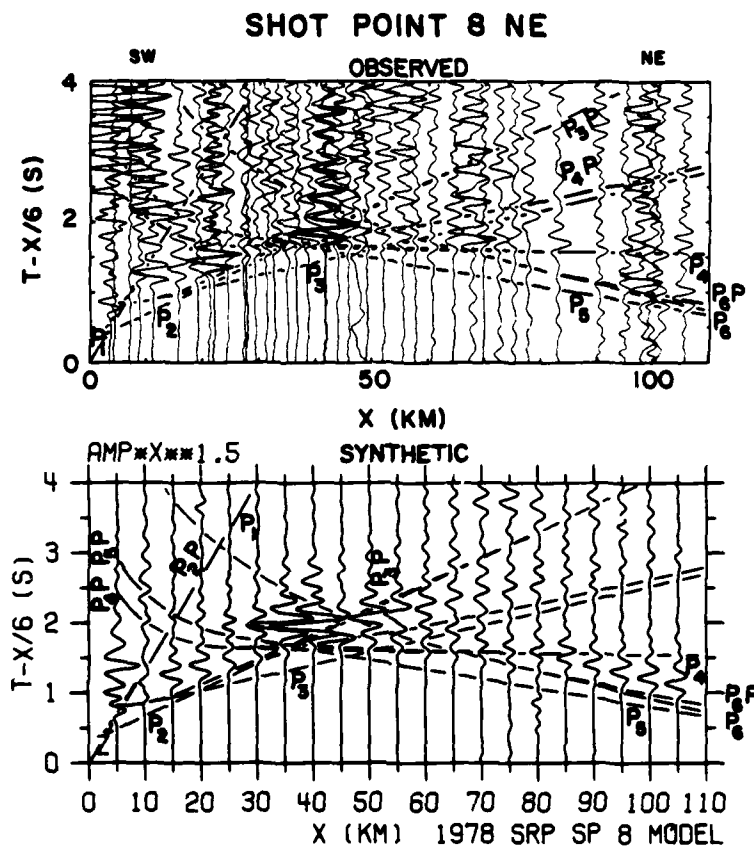


Figure 2.

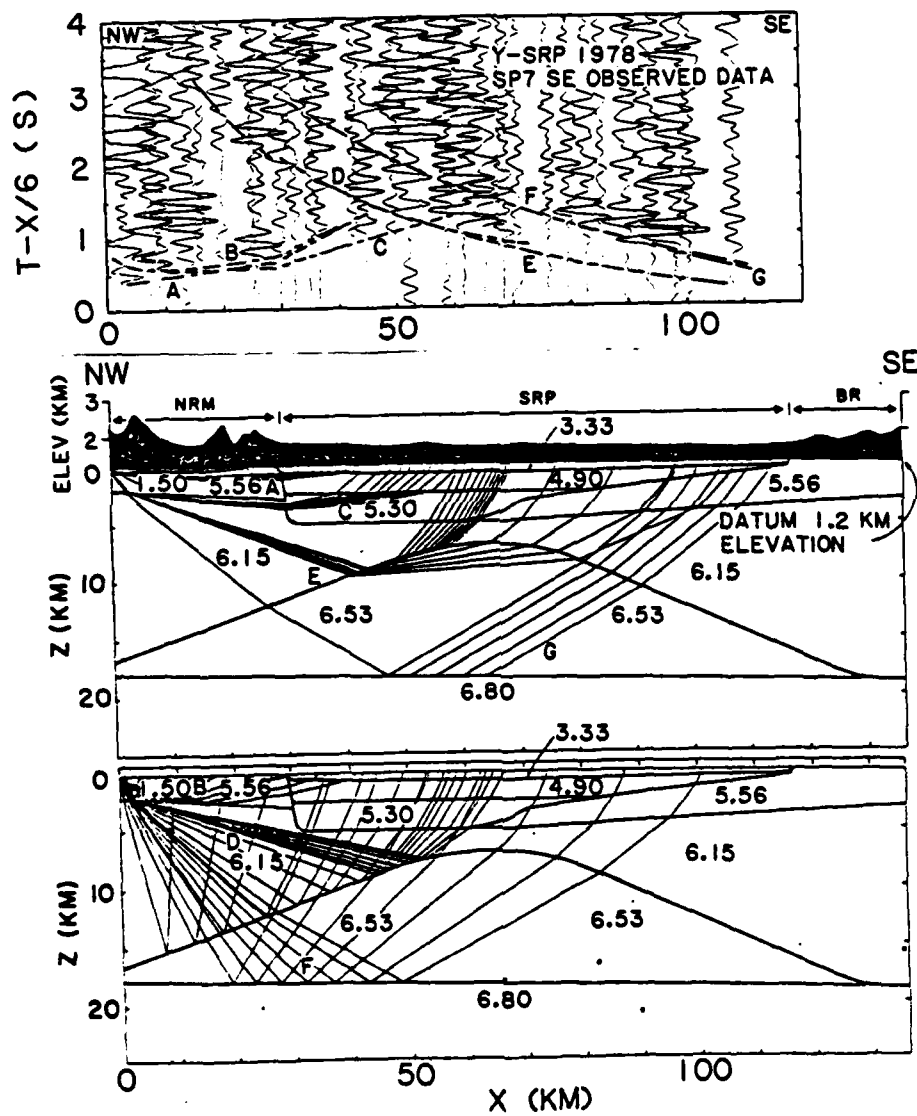


Figure 3.

# FINITE DIFFERENCE MODEL

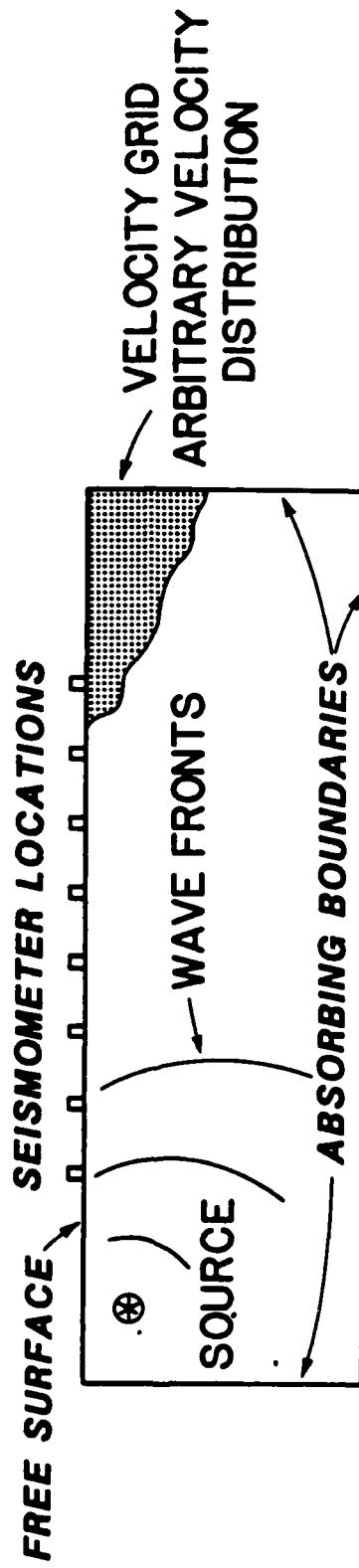


Figure 4.

TWO DIMENSIONAL EQUATIONS OF MOTION  
FOR DISPLACEMENT  
( HETEROGENEOUS, ISOTROPIC MEDIA )

$$\rho \frac{\partial^2 u}{\partial t^2} = \frac{\partial}{\partial x} \left[ \lambda \left( \frac{\partial u}{\partial x} + \frac{\partial w}{\partial z} \right) + 2\mu \frac{\partial u}{\partial x} \right] + \frac{\partial}{\partial z} \left[ \mu \left( \frac{\partial w}{\partial x} + \frac{\partial u}{\partial z} \right) \right]$$

$$\rho \frac{\partial^2 w}{\partial t^2} = \frac{\partial}{\partial x} \left[ \lambda \left( \frac{\partial u}{\partial x} + \frac{\partial w}{\partial z} \right) + 2\mu \frac{\partial w}{\partial z} \right] + \frac{\partial}{\partial x} \left[ \mu \left( \frac{\partial w}{\partial x} + \frac{\partial u}{\partial z} \right) \right]$$

WHERE:  $u(x, z)$  AND  $w(x, z)$  ARE DISPLACEMENTS  
IN  $x$  AND  $z$  DIRECTIONS

$\alpha = \sqrt{\frac{\lambda + 2\mu}{\rho}}$  IS THE COMPRESSIONAL  
VELOCITY

$\beta = \sqrt{\frac{\mu}{\rho}}$  IS THE SHEAR VELOCITY

$\rho$  IS THE DENSITY

Figure 5.

# FINITE DIFFERENCE APPROXIMATIONS ( EXPLICIT CASE )

## SECOND ORDER SPATIAL DERIVATIVES

$$\frac{\partial}{\partial x} \left[ \alpha^2(x, z) \frac{\partial}{\partial x} u(x, z, t) \right] = \left\{ \alpha^2(m + \frac{1}{2}, n) [u(m+1, n, l) - u(m, n, l)] \right. \\ \left. - \alpha^2(m - \frac{1}{2}, n) [u(m, n, l) - u(m-1, n, l)] \right\} / (\Delta H)^2$$

## CROSS PRODUCT SPATIAL DERIVATIVES

$$\frac{\partial}{\partial z} \left[ \alpha^2(x, z) \frac{\partial}{\partial x} u(x, z, t) \right] = \left\{ \alpha^2(m, n+1) [u(m+1, n+1, l) - u(m-1, n+1, l)] \right. \\ \left. - \alpha^2(m, n-1) [u(m+1, n-1, l) - u(m-1, n-1, l)] \right\} / 4(\Delta H)^2$$

## SECOND ORDER TIME DERIVATIVE

$$u(m, n, l+1) = 2u(m, n, l) - u(m, n, l-1) + \tau \left[ \text{Spatial derivatives} \right]$$

$$\text{WHERE: } \alpha^2(m \pm \frac{1}{2}, n) = \left[ \alpha^2(m \pm 1, n) + \alpha^2(m, n) \right] / 2$$

m AND n REFER TO THE x AND z DIRECTION  
GRID POINTS AND l IS THE TIME STEP

Figure 6.

## PRACTICAL ASPECTS OF EXPLICIT FINITE DIFFERENCE SYNTHETIC SEISMOGRAM CALCULATION

- TWO DIMENSIONAL APPLICATION
- SOURCE GENERATION
- FREE SURFACE BOUNDARY CONDITION
- ABSORBING BOUNDARIES AT EDGES OF MODEL
- STABILITY CONDITION (SMALL TIME STEP)
- ACCURACY CONDITION (SMALL GRID SPACING)
- NUMBER OF TIME STEPS (LENGTH OF SEISMOGRAMS)
- NUMBER OF GRID POINTS
- LARGE COMPUTER TIME AND STORAGE REQUIREMENTS

Figure 7.

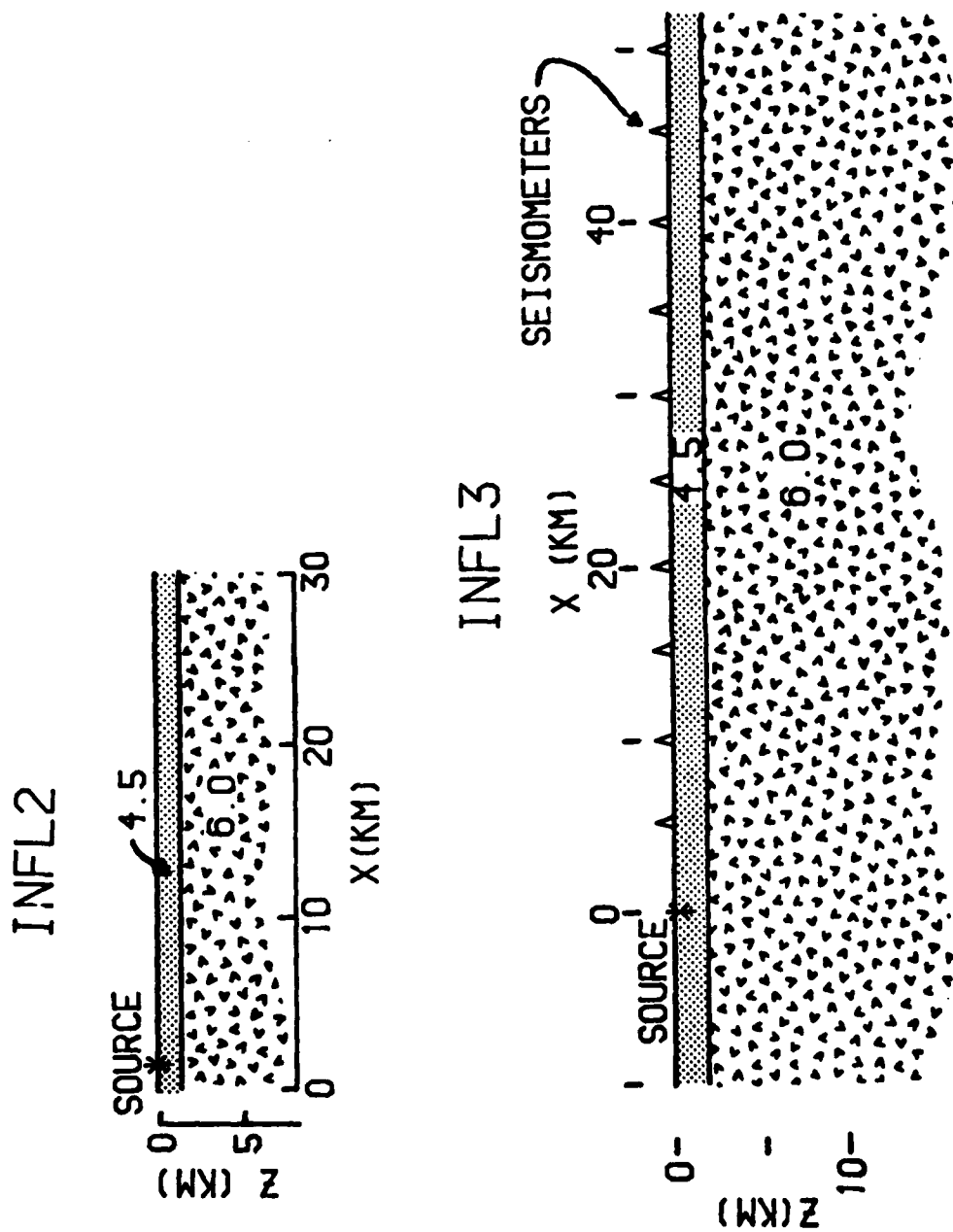


Figure 8.

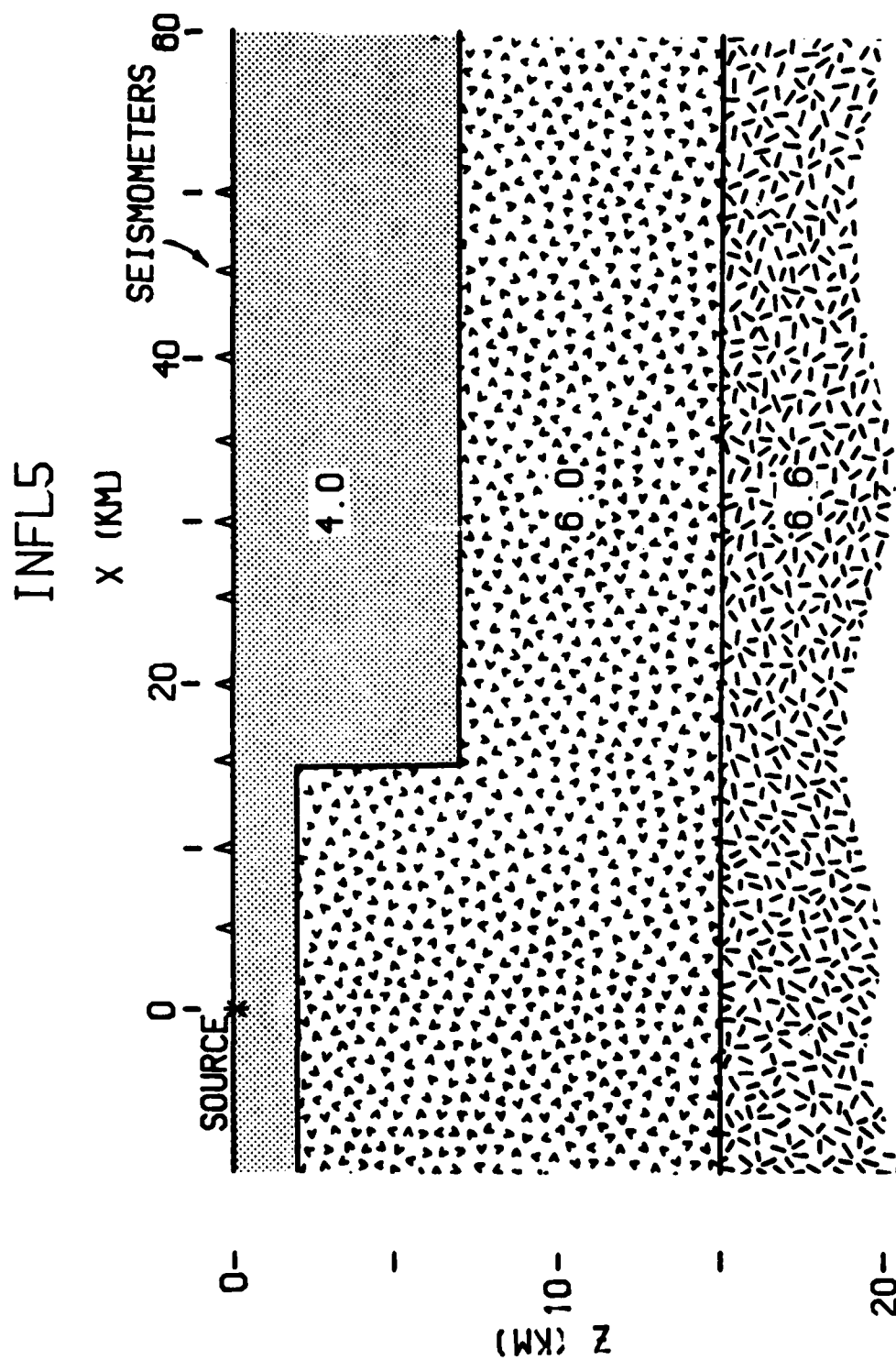


Figure 8. (cont.)

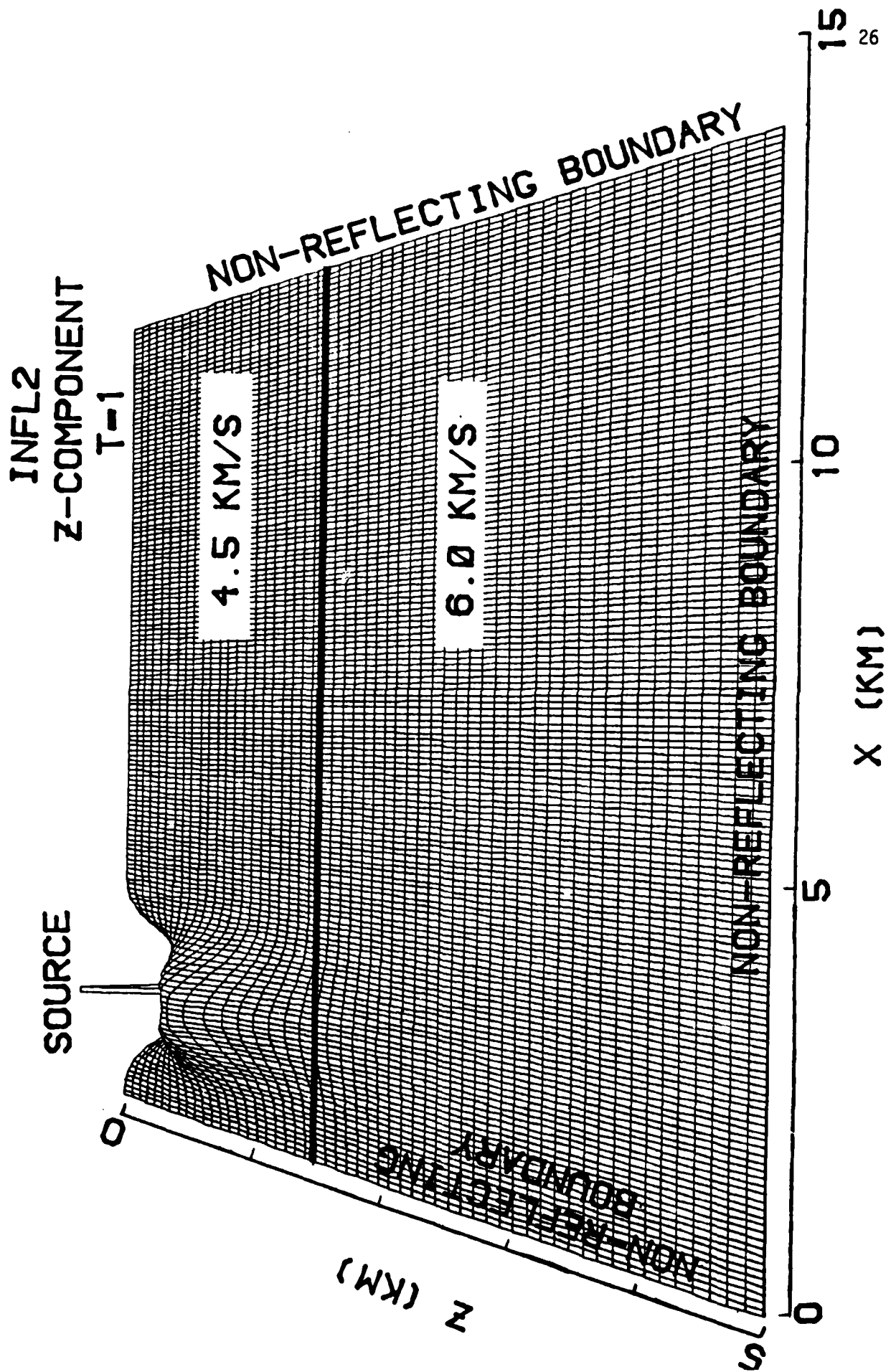


Figure 9A.

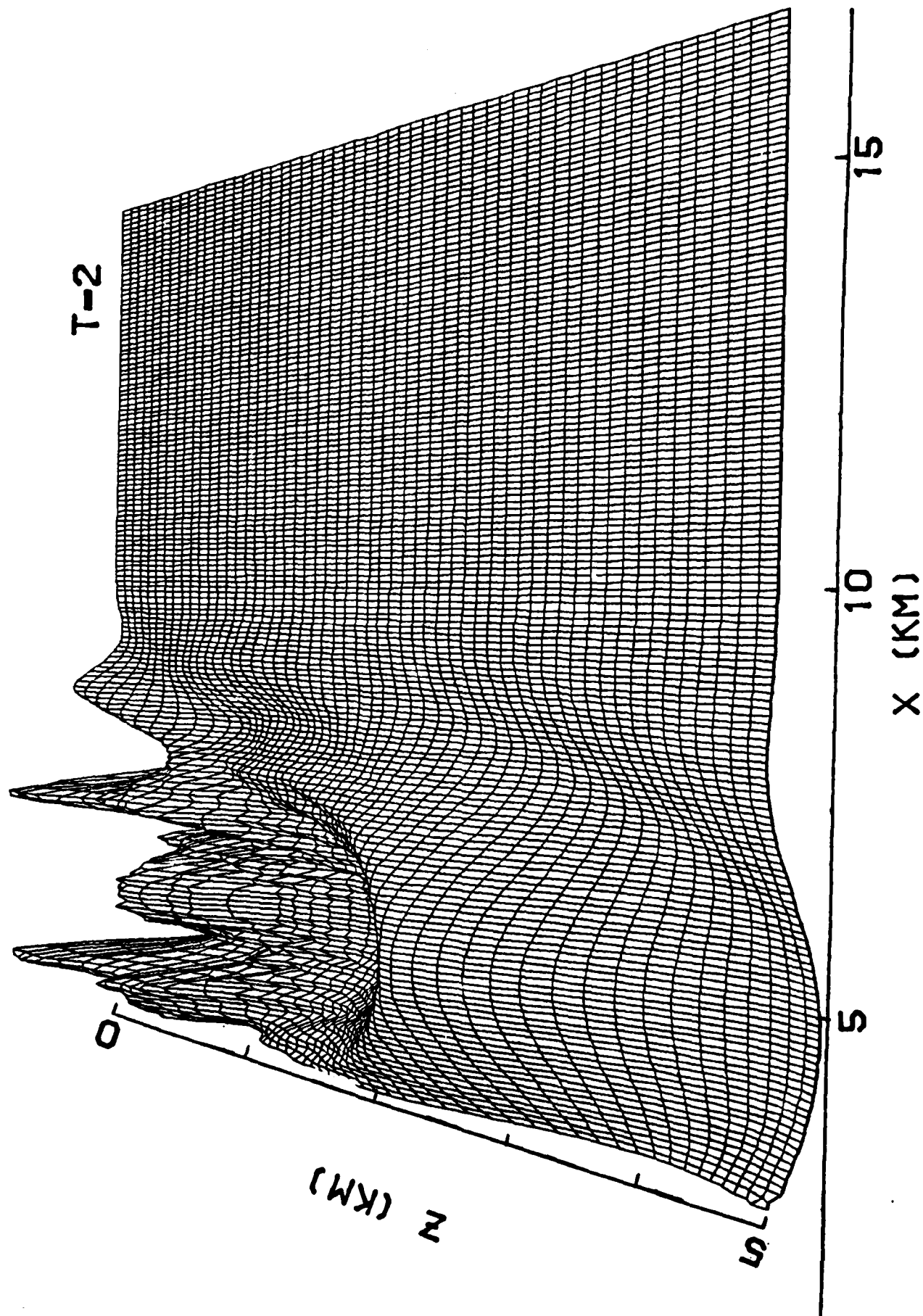


Figure 9B.

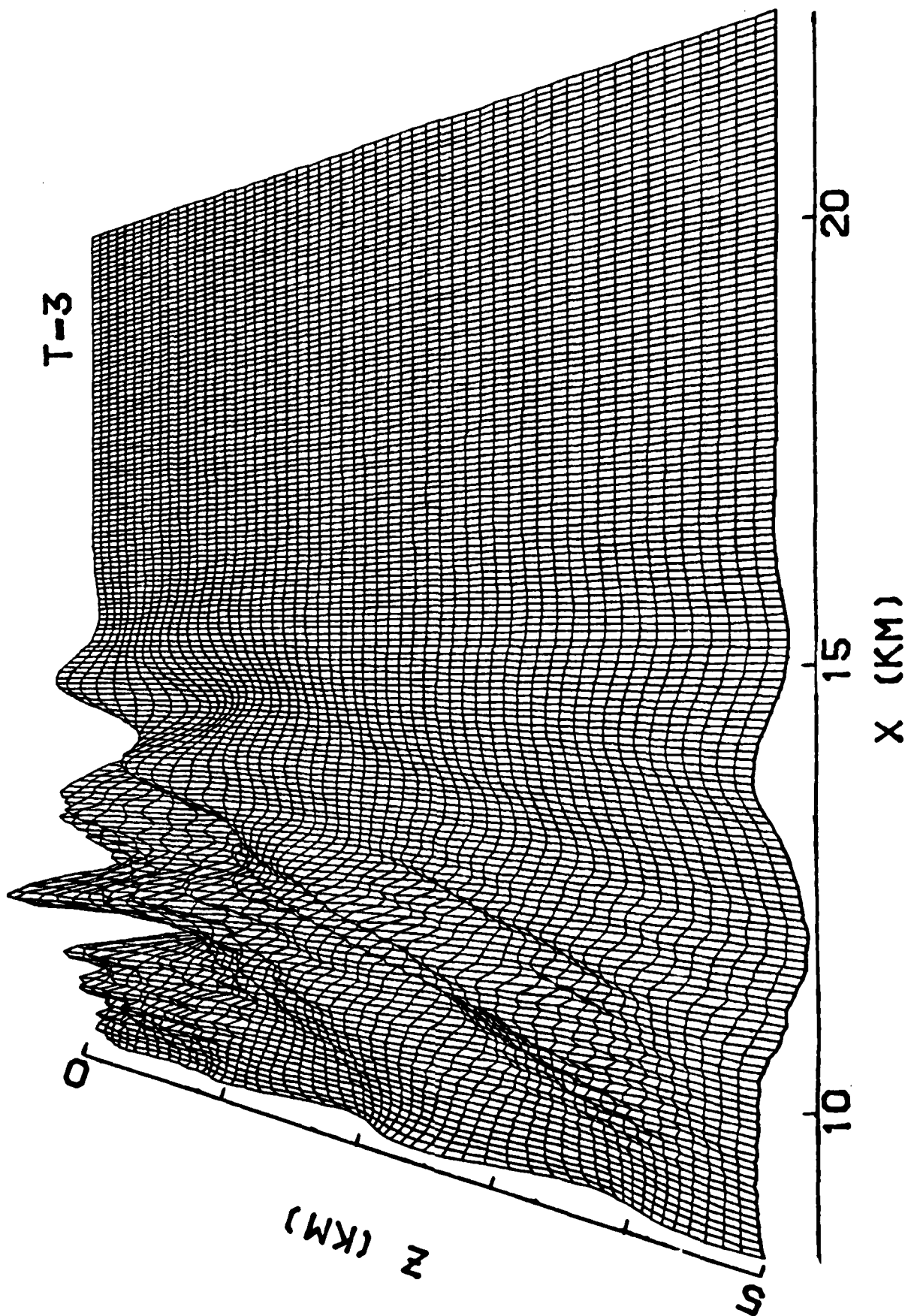


Figure 9C.

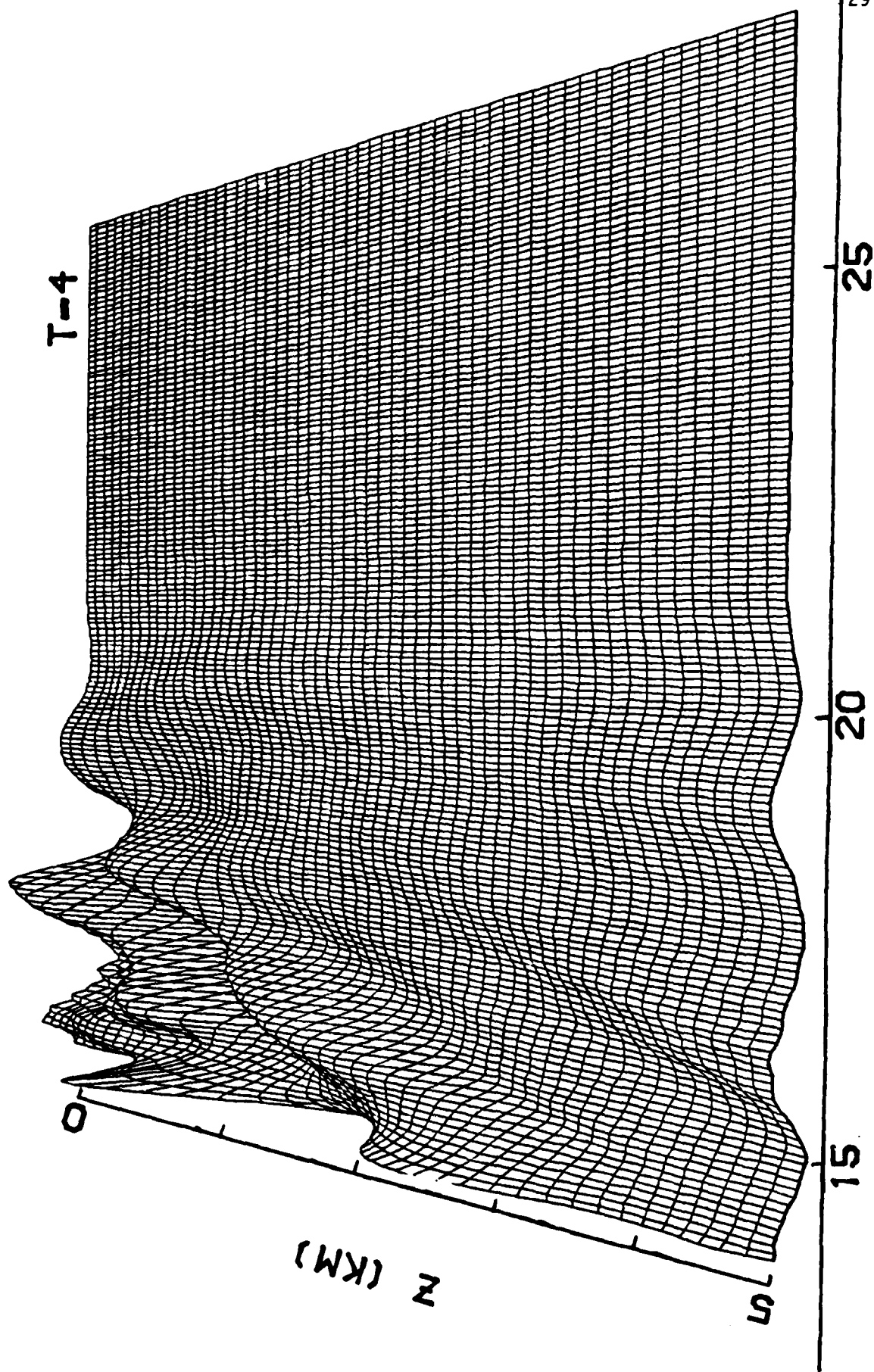


Figure 90.

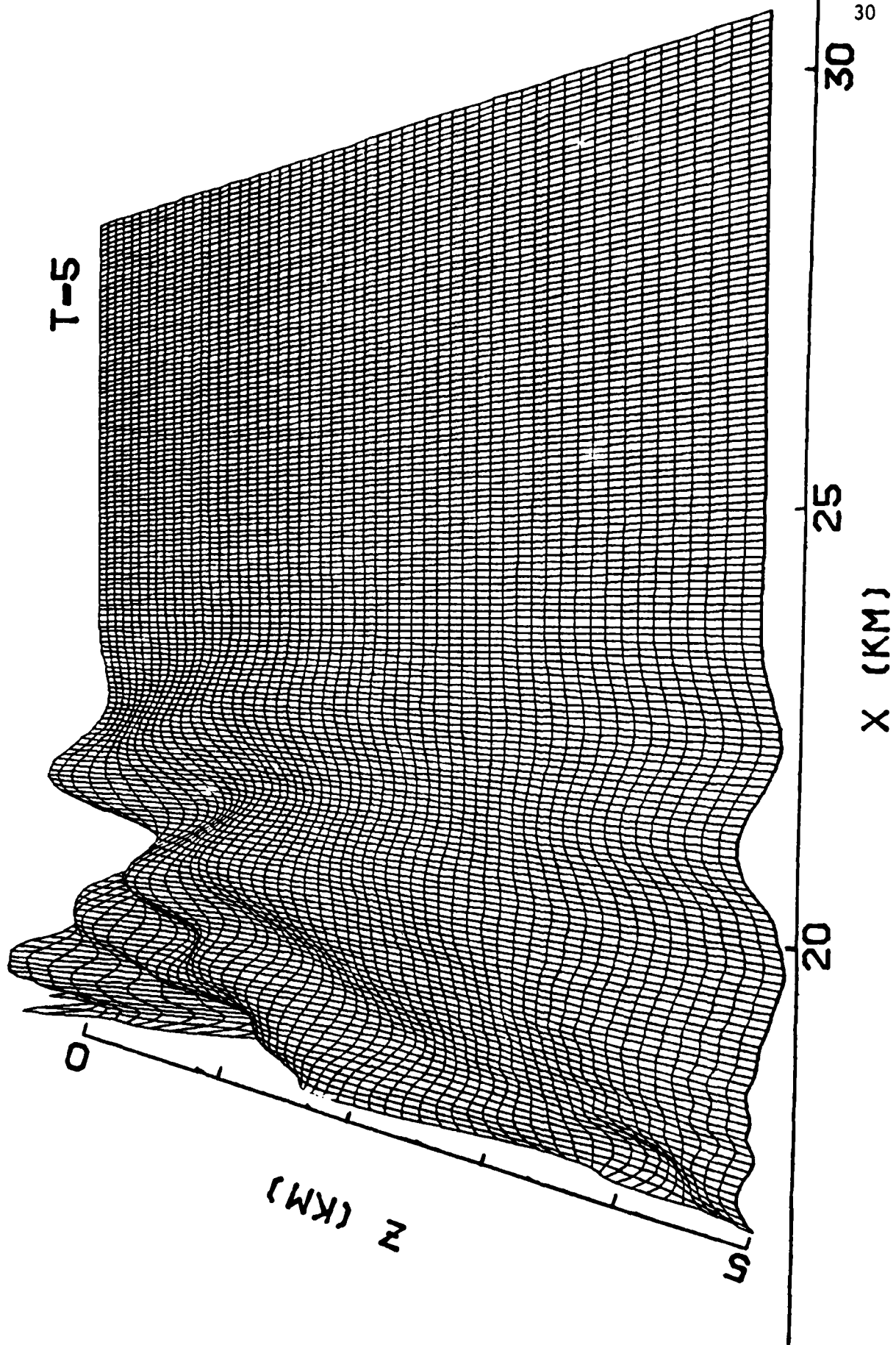


Figure 9E.

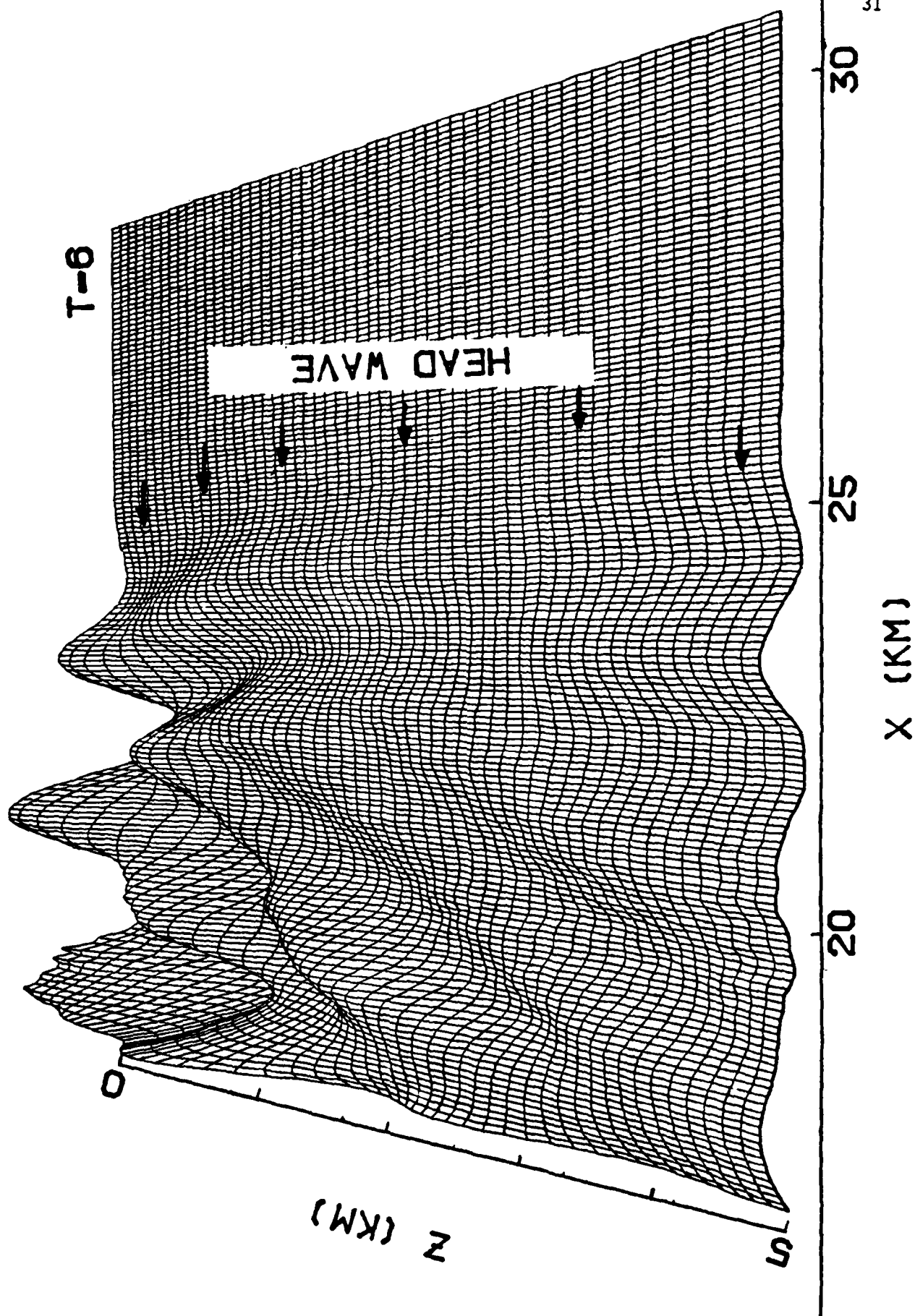


Figure 9F.

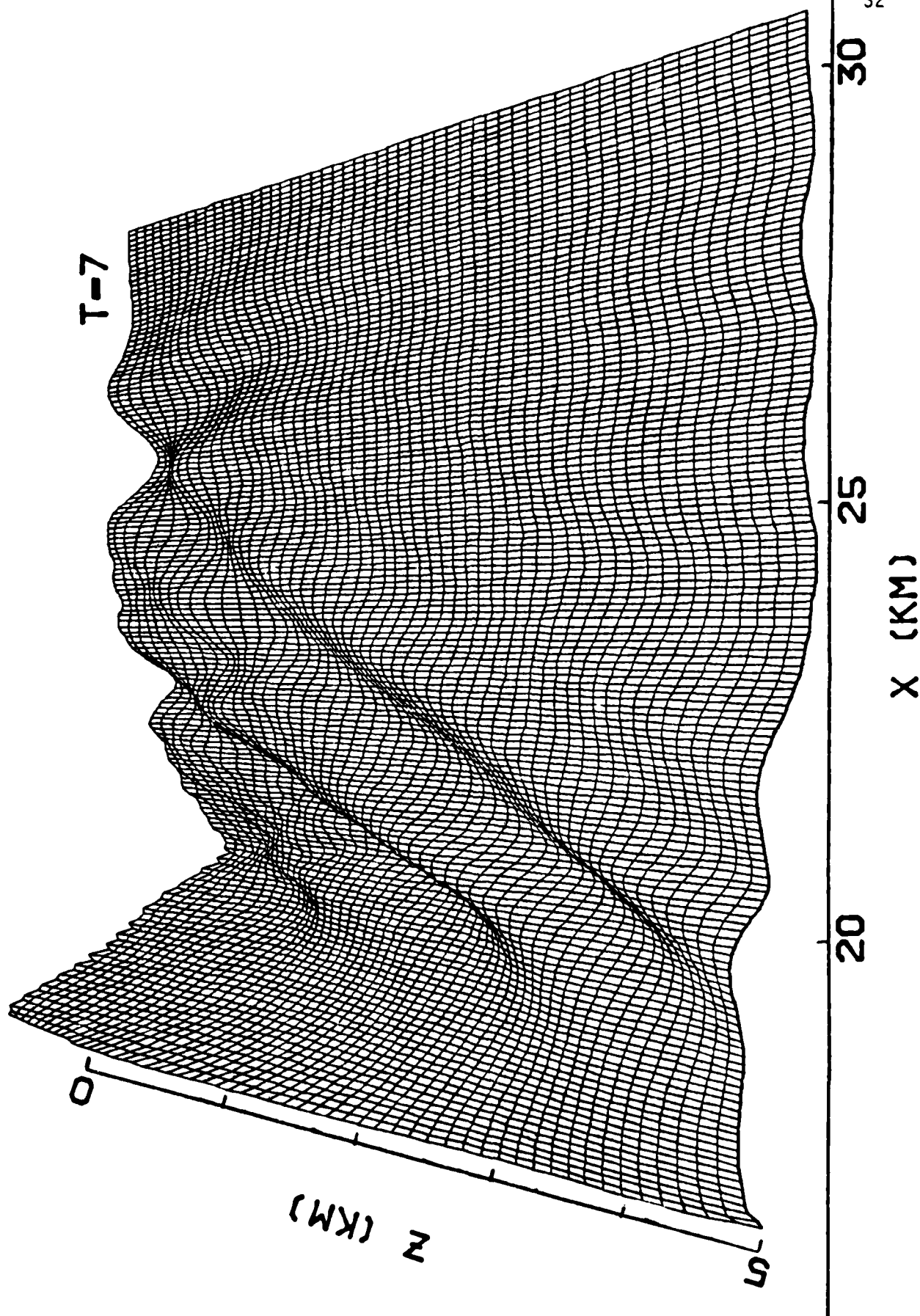


Figure 96.

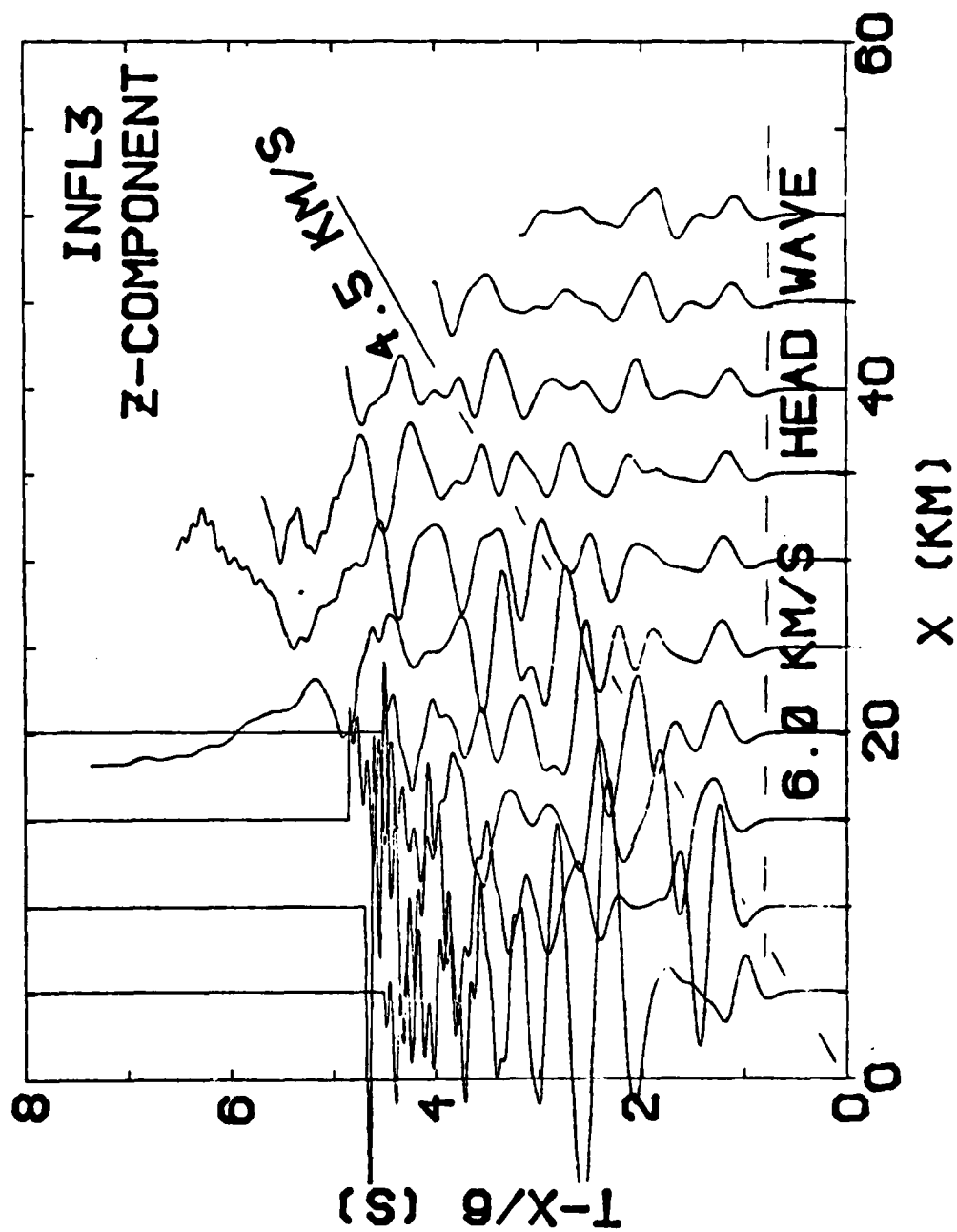


Figure 10A.

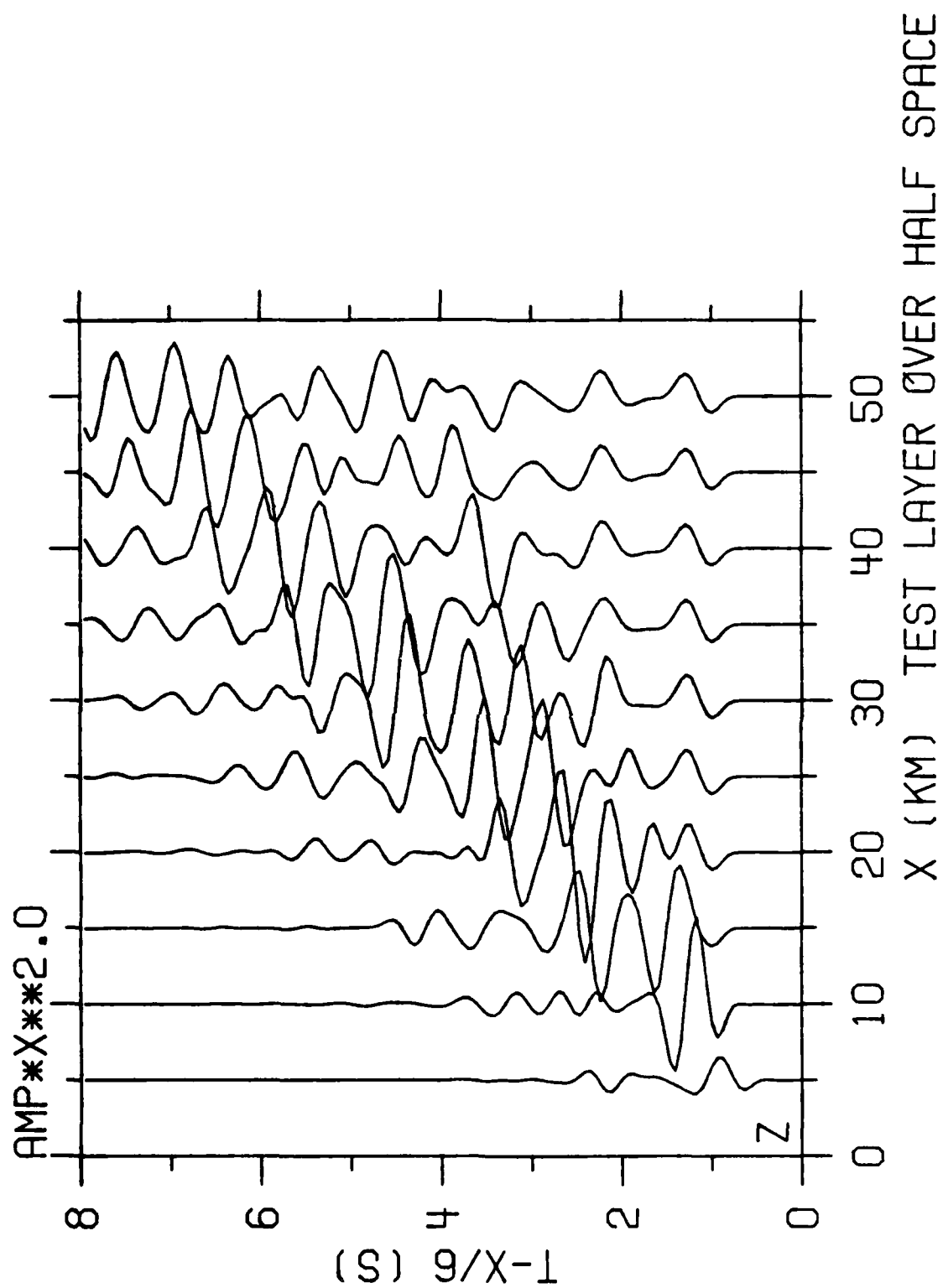


Figure 10B.

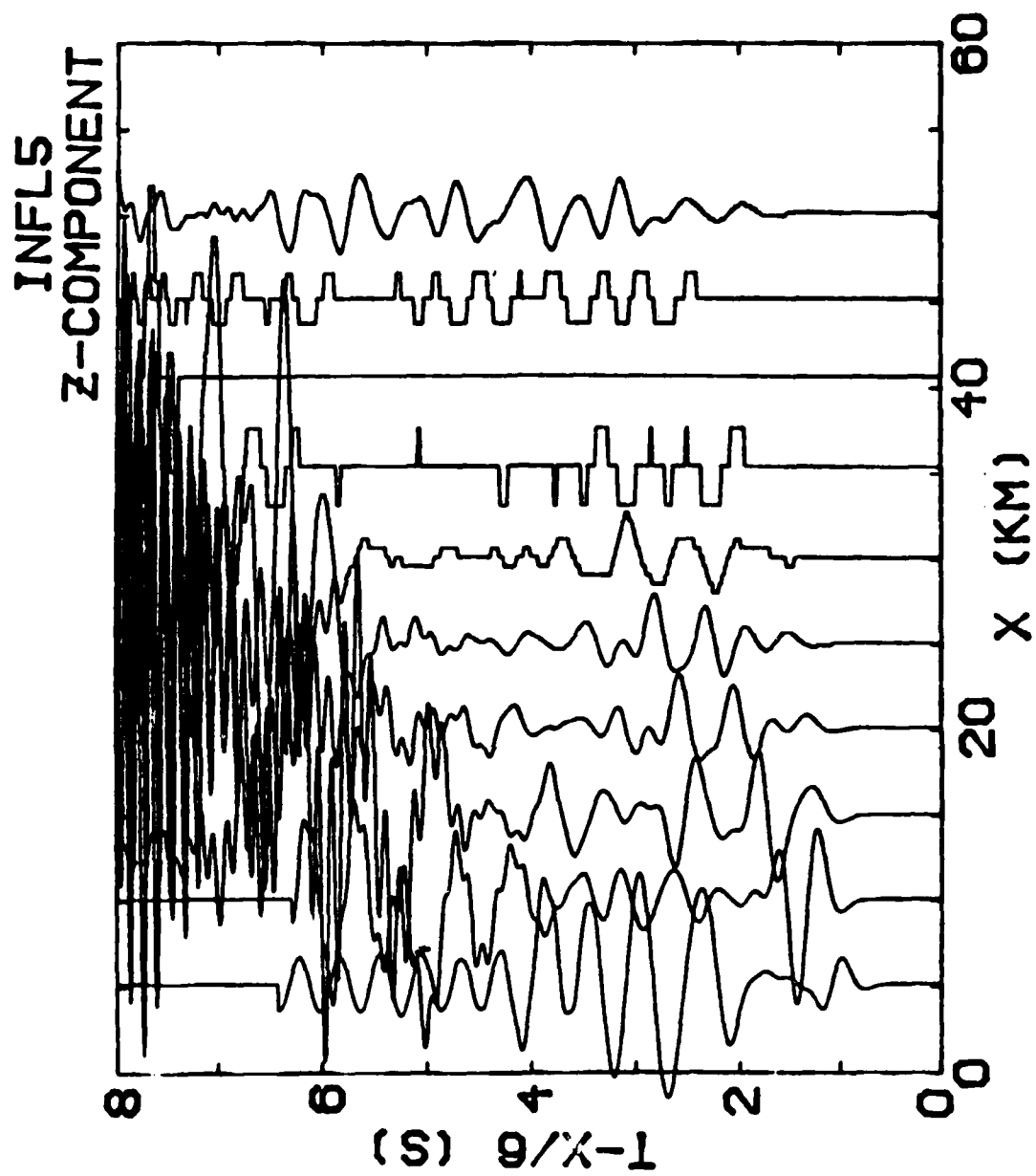


Figure 11A.

## FINITE DIFFERENCE SYNTHETIC SEISMOGRAMS

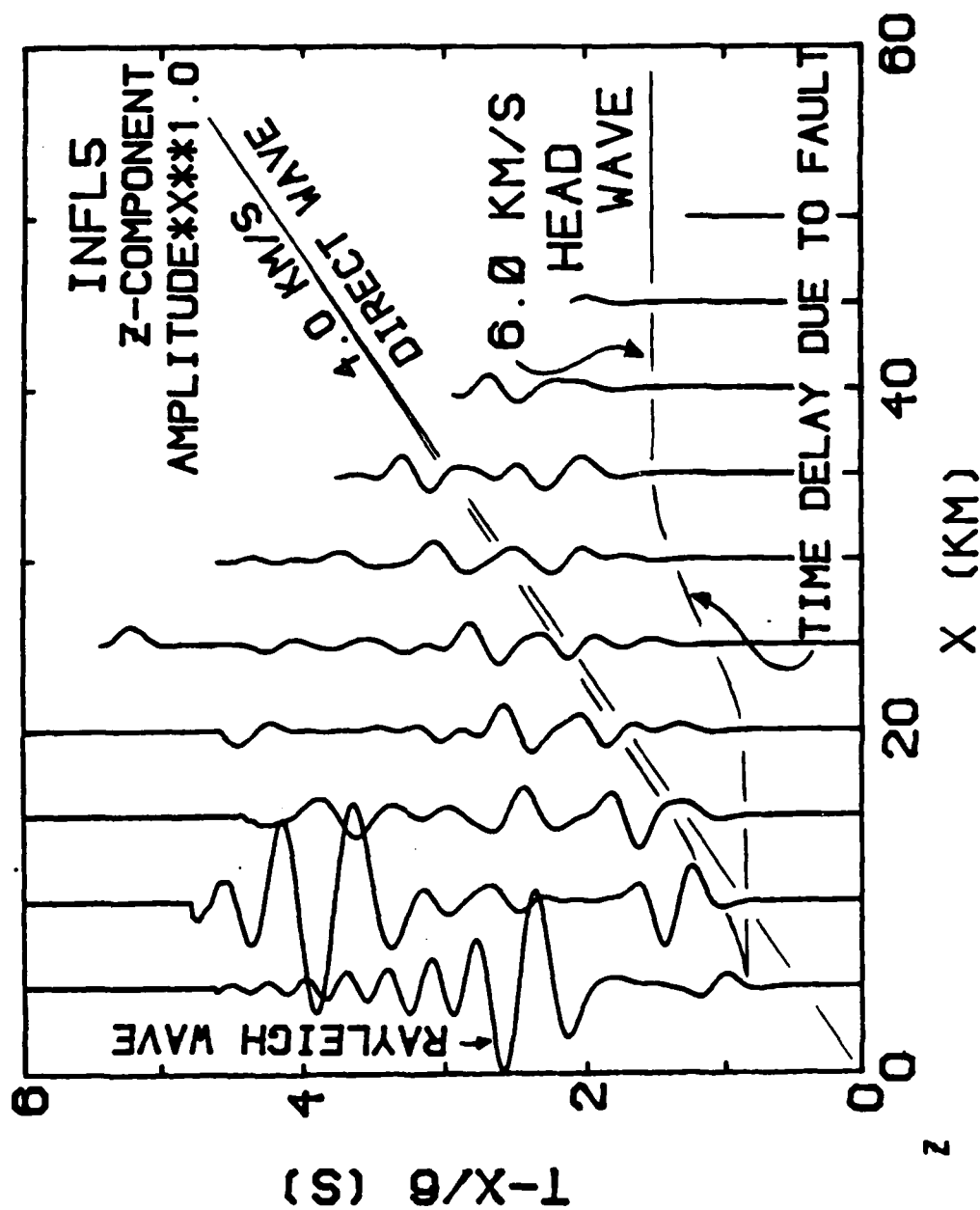


Figure 11B.

# FINITE DIFFERENCE SYNTHETIC SEISMOGRAMS

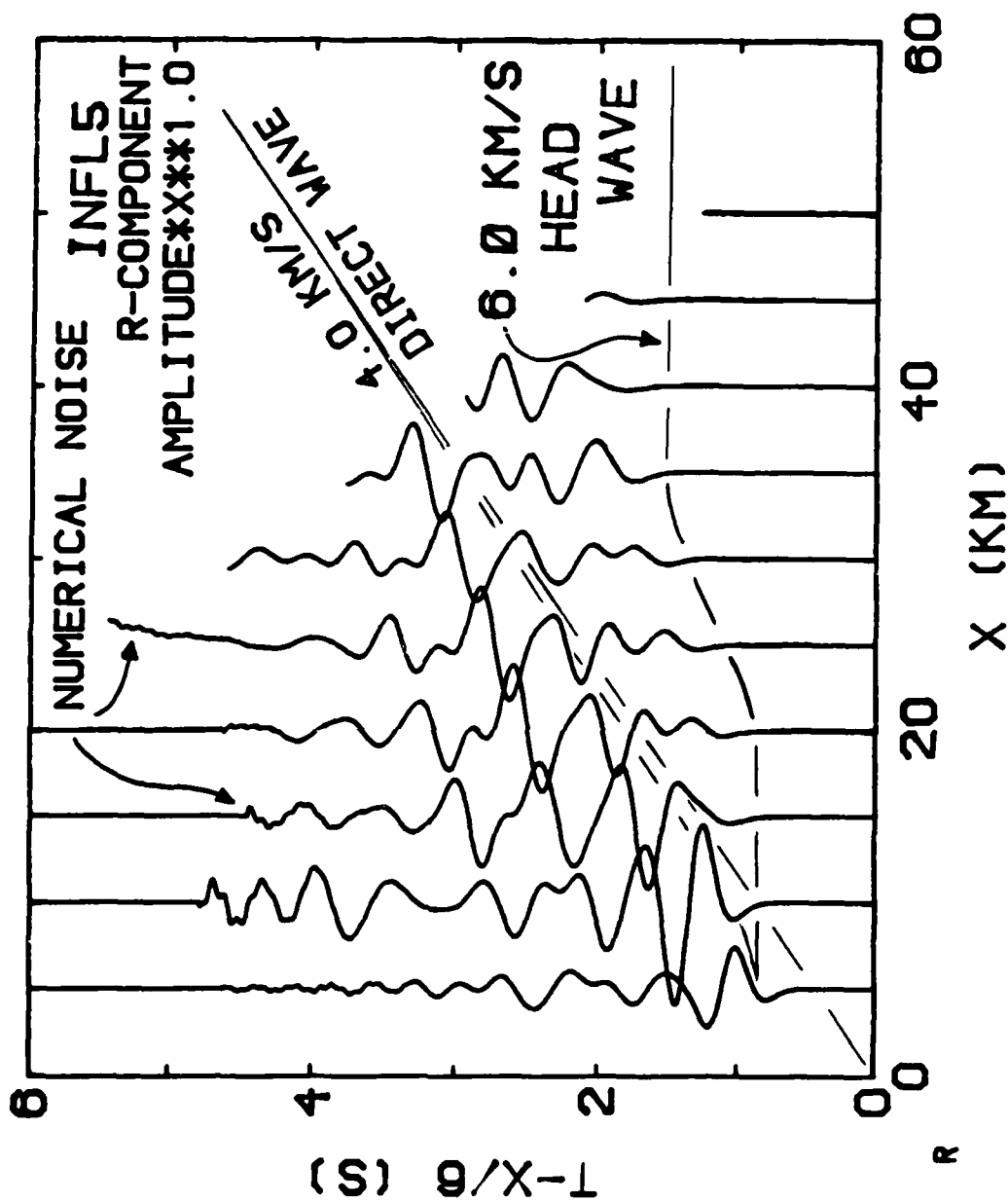


Figure 11C.

## DISTRIBUTION LIST

Chief of Naval Research  
Department of the Navy  
800 North Quincy Street  
Arlington, Virginia 22217

Code 100C1 (1)  
Code 460 (1)  
Code 463 (5)  
Code 480 (1)  
Code 420 (1)

ONR Resident Representative  
Ohio State Univ. Research Center  
1314 Kinnear Road  
Columbus, OH 43212 (1)

Director  
Naval Research Laboratory  
Code 2627  
Washington, DC 20375 (6)

Director  
Defense Advanced Research  
Projects Agency  
1400 Wilson Boulevard  
Arlington, VA 22209 (1)

Office of Naval Research  
Branch Office/Chicago  
536 South Clark St.  
Chicago, IL 60605 (1)

Director, Environmental Sciences Directorate  
Geophysical Sciences Division  
Office of Naval Research  
800 North Quincy Street  
Arlington, VA 22217 (1)

Air Force Office of Scientific Research  
Department of the Air Force  
Directorate of Physics (MPG)  
Building 410  
Bolling Air Force Base  
Washington, DC 20332 (1)

Army Research Office  
Department of the Army  
Geosciences Division  
Box 12211  
Research Triangle Park, NC 27709 (1)

Defense Technical Information Center  
Building 5  
Cameron Station  
Alexandria, VA 22314 (12)

Procuring Contracting Officer, Code 614B:DAW  
Office of Naval Research  
Department of the Navy  
800 North Quincy Street  
Arlington, VA 22217 (1)

## SUPPLEMENTARY DISTRIBUTION LIST

Division of Sponsored Programs  
Purdue University  
West Lafayette, IN 47907 (1)

Dr. Robert B. Smith  
Dept. of Geology & Geophysics  
University of Utah  
Salt Lake City, UT 84112 (1)

Dr. John Kuo  
Henry Krumb School of Mines  
Columbia University  
New York, NY 10027 (1)

Dr. G.R. Keller  
Dept. of Geological Sciences  
University of Texas, El Paso  
El Paso, TX 79968 (1)

Dr. Ken Olsen  
LASL, Group G-7  
MS 676  
PO Box 1663  
Los Alamos, NM 87545 (1)

Dr. Mark Odegard  
Dept. of Physics  
New Mexico State University  
Las Cruces, NM 88003 (1)

Dr. Robert E. Houtz  
Lamont-Doherty Geological Obs.  
Columbia University  
New York, NY 10029 (1)

Dr. John G. Heacock  
Earth Physics Program, Code 463  
Office of Naval Research  
Arlington, VA 22217

Dr. R.F. Obrochta  
Office of Naval Research  
800 N. Quincy Street  
Arlington, VA 22217 (1)

Dr. Murray MacDonald  
Code 425  
Geology & Geophysics  
Office of Naval Research  
Bay St. Louis, MS 39522 (1)

## APPENDIX I

The following papers or abstracts of theses reporting research supported by the Earth Physics Program of the Office of Naval Research have been published or are in press. Copies of the papers or abstracts are included in this appendix.

Black, P.R. and L.W. Braile, Pn velocity and cooling of the continental lithosphere, J. Geophys. Res., 87, 10557-10568, 1982.

Olsen, K.H. and L.W. Braile, Seismograms of explosions at regional distances in the western United States: Observations and reflectivity method modeling, in Identification of Seismic Sources - Earthquake or Underground Explosion, edited by E.S. Husebye and S. Mykkeltveit, 453-466, Reidel, 1981.

Olsen, K.H., L.W. Braile and P.A. Johnson, Seismic velocity and Q-structure of the upper mantle lid and low velocity zone for the eastern Great Basin, Geophys. Res. Letters, 7, 1029-1032, 1980.

Olsen, K.H., L.W. Braile and J.N. Stewart, Modeling short-period crustal phases (P, Lg) for long-range refraction profiles, Phys. of the Earth and Planet. Interiors, 31, (in press), 1982.

Banda, E., N. Deichmann, L.W. Braile and J. Ansorge, Amplitude study of the Pg phase, J. Geophysics, (in press), 1982.

Espindola, J.M., Finite difference synthetic seismograms for kinematic models of the earthquake source, Ph.D. thesis, Purdue Univ., West Lafayette, IN, 151 p., 1979.

Mazzella, F.E., The generation of synthetic seismograms for laterally heterogeneous models using the finite difference technique, Ph.D. Thesis, Purdue Univ., West Lafayette, IN, 225 p., 1979.

$P_n$  VELOCITY AND COOLING OF THE CONTINENTAL LITHOSPHEREPaul R. Black<sup>1</sup> and Lawrence W. Braile

Department of Geosciences, Purdue University, West Lafayette, Indiana 47907

**Abstract.** Average upper mantle  $P_n$  velocities and heat flow were computed within continental physiographic provinces in North America from published data.  $P_n$  velocity and heat flow data display an inverse relationship and were found to correlate with a statistically significant correlation coefficient. Temperatures at the crust-mantle boundary were estimated from the heat flow values, and these were used to demonstrate a correlation between  $P_n$  velocity and temperature of upper-mantle material. The value of  $(\partial P_n / \partial T)_p$  thus obtained ( $-4.4 \times 10^{-4}$  to  $-8.1 \times 10^{-4}$  km s<sup>-1</sup> °C<sup>-1</sup>) is within the range of temperature derivatives determined from laboratory studies of ultramafic rocks. This dependency of  $P_n$  velocity on temperature implies that one possible explanation for the observed geographical distribution in upper-mantle seismic velocity is that the variation in  $P_n$  velocity is primarily a temperature effect. Combined with the relationship between heat flow and crustal age for continents, the  $P_n$  versus heat flow correlation suggests a relationship between  $P_n$  velocity and crustal age, probably due to progressive cooling of the continental lithosphere after a thermotectonic event.

## Introduction

Seismologists have been aware of variations of continental upper-mantle compressional-wave velocity ( $P_n$  velocity at the Mohorovičić discontinuity) on a regional scale since about 1960 (Harris, 1969). The implications of this observation are not clearly understood, however, and several possible explanations have been suggested. Horai and Simmons [1968] found a correlation between travel-time anomalies for the Longshot nuclear explosion and heat flow. They could not demonstrate a similar correspondence with gravity. They concluded that thermal anomalies in the upper mantle (perhaps 50-km deep) were the probable cause of travel-time anomalies. Pakiser and Steinhart [1964], and Warren and Healy [1973], on the other hand, related  $P_n$  and mean crustal velocities to density variations. Chung [1977] attributed variations in  $P_n$  to compositional differences in the upper mantle. Fagerne and Kanestrom [1973] found that variations in the ratio of  $P_n$  velocity to  $S_n$  velocity within a region were too large to be explained solely by temperature variations, and proposed density variations as the cause. Pakiser [1963], noting that  $P_n$  and crustal thickness are related, found that

the assumption of isostasy requires variations of density in the upper mantle and hence a relationship between  $P_n$  and density. He notes, however, that '...elevated temperatures may affect velocity more than density' (Pakiser, 1963, p. 5754).

This study was undertaken in an attempt to quantitatively determine the relationship between continental  $P_n$  velocities and heat flow, and to determine whether the implied temperature variations alone are sufficient to be a viable explanation for the variation in upper mantle seismic velocity. The continental crust and upper mantle of North America was selected for study because of the large number of seismic refraction profiles and heat flow measurements available and because of the range of heat flow values present. Because the locations of seismic and thermal observations do not coincide, and because of large uncertainties which are possible in any given observation, the data were grouped by provinces and mean values for each province analyzed.

## Seismic Data

One-hundred thirty-one seismic refraction profiles for the continental crust and upper mantle of North America were compiled from published literature and other sources (Table 1). Observed  $P_n$  velocities and crustal thickness were tabulated from the profiles resulting in 153 observations of the continental  $P_n$  velocity. The data were sorted according to physiographic province (Fenneman [1946] for the United States and Douglas and Price [1972] for Canada) and mean  $P_n$  velocity and crustal thickness were calculated for each province (Table 2). The locations of the seismic profiles and the physiographic provinces are shown in Figure 1. Estimated errors for the mean  $P_n$  velocity and crustal thickness were taken to be the estimated standard deviation of the mean,  $S = \sigma/\sqrt{N}$ , where  $\sigma$  is the standard deviation of the data ( $P_n$  or  $H_c$  for a given province) and  $N$  is the number of observations. The estimated standard deviation of the mean provides a reasonable choice for estimating the uncertainty of the mean  $P_n$  velocity for each province because possible errors of individual  $P$  observations are generally not given. However,  $S$  is likely to be a poor estimate of the uncertainty of the mean  $P_n$  value for provinces containing only a small number of observations such as the Cascade Range, middle Rocky Mountains, southern Rocky Mountains, and Columbia Plateau provinces.

Two possible sources of errors in the  $P_n$  observations have not been analyzed in detail, but are expected to be negligible for the purpose of correlation of  $P_n$  velocity and heat flow by province. They are velocity anisotropy and differences in the apparent and true  $P_n$  velocity due to the earth's sphericity. Although velocity anisotropy in the upper mantle of

<sup>1</sup>Now at Eureka Resources Associates, Berkeley, California 94704.

Black and Braille:  $P_n$  Velocity and Cooling of the Lithosphere

TABLE 1. Seismic Refraction Profiles for North America

Profile	Reference	Profile	Reference
1	Richards and Walker [1959]	178	Hales and Nation [1973]
2,3	Johnson and Couch [1970]	179	Hill [1972]
4,5,6,7	Ewing et al. [1966]	184	Jackson and Pakiser [1965]
8,9	Stewart [1968a]	185	Braille et al. [1974]
10	Roller [1965]	193	Keller et al. [1975]
11	Diment et al. [1961]	194	Hales and Nation [1973]
11	Roller [1964]; Prodehl [1979]	195	Olsen et al. [1979]
11	Langston and Helmberger [1974]	198	Barr [1971]
12	Hamilton et al. [1964]	199	Mereu and Hunter [1969]
13	Berg et al. [1966]	200	Hodgson [1953]
14	Johnson [1965]	201,202	Hall and Hajnal [1973]
15,16	Mitchell and Landisman [1971]	204,205	Green et al. [1980]
17	Topposada and Sanford [1976]	206	Lyons et al. [1980]
18,19	Healy [1963]	207	White and Savage [1965]
20	Roller and Jackson [1966]	208	Warren et al. [1972]
21,22,23	Katz [1954]	212	Hill and Pakiser [1966]
28,29	Eaton [1963]	216	Carder [1973]
31	Gibbs and Roller [1966]	217	Forsyth et al. [1974]
32	Carder et al. [1970]	218,219	Hobson et al. [1967]
33	Ryall and Stuart [1963]	220	Gish et al. [1981]
35	Berry and West [1966]	221	Smith et al. [1982]
36,37	Cohen and Meyer [1966]	222	Sparlin et al. [1982]
38	Cram [1961]	223	Baldwin [1980]
39	Dorman et al. [1972]	225	Hall and Hajnal [1969]
40	McCamy and Meyer [1966]	226	Sinno et al. [1981]
41	Merkal and Alexander [1969]	227,228	Shor et al. [1968]
42	Warren et al. [1966]	229	Keller et al. [1975]; Mueller and Landisman [1971]
43,44	Warren [1969]	230	Clee et al. [1974]
45	Hales et al. [1970]	231	Martin [1978]
46	Willden [1965]	232	Mereu and Jobidon [1971]
47	Jackson et al. [1963]	233,234	
48	Jackson and Pakiser [1965]; Prodehl and Pakiser [1980]	235,236	Berry and Forsyth [1975]
49	Chandra and Cummings [1972]	237,238	Eaton [1966]
50	Bennett et al. [1975]	239,240	Stewart [1968b]
51,52	Johnson et al. [1972]	241	Braille et al. [1982]
53,54,55	Berry and Fuchs [1973]	242,243	
56,57,58		244,245	
59,60,61		246,247	
62,63	McCamy and Meyer [1964]	248	Prodehl [1979]
64	Roller and Healy [1963]	249,250	
66	Ewing et al. [1955]	251	Warren and Jackson [1968]
68,69	Hersey et al. [1959]	252,253	Romney et al. [1962]
72	Mereu et al. [1976]	254,255	James et al. [1968]
75,76	Stauber and Boore [1978]	256	Bates and Hall [1975]
86,87	Barratt et al. [1964]	257	Tuve [1951]; Steinhart and Meyer [1961]
154	Shor [1962]	258	Steinhart and Meyer [1961]
157	Steinhart and Meyer [1961]	259	Tuve [1953]; Steinhart and Meyer [1961]
158	Slichter [1951]; Steinhart and Meyer [1961]	260	Tuve [1954]; Steinhart and Meyer [1961]
163	Steinhart and Meyer [1961]	261	Warren [1968]
167	Press [1960]	262	Steinhart et al. [1964]
173,174	Slichter [1951]; Steinhart and Meyer [1961]	263	Hales et al. [1968]
175	Berg et al. [1960]		

continents has been reported [Bamford, 1973], an analysis of western United States data by Bamford et al. [1979] found a relatively small and poorly defined anisotropy of about 3%. Because the azimuths of the seismic refraction profiles within each province are randomly distributed, any anisotropy present would contribute to a larger estimated standard deviation of the mean for the  $P_n$  measurements for the

province but would not be expected to significantly affect the mean value of  $P_n$ . Of course, for provinces that have only a few observations, the effect could be more pronounced. Possible errors due to neglect of consideration of the spherical earth can be evaluated and shown to be small. The errors are due to the fact that many analyses of seismic velocities utilize a flat-earth formulation in which apparent velo-

TABLE 2. Heat Flow,  $P_n$  Velocity, Estimated Temperature at the Mohorovicic Discontinuity and Crustal Thickness Averaged by Province for North America

Province	Symbol	Mean Heat Flow, $q_0$ $mW/m^2$	Estimated Standard Deviation of $q_0$ $mW/m^2$	Sample Size for $q_0$	Mean $P_n$ velocity, $km/s$	Estimated Standard Deviation of $P_n$ $km/s$	Sample Size for $P_n$	Mean $H_c$ , $km$	Estimated Standard Deviation of $H_c$ $km$	$T_m$ , $^{\circ}C$	Estimated Error Limits, $^{\circ}C$
Pacific Border	PB	67.4	2.5	50	8.06	0.037	11	23.7	2.05	420	80
Sierra Nevada	SN	33.9	3.3	12	7.92	0.020	7	41.0	3.54	270	100
Columbia Plateau	CA	86.2	7.5	14	7.82	0.042	5	36.8	2.29	1100	200
Basin and Range	BR	85.4	1.7	213	7.79	0.025	30	29.2	0.85	850	80
Colorado Plateau	CO	64.0	4.6	17	7.83	0.022	6	39.7	1.38	820	150
Middle Rocky Mtns.	MR	69.1	9.2	10	7.86	0.040	2	35.9	2.10	770	180
Northern Rocky Mtns.	NR	86.7	6.7	31	8.02	0.037	10	39.1	1.95	1090	200
Southern Rocky Mtns.	SR	97.1	6.3	26	7.90	0.024	4	44.0	0.96	1400	200
Cascade Range	CR	50.7	5.0	8	7.99	0.013	3	31.2	0.60	440	100
Coastal Plain	CP	41.4	1.3	4	8.20	0.042	11	29.1	3.28	330	80
Canadian Shield	CS	37.7	2.9	12	8.08	0.029	13	36.8	0.99	380	80
Midcontinent	MC	52.7	2.1	63	8.10	0.020	36	43.9	0.92	670	100
Appalachians	AP	53.6	2.1	47	8.21	0.054	15	37.2	1.27	570	100

 $q_0$  - Mean of observed heat flow. $P_n$  - Mean of seismic compressional wave velocity at the Moho. $H_c$  - Mean of crustal thickness. $T_m$  - Temperature estimate at the Moho (interpolated from the geothermal gradient curve of Lachenbruch and Sasa [1977]).

NR - Includes Northern Rocky Mountains and Canadian Cordillera provinces.

CS - Includes Superior, Grenville, Churchill, Slave, Bear and Hudson Platform provinces.

MC - Includes Great Plains, Ozark and Interior Platform provinces.

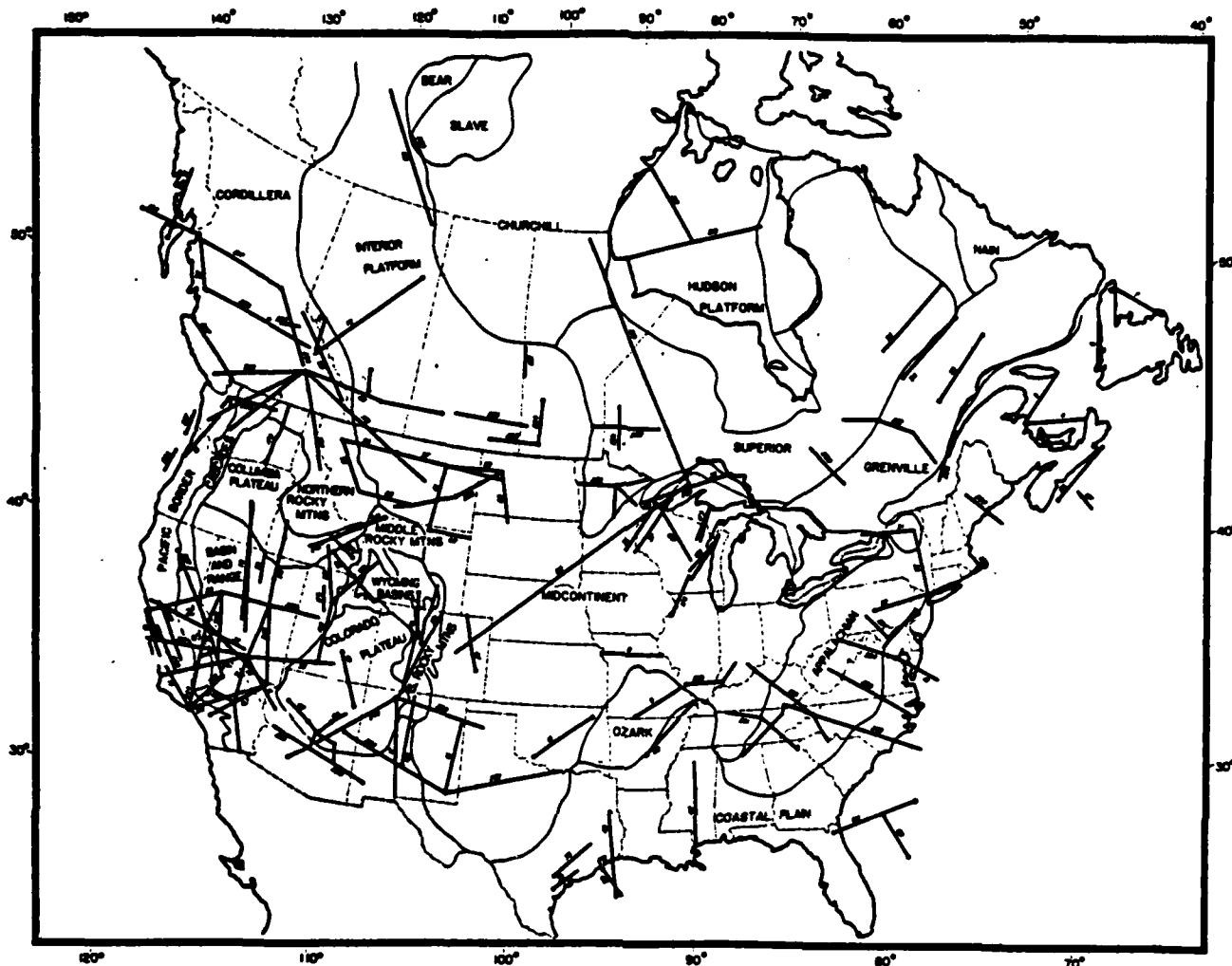


Fig. 1. Locations of refraction profiles for the continental crust and upper mantle of North America. References for the profiles are given in Table 1. Province boundaries are from Fenneman [1946] for the United States and from Douglas and Price [1972] for Canada.

city along the surface of the  $P_n$  arrivals in the absence of dip on the Moho is equal to the upper mantle velocity. Consideration of a spherical earth indicates that the true velocity of the upper mantle is slightly lower than the apparent velocity. The difference is dependent on the velocity and the depth of the refractor (the crustal thickness) but varies from  $-0.03$  to  $-0.06$  km/s for the range of velocities and thicknesses included here. These corrections have not been applied to the  $P_n$  data used here because publications that report the  $P_n$  data generally do not include an indication as to whether spherical-earth or flat-earth calculations were utilized. Including this correction would have no significant effect on the correlation analysis discussed below.

Variations in the  $P_n$  velocities due to differences in crustal thickness were corrected for pressure by recalculating each to a common depth of 35 km. To do this, the pressure gradient was assumed to be lithostatic, i.e.,  $dP/dZ = \rho g$  where  $P$  is pressure,  $Z$  is depth,  $\rho$  is density, and  $g = 980$  cm/s<sup>2</sup>, the accelera-

tion of gravity. The variation of velocity with depth will then be  $dV/dZ = (\partial V/\partial P)_T (dP/dZ) = (\partial V/\partial P)_T \rho g$ . On the basis of experimental studies [Christensen, 1974; Manghani et al., 1974],  $(\partial V/\partial P)_T$  was taken to be  $0.015$  km s<sup>-1</sup> kbar<sup>-1</sup>. The average crustal density was taken as  $2.9$  gm/cm<sup>3</sup> [Verhoogen et al., 1970, p. 617]. The pressure correction is then  $4.2 \times 10^{-3}$  km s<sup>-1</sup> km<sup>-1</sup>  $\times (35 - H_c)$  km where  $H_c$  is the average crustal thickness for the province calculated from the seismic data. Varying the pressure correction over a fairly wide range (or neglecting the correction completely) does not significantly affect the correlation analysis discussed below.

#### Heat Flow Data

Heat flow values for the United States published through 1976 were compiled by Sass et al. [1976]. These values were supplemented by data taken from Henyey and Lee [1976], Pollack and Chapman [1977], and Costain et al. [1980].

TABLE 3. Regression Parameters for  $P_n = A + Bq_0$  and  $P_n = A + BT_m$ 

Case	Regression Variables	Method	Provinces Excluded	N	A	$\sigma_A$	B( $\times 10^4$ )	$\sigma_B(\times 10^4)$	r	$\alpha$
1	$q_0 - P_n$	RMA	-	13	8.420	0.123	-68.8	15.9	-0.550	0.10
2	$q_0 - P_n$	LSQC	-	13	8.386	0.121	-68.0	19.4	-0.550	0.10
3	$q_0 - P_n$	RMA	SN	12	8.487	0.131	-75.6	16.0	-0.679	0.05
4	$q_0 - P_n$	LSQC	SN	12	8.516	0.113	-82.9	17.4	-0.679	0.05
5	$T_m - P_n$	RMA	-	13	8.271	0.097	-4.11	0.97	-0.519	0.10
6	$T_m - P_n$	LSQC	-	13	8.490	0.135	-8.46	2.15	-0.519	0.10
7	$T_m - P_n$	RMA	SN	12	8.312	0.102	-4.40	1.00	-0.619	0.05
8	$T_m - P_n$	LSQC	SN	12	8.456	0.112	-7.29	1.70	-0.619	0.05
9	$T_m - P_n$	RMA	SN,SR	11	8.370	0.119	-5.53	1.26	-0.653	0.05
10	$T_m - P_n$	LSQC	SN,SR	11	8.488	0.117	-8.08	1.88	-0.653	0.05
11	$q_0 - P_n$	LSQ	-	13	8.223	0.115	-37.8	17.3	-0.550	0.10
12	$q_0 - P_n$	LSQ	SN	12	8.327	0.120	-51.3	17.5	-0.679	0.05
13	$T_m - P_n$	LSQ	-	13	8.133	0.082	-2.13	1.06	-0.519	0.10
14	$T_m - P_n$	LSQ	SN	12	8.189	0.088	-2.72	1.09	-0.619	0.05
15	$T_m - P_n$	LSQ	SN,SR	11	8.240	0.101	-3.61	1.40	-0.653	0.05

$q_0$  - heat flow averaged by province;  $P_n$  - upper mantle compressional wave velocity averaged by province (km/s);  $T_m$  - temperature estimate at the Moho ( $^{\circ}\text{C}$ ); RMA - reduced major axis method; LSQC - least squares cubic method; LSQ - standard least squares linear regression; SN - Sierra Nevada province; SR - southern Rocky Mountains province; N - number of data points; A - intercept;  $\sigma_A$  - estimated standard deviation of A; B - slope;  $\sigma_B$  - estimated standard deviation of B; r - correlation coefficient;  $\alpha$  - level of significance for r.

Heat flow values were sorted by province, and the mean and estimated standard deviation of the mean were calculated for each province (Table 2). Values of heat flow greater than  $200 \text{ mW/m}^2$  were considered anomalous and eliminated. Such a high value for observed heat flow generally implies the action of hydrothermal systems or other near-surface conditions not representative of the regional heat flow.

#### Temperatures

In order to evaluate the possible dependence of the  $P_n$  velocity on temperature, the temperature at the Mohorovičić discontinuity (Moho) for each province must be calculated. Such thermal calculations would require additional information on the thermal conductivity and heat generation values for each province. In addition, assumptions pertaining to thermal equilibrium, the distribution of heat producing elements and the possible contributions of thermal convection to the heat flow would have to be made for each province. Such an analysis is beyond the scope of this study and, therefore, we have estimated the temperature at the Moho beneath each province by utilizing the geothermal gradient curves presented by Lachenbruch and Sasa [1977]. The temperature estimates were interpolated from the curves of Lachenbruch and Sasa [1977], using the average heat flow and crustal thickness calculated here (Table 2). Temperature error estimates are based on the

estimated uncertainties in heat flow and crustal thickness for each province (Table 2).

#### Correlation

The correlations of continental upper mantle seismic velocity ( $P_n$ ) and heat flow ( $q_0$ ) as well as  $P_n$  velocity and temperature estimated at the Moho ( $T_m$ ) were evaluated by least-squares linear regression of the form  $y = A + Bx$  where y is the  $P_n$  variable and x is  $q_0$  or  $T_m$ . The coefficients A (intercept), B (slope), and the correlation coefficient (r), as well as standard deviations estimates of A ( $\sigma_A$ ) and B ( $\sigma_B$ ), were calculated and are given in Table 3. It is well-known that standard linear regression methods (x considered the independent variable and y considered the dependent variable) yield unreliable estimates of the A and B coefficients for the situation in which both the x and y variables are subject to error. This can be easily demonstrated by comparing the results of the regressions for y on x and for x on y. Because both the x ( $q_0$  or  $T_m$ ) and y ( $P_n$ ) variables analyzed here are subject to error, the 'reduced major axis' (RMA) and the 'least-squares cubic' (LSQC) methods of linear regression were utilized in order to evaluate the correlation of  $P_n$  versus  $q_0$  and  $P_n$  versus  $T_m$ . In the RMA method [Kernack and Haldane, 1950], the x and y variables are scaled by standard deviations of the data and the perpendicular distances of points to the least squares line are minimized.

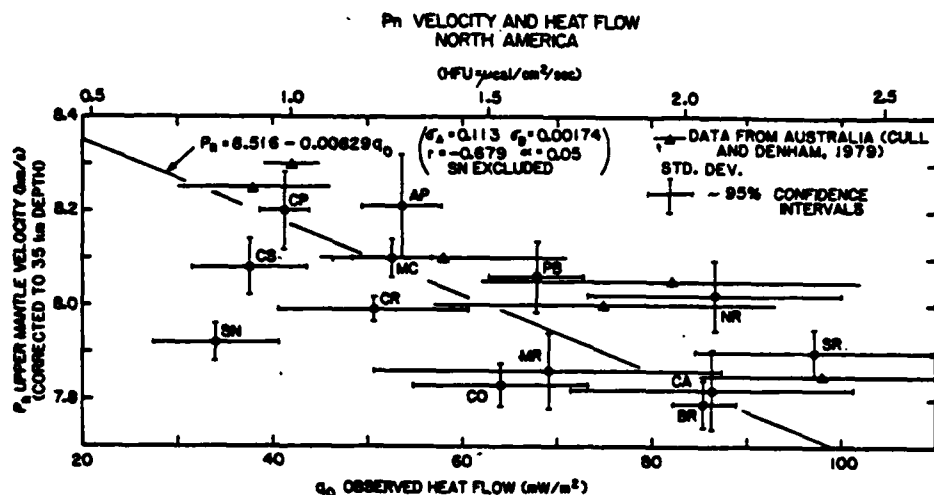


Fig. 2.  $P_n$  velocity and heat flow data averaged by province for North America. The province abbreviations and the data are given in Table 2. Error bars correspond to plus and minus two estimated standard errors of the mean for the  $P_n$  and heat flow observations. The best fitting regression line for the case of the Sierra Nevada province excluded is shown along with the regression parameters (case 4, Table 3). Data from Australia [Cull and Denham, 1979] are shown by triangles with error bars (for heat flow only) indicating plus and minus one standard deviation. Each of the Australian data points corresponds to an individual geological province. The data from Australia were not used in the regression line calculation.

In the LSQC method [York, 1966, 1967], each observation is weighted according to its estimated error in both the x and y directions. The solution of a cubic equation yields the coefficients A and B and estimates of their standard deviations. Because each data point is individually weighted, and because errors in both variables are considered, this method has the advantage that data points with the smallest errors have the greatest effect on the regression line. The regression parameters for the correlations of  $P_n$  velocity and heat flow and for  $P_n$  velocity and temperature are

given in Table 3. Regression parameters for standard least squares fit to the  $q_0$ - $P_n$  and  $T_m$ - $P_n$  data are shown for comparison with the RMA and LSQC methods as cases 11 to 15 in Table 3. The correlation coefficient r and the associated level of significance  $\alpha$  are determined from the linear correlation of the observation without regard to estimated errors in the data and, therefore, are the same for the three methods.

The  $P_n$  velocity data are plotted versus heat flow and estimated temperature at the Moho in Figures 2 and 3. Error bars for the mean  $P_n$

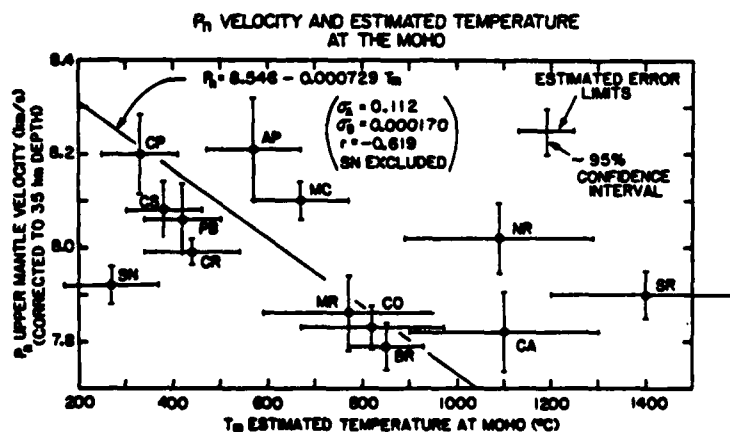


Fig. 3.  $P_n$  velocity and estimated temperature at the Moho data averaged by province for North America. The province abbreviations and data are given in Table 2. Error bars correspond to plus and minus two estimated standard deviations of the mean calculated for the  $P_n$  data and estimated error limits for the temperatures. The best fitting regression line for the case of the Sierra Nevada province excluded is shown along with the regression parameters (case 8, Table 3).

TABLE 4. Comparison of Temperature Derivatives Inferred From  $P_n - T_m$  Regression with Laboratory Determinations of  $(\partial V_p / \partial T)_P$  for Ultramafic Rocks

$\left(\frac{\partial V_p}{\partial T}\right)_P \times 10^4$ km/s/°C	Reference
-4.4 to -8.1	Regression of $P_n$ and T [this study]
-4.12	Dunite [Kern and Richter, 1981]
-4.94	Peridotite [Kern and Richter, 1981]
-5.6	Dunite [Christensen, 1979]
-6.1	Dunite [Ramanantoandro and Manghani, 1978]
-4.4	Peridotite, data from Fielitz [1976]
-6.5	Harzburgite [Peselnick and Nicolas, 1978]
-6.7	Harzburgite [Peselnick and Nicolas, 1978]
-5.6	Harzburgite [Peselnick and Nicolas, 1978]
-7.1	Lherzolite [Peselnick and Nicolas, 1978]
-6.7	Lherzolite [Peselnick and Nicolas, 1978]
-6.2	Harzburgite [Peselnick et al., 1977] (corrected values by Peselnick and Nicolas [1978])
-6.9	Harzburgite [Peselnick et al., 1977] (corrected values by Peselnick and Nicholas [1978])

velocity and heat flow values are scaled to plus and minus two estimated standard deviations of the mean that correspond approximately to 95% confidence intervals. The error bars for temperature at the Moho are estimated by the range of temperatures read from the geothermal gradient curves of Lachenbruch and Sass [1977], corresponding to the 95% confidence interval ranges of observed heat flow and crustal thickness. The best fitting regression lines for the case of the Sierra Nevada province excluded are also shown in Figures 2 and 3.

If the Sierra Nevada data point is excluded from the least squares calculations, the correlations between heat flow and  $P_n$  velocity and between temperature and  $P_n$  velocity are statistically significant at the  $\alpha = 0.05$  level of significance (cases 3, 4, 7, 8, 9 and 10, Table 3). The Sierra Nevada data point is one of the most discrepant points on the plots shown in Figures 2 and 3 and its exclusion from the regression calculations is based on the fact that the estimated mantle heat flow for the Sierra Nevada is anomalously low [Blackwell, 1971] and thus the estimated temperature at the Moho based on average surface heat flow may be substantially in error. The estimated temperature at the Moho for the Southern Rocky Mountains (SR) province also appears highly anomalous (Figure 3). The high value of inferred temperature is due to the large average crustal thickness of the SR Province and the relatively high observed heat flow (Table 2). Such a high temperature should not exist at the Moho because it is above the melting points for likely mantle and lower crustal rocks. However, because of the large error bars associated with the SR data point, its inclusion in the regression analysis has little effect on the resulting slope estimates (compare cases 7 and 9 or 8 and 10 from Table 3). Although

the correlations of  $q_0$  and  $P_n$  or  $T_m$  and  $P_n$  are statistically significant, the differences between the intercept and slope coefficients for the various regressions shown in Table 3 (cases 1-4 for  $q_0$  and  $P_n$ ; cases 5-10 for  $T_m$  and  $P_n$ ) are not significant.

#### Laboratory Data

To determine whether the regional variations in temperature calculated from heat flow are sufficient to explain the entire variation in continental  $P_n$  velocities, experimental values of  $(\partial V_p / \partial T)_P$  must be considered. The regression line values found in this study  $-4.4 \times 10^{-4}$  to  $-8.1 \times 10^{-4}$  km/s/°C compare well with the range of experimental measurements of the temperature derivatives of compressional velocity for ultramafic rocks as shown in Table 4. Although other factors could also have a significant effect, these results are consistent with the hypothesis that temperature effects could explain the entire observed variation in  $P_n$  velocity between provinces.

#### Discussion

This study has demonstrated a statistically significant relationship between continental  $P_n$  velocity and heat flow on a regional scale for North America. Heat flow has also been related to crustal age [Polyak and Smirnov, 1968] and to thickness of the lithosphere [Crough and Thompson, 1976; Pollack and Chapman, 1977; Kono and Amano, 1978]. Figure 4 shows the observed relationship between  $P_n$  velocity, crustal age, and heat flow which was obtained by using the relationship between heat flow and age determined by Polyak and Smirnov [1968] (as plotted by Chapman and Pollack [1975]) and the relationship between heat flow and  $P_n$  velocity found in this study.

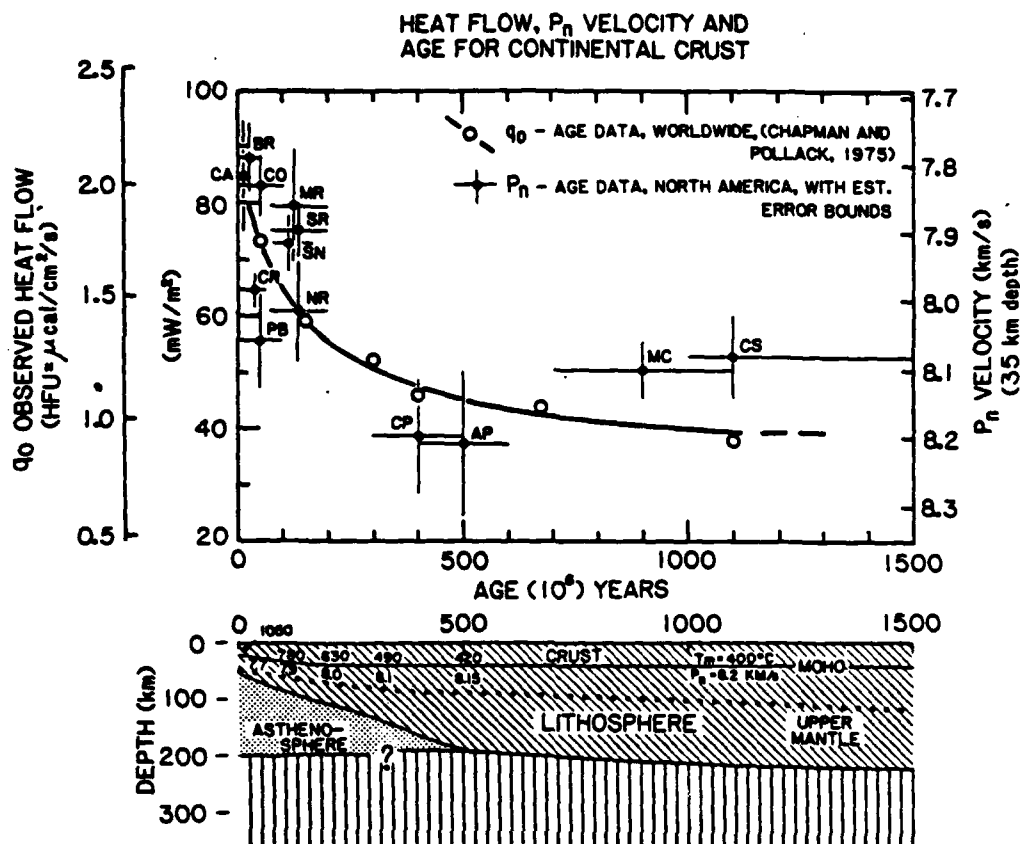


Fig. 4. Relationship of observed heat flow, crustal age and  $P_n$  velocity. Heat flow age data are from Polyak and Smirnov [1968] as plotted by Chapman and Pollack [1975] for continents.  $P_n$  velocity - heat flow relation is inferred by the linear regression for North American data shown in Figure 2. Crustal age is interpreted as time since the last thermal event affecting the continental lithosphere. Lower schematic diagram illustrates the evolution of the continental lithosphere and upper mantle velocity as a function of time (cooling of the lithosphere).  $P_n$  values are in km/s inferred from the  $q_0 - P_n$  - age curve above and the  $T_m$  estimates (in  $^{\circ}\text{C}$ ) are inferred from the  $P_n - T_m$  relationship illustrated in Figure 3. The depth to the base of the lithosphere is shown based on the depth to the estimated temperature of partial melting of upper mantle materials from the model of Pollack and Chapman [1977]. The dotted line in the lower part of the figure shows the lithosphere-asthenosphere boundary according to the relation determined by Kono and Amano [1978].

Although correlations of heat flow age and heat flow  $P_n$  velocity do not necessarily imply a causal relationship between age and  $P_n$  velocity, the  $P_n$  versus age estimates for provinces in North America shown in Figure 4 suggest that this relationship is valid. Lithospheric thickness estimates from Pollack and Chapman [1977] and Kono and Amano [1978] are also shown in Figure 4. These results suggest that thickening of the lithosphere and an increase in upper mantle  $P_n$  velocity are related processes caused by cooling of the continental lithosphere with time after a thermo-tectonic event. The observed range of continental upper mantle  $P_n$  velocities ( $\approx 7.6 - 8.3$  km/s) can be explained as primarily the results of regional differences in temperature at the Moho discontinuity.

Alternative explanations for the heat flow,  $P_n$  and crustal age data are (1) that  $P_n$  velocity is a function of composition that may vary with age (for example, by loss of volatiles or

differentiation by magmatic processes) and, (2) that variations in  $P_n$  velocity are due to anisotropy in which the degree of orientation of anisotropic mineral grains varies with time. Rybach and Buntebarth [1982] have recently presented data to indicate that seismic velocity and heat generation in crystalline rocks are inversely related and thus variations in composition (and, therefore, heat generation) could be a controlling factor in variations in upper mantle seismic velocity. However, the agreement of  $(\partial P_n / \partial T)_P$ , estimated from the regression of  $T_m$  and  $P_n$ , with experimentally determined temperature derivatives for ultramafic rocks suggests that the entire variation may be due to temperature effects.

Data from North America were selected for the analysis of the relation between  $P_n$  velocity and heat flow because the volume and geographical distribution of data were sufficient to permit statistical analysis. A

similar  $P_n$  versus heat flow relationship (Figure 2) was suggested by Cull and Denham [1979] for Australia. Although no detailed analysis has been performed, a brief examination of the  $P_n$  and heat flow data for Europe and Asia suggests that a similar relationship will be found for these continental regions.

**Acknowledgments.** This research was supported by the Office of Naval Research, Earth Physics Program, contract N00014-75-C-0972, by the National Aeronautics and Space Administration, contract NCC521, by contract 9-X60-2133K-1 with Los Alamos National Laboratory, and by a Purdue University Research Foundation David Ross grant. We are grateful to Mark Sparlin, Kevin Martindale, Neil Stillman, and John McGinnis, who aided in the compilation of data used in this research.

#### References

- Baldwin, J. L., A crustal seismic refraction study in Southwestern Indiana and Southern Illinois, M.S. thesis, Purdue Univ., West Lafayette, IN, 1980.
- Bamford, D., Refraction data in western Germany - A time-term interpretation, J. Geophys., **39**, 907-927, 1973.
- Bamford, D., M. Jentsch, and C. Prodehl,  $P_n$  anisotropy in northern Britain and the eastern and western United States, Geophys. J. R. Astron. Soc., **57**, 397-429, 1979.
- Barr, K. G., Crustal refraction experiment: Yellowstone 1966, J. Geophys. Res., **76**, 1929-1948, 1971.
- Barrett, D. L., M. Berry, J. E. Blanchard, M. J. Keen, and R. E. McAllister, Seismic studies on the eastern seaboard of Canada: The Atlantic coast of Nova Scotia, Can. J. Earth Sci., **1**, 10-22, 1964.
- Bates, A., and D. H. Hall, Upper mantle structure in southern Saskatchewan and western Manitoba from project Edzo, Can. J. Earth Sci., **12**, 2134-2144, 1975.
- Bennett, G. T., R. M. Clowes, and R. M. Ellis, A seismic refraction survey along the southern Rocky Mountain trench, Canada, Bull. Seismol. Soc. Am., **65**, 37-54, 1975.
- Berg, J. W., Jr., K. L. Cook, H. D. Narans, Jr., and W. M. Dolan, Seismic investigation of crustal structure in the eastern part of the Basin and Range Province, Bull. Seismol. Soc. Am., **50**, 511-535, 1960.
- Berg, J. W., Jr., L. Trembly, D. A. Emilia, J. R. Hutt, J. M. King, L. T. Long, W. R. McKnight, S. K. Sarmah, R. Souders, J. V. Thiruvathukal, and D. A. Vossler, Crustal refraction profile, Oregon coast range, Bull. Seismol. Soc. Am., **56**, 1357-1362, 1966.
- Berry, M. J., and D. A. Forsyth, Structure of the Canadian Cordillera from seismic refraction and other data, Can. J. Earth Sci., **12**, 182-208, 1975.
- Berry, M. J., and K. Fuchs, Crustal structure of the Superior and Grenville provinces of the northeastern Canadian shield, Bull. Seismol. Soc. Am., **63**, 1393-1432, 1973.
- Berry, M. J., and G. F. West, A time-term interpretation of the first-arrival data of the 1963 Lake Superior experiment, in The Earth Beneath the Continents, Geophys. Monogr. Ser., Vol. 10, edited by J. S. Steinhardt and T. J. Smith, pp. 166-180, AGU, Washington, D.C., 1966.
- Blackwell, D., The thermal structure of the continental crust, in The Structure and Physical Properties of the Earth's Crust, Geophys. Monogr. Ser., Vol. 14, edited by J. G. Heacock, AGU, Washington, D.C., 1971.
- Braille, L. W., R. B. Smith, G. R. Keller, R. M. Welch, and R. P. Meyer, Crustal structure across the Wasatch front from detailed seismic refraction studies, J. Geophys. Res., **79**, 2669-2766, 1974.
- Braille, L. W., R. B. Smith, J. Ansorge, M. R. Baker, M. Sparlin, C. Prodehl, M. M. Schilly, J. H. Healy, St. Mueller, and K. H. Olsen, The Yellowstone-Snake River plain seismic profiling experiment: Crustal structure of the eastern Snake River plain, J. Geophys. Res., **87**, 2597-2609, 1982.
- Carder, D. S., Trans-California seismic profile, Death Valley to Monterey Bay, Bull. Seismol. Soc. Am., **63**, 571-586, 1973.
- Carder, D. S., A. Qamar, and T. V. McEvilly, Trans-California seismic profile Pahute Mesa to San Francisco Bay, Bull. Seismol. Soc. Am., **60**, 1829-1846, 1970.
- Chandra, N. N., and G. L. Cumming, Seismic refraction studies in Western Canada, Can. J. Earth Sci., **9**, 1099-1109, 1972.
- Chapman, D. S., and H. N. Pollack, Global heat flow: A new look, Earth Planet. Sci. Lett., **28**, 23-32, 1975.
- Christensen, N. I., Compressional wave velocity in rocks at high temperatures and pressures: Critical thermal gradients, and crustal low-velocity zones, J. Geophys. Res., **84**, 6849-6857, 1979.
- Christensen, N. I., Compressional wave velocity in possible mantle rocks to pressures of 30 kilobars, J. Geophys. Res., **79**, 407-412, 1974.
- Chung, D. J.,  $P_n$  velocity and partial melting - Discussion, Tectonophysics, **42**, T35-T42, 1977.
- Clee, T. E., K. G. Barr, and M. J. Berry, Fine structure of the crust near Yellowstone, Can. J. Earth Sci., **11**, 1534-1549, 1974.
- Cohen, T. J., and R. P. Meyer, The midcontinent gravity high: Gross crustal structure, in The Earth Beneath the Continents, Geophys. Monogr. Ser., Vol. 10, edited by J. S. Steinhardt and T. J. Smith, pp. 141-165, AGU, Washington, D.C., 1966.
- Costain, J. K., L. Glover III, and A. K. Sinha, Low-temperature geothermal resources in the eastern United States, Eos Trans. AGU, **61**, 1, 1980.
- Cram, I. H., Jr., Crustal structure refraction survey in South Texas, Geophysics, **26**, 560-573, 1961.
- Crough, S. T., and G. A. Thompson, Thermal model of a continental lithosphere, J. Geophys. Res., **81**, 4857-4862, 1976.
- Cull, J. P., and D. Denham, Regional variations in Australian heat flow, BMJ. J. Aust. Geol. Geophys., **4**, 1-13, 1979.
- Diment, W. H., S. W. Stewart, and J. C. Roller, Crustal structure from the Nevada test site to Kingman, Arizona, from seismic and gravity observations, J. Geophys. Res., **66**, 201-213, 1961.

- Dorman, J., J. L. Worzel, R. Leyden, T. M. Cook, and M. Hatzemanuel, Crustal section from seismic refraction measurements near Victoria, Texas, Geophysics, **37**, 225-336, 1972.
- Douglas, R. J. W., and R. A. Price, Nature and significance of variations in tectonic styles in Canada, in Variations in Tectonic Styles in Canada, Geol. Soc. Canada Spec. Pap. **11**, edited by R. A. Price and R. J. W. Douglas, pp. 625-688, 1972.
- Eaton, J. P., Crustal structure from San Francisco, California, to Eureka, Nevada, from seismic-refraction measurements, J. Geophys. Res., **68**, 5789-5806, 1963.
- Eaton, J. P., Crustal structure in northern and central California from seismic evidence in geology of northern California, Calif. Div. Mines Geol. Bull., **190**, 419-426, 1966.
- Ewing, M., J. L. Worzel, D. B. Ericson, and B. C. Heezen, Geophysical and geological investigations in the Gulf of Mexico, Part I, Geophysics, **20**, 1-18, 1955.
- Ewing, G. N., A. M. Dainty, J. E. Blanchard, and M. J. Keen, Seismic studies on the eastern seaboard of Canada: The Appalachian system I, Can. J. Earth Sci., **3**, 89-109, 1966.
- Fagerne, V., and R. Kanestrom, Variations in the upper mantle structure as derived from  $P_n$  and  $S_n$  waves, Pure Appl. Geophys., **109**, 1762-1772, 1973.
- Fenneman, N. M., Physical divisions of the United States, U.S. Geological Survey Map, scale 1:7,000,000, 1946.
- Fielitz, K., Compressional and shear wave velocities as a function of temperature in rocks at high pressure, in Explosion Seismology in Western Europe, edited by P. Giese, C. Prodehl, and A. Stein, pp. 40-44, Springer-Verlag, New York, 1976.
- Forsyth, D. A., M. J. Berry, and R. M. Ellis, A refraction survey across the Canadian Cordillera at 54°N, Can. J. Earth Sci., **11**, 533-548, 1974.
- Gibbs, J. P., and J. C. Roller, Crustal structure determined by seismic-refraction measurements between the Nevada test site and Ludlow, California, U.S. Geol. Survey Prof. Pap., **550-D**, D125-D131, 1966.
- Gish, D. M., G. R. Keller, and M. L. Sbar, A refraction study of deep crustal structure in the basin and range: Colorado plateau of eastern Arizona, J. Geophys. Res., **86**, 6029-6038, 1981.
- Green, A. G., O. G. Stephenson, G. D. Mann, E. R. Kanasewich, G. L. Cumming, Z. Hajnal, J. A. Mair, and G. F. West, Cooperative seismic surveys across the Superior-Churchill boundary zone in southern Canada, Can. J. Earth Sci., **17**, 617-632, 1980.
- Hales, A. L., and J. B. Nation, A seismic refraction survey in the northern Rocky Mountains: More evidence for an intermediate crustal layer, Geophys. J. R. Astron. Soc., **35**, 381-399, 1973.
- Hales, A. L., C. E. Helsley, J. J. Dowling, and J. B. Nation, The east coast onshore-offshore experiment, 1, The first arrival phases, Bull. Seismol. Soc. Am., **58**, 757-819, 1968.
- Hales, A. L., C. E. Helsley, and J. B. Nation, Crustal structure study on Gulf Coast of Texas, Am. Assoc. Petrol. Geol. Bull., **54**, 2040-2057, 1970.
- Hall, D. H., and Z. Hajnal, Crustal structure of northwestern Ontario: Refraction seismology, Can. J. Earth Sci., **6**, 81-99, 1969.
- Hall, D. H., and Z. Hajnal, Deep seismic crustal studies in Manitoba, Bull. Seismol. Soc. Am., **63**, 883-910, 1973.
- Hamilton, R. M., A. Ryall, and E. Berg, Crustal structure southwest of the San Andreas fault from quarry blasts, Bull. Seismol. Soc. Am., **54**, 67-77, 1964.
- Healy, J. H., Crustal structure along the coast of California from seismic-refraction measurements, J. Geophys. Res., **68**, 5777-5787, 1963.
- Heney, T. L., and T. C. Lee, Heat flow in Lake Tahoe, California-Nevada, and the Sierra Nevada-basin and range transition, Geol. Soc. Am. Bull., **87**, 1179-1187, 1976.
- Herrin, E., Regional variations of P-wave velocity in the upper mantle beneath North America, in The Earth's Crust and Upper Mantle, Geophys. Monogr. Ser., Vol. 13, edited by P. J. Hart, AGU, Washington, D.C., 1969.
- Hersey, J. B., E. T. Bunce, R. F. Wyrick, and F. T. Dietz, Geophysical investigation of the continental margin between Cape Henry, Virginia and Jacksonville, Florida, Geol. Soc. Am. Bull., **70**, 437-465, 1959.
- Hill, D. P., and L. C. Pakiser, Crustal structure between the Nevada test site and Boise, Idaho, from seismic-refraction measurements, in The Earth Beneath the Continents, Geophys. Monogr. Ser., Vol. 10, edited by J. S. Steinhardt and T. J. Smith, pp. 391-419, AGU, Washington, D.C., 1966.
- Hill, D. P., Crustal and upper mantle structure of the Columbia plateau from long range seismic-refraction measurements, Geol. Soc. Am. Bull., **83**, 1639-1648, 1972.
- Hobson, G. D., A. Overton, D. N. Clay, and W. Thatcher, Crustal structure under Hudson Bay, Can. J. Earth Sci., **4**, 929-947, 1967.
- Hodgson, J. H., A seismic survey in the Canadian Shield, 1, Refraction studies based on rockbursts at Kirkland Lake, Ontario, Publ. Dom. Obs. Ottawa, **16**, 111-163, 1953.
- Horai, K., and G. Simmons, Seismic travel time anomaly due to anomalous heat flow and density, J. Geophys. Res., **73**, 7577-7588, 1968.
- Jackson, W. H., S. W. Stewart, and L. C. Pakiser, Crustal structure in eastern Colorado from seismic-refraction measurements, J. Geophys. Res., **68**, 5767-5776, 1963.
- Jackson, W. H., and L. C. Pakiser, Seismic study of crustal structure in the Southern Rocky Mountains, U.S. Geol. Survey Prof. Pap., **525-D**, D85-D92, 1965.
- James, D. W., T. J. Smith, and J. S. Steinhardt, Crustal structure of the middle Atlantic states, J. Geophys. Res., **73**, 1983-2007, 1968.
- Johnson, L. R., Crustal structure between Lake Mead, Nevada, and Mono Lake, California, J. Geophys. Res., **70**, 2863-2872, 1965.
- Johnson, S. H., and R. W. Couch, Crustal structure in the North Cascade Mountains of Washington and British Columbia from seismic refraction measurements, Bull. Seismol. Soc. Am., **60**, 1259-1269, 1970.
- Johnson, S. H., R. W. Couch, M. Gempferle, and E. R. Banks, Seismic refraction measurements in southeast Alaska and western British Columbia, Can. J. Earth Sci., **9**, 1756-1765, 1972.

- Katz, S., Seismic study of crustal structure in Pennsylvania and New York, Bull. Seismol. Soc. Am., 44, 303-325, 1954.
- Keller, G. R., R. B. Smith, and L. W. Braille, Crustal structure along the Great Basin-Colorado Plateau transition from seismic refraction studies, J. Geophys. Res., 80, 1093-1097, 1975.
- Kermack, K. A., and J. B. S. Haldane, Organic correlation and allometry, Biometrika, 37, 30-41, 1950.
- Kern, H., and A. Richter, Temperature derivatives of compressional and shear wave velocities in crustal and mantle rocks at 6 kbar confining pressure, J. Geophys. Res., 49, 47-56, 1981.
- Kono, Y., and M. Amano, Thickening model of the continental lithosphere, Geophys. J. R. Astron. Soc., 54, 405-416, 1978.
- Langston, C. A., and D. V. Helmberger, Interpretation of body and Rayleigh waves from NTS to Tucson, Bull. Seismol. Soc. Am., 64, 1919-1929, 1974.
- Lachenbruch, A. H., and J. H. Sass, Heat flow in the United States and the thermal regime of the crust, in The Earth's Crust, Geophys. Monogr. Ser., Vol. 20, edited by J. G. Heacock, AGU, Washington, D.C., 1977.
- Lyons, J. A., D. A. Forsyth, and J. A. Mair, Crustal studies in the La Malbaie Region Quebec, Can. J. Earth Sci., 17, 478-490, 1980.
- Manghnani, N. H., R. Ramanantoandro, and S. P. Clark, Compressional and shear wave velocities in granulite facies rocks and eclogites to 10 kbar, J. Geophys. Res., 79, 5427-5446, 1974.
- Martin, W. R., A seismic refraction study of the northeastern basin and range and its transition with the eastern Snake River plain, M.S. Thesis, Univ. of Texas, El Paso, 1978.
- McCamy, K., and R. P. Meyer, A correlation method of apparent velocity measurement, J. Geophys. Res., 69, 691-699, 1964.
- McCamy, K. and R. P. Meyer, Crustal results of fixed multiple shots in the Mississippi embayment, in The Earth Beneath the Continents, Geophys. Monogr. Ser., Vol. 10, edited by J. S. Steinhardt and T. J. Smith, pp. 166-180, AGU, Washington, D.C., 1966.
- Mereu, R. F., and J. A. Hunter, Crustal and upper mantle structure under the Canadian shield from project early rise data, Bull. Seismol. Soc. Am., 59, 147-165, 1969.
- Mereu, R. F., and G. Jobidon, A seismic investigation of the crust and mocho on a line perpendicular to the Grenville Front, Can. J. Earth Sci., 8, 1553-1583, 1971.
- Mereu, R. F., S. C. Majumdar, and R. E. White, The structure of the crust and upper mantle under the highest ranges of the Canadian Rockies from a seismic refraction survey, Can. J. Earth Sci., 14, 196-208, 1976.
- Merkel, R. H., and S. S. Alexander, Use of correlation analysis to interpret continental margin ECOOE refraction data, J. Geophys. Res., 74, 2683-2697, 1969.
- Mitchell, B. J., and M. Landisman, Geophysical measurements in the southern great plains, in The Structure and Physical Properties of the Earth's Crust, Geophys. Monogr. Ser., Vol. 14, edited by J. G. Heacock, pp. 77-93, AGU, Washington, D.C., 1971.
- Mueller, S., and M. Landisman, An example of the unified method of interpretation for crustal seismic data, Geophys. J. R. Astron. Soc., 23, 365-371, 1971.
- Olsen, K. H., G. R. Keller, and J. N. Stewart, Crustal structure along the Rio Grande rift from seismic refraction profiles, in Rio Grande Rift: Tectonics and Magmatism, edited by R. E. Riecker, pp. 127-143, AGU, Washington, D.C., 1979.
- Pakiser, L. C., Structure of the crust and upper mantle in the western United States, J. Geophys. Res., 68, 5747-5756, 1963.
- Pakiser, L. C., and J. S. Steinhardt, Explosion seismology in the western hemisphere, in Research in Geophysics, 2, Solid Earth and Interface Phenomena, edited by J. Odishaw, pp. 123-142, MIT Press, Cambridge, Mass., 1964.
- Peselnick, L., J. P. Lockwood, and R. M. Stewart, Anisotropic elastic velocities of some upper mantle xenoliths underlying the Sierra Nevada batholith, J. Geophys. Res., 82, 2005-2010, 1977.
- Peselnick, L., and A. Nicolas, Seismic anisotropy in an ophiolite peridotite: Application to oceanic upper mantle, J. Geophys. Res., 83, 1227-1235, 1978.
- Pollack, H. N., and D. S. Chapman, On the regional variation of heat flow, geotherms, and lithospheric thickness, Tectonophysics, 38, 279-296, 1977.
- Polyak, B. G., and Ya. B. Smirnov, Relationship between terrestrial heat flow and the tectonics of continents, Geotectonics, 4, 205-213, 1968.
- Press, F., Crustal structure in the California-Nevada Region, J. Geophys. Res., 65, 1039-1051, 1960.
- Prodehl, C., Crustal structure of the western United States, U.S. Geol. Surv. Prof. Pap., 1034, 1979.
- Prodehl, C., and L. C. Pakiser, Crustal structure of the southern Rocky Mountains from seismic measurements, Geol. Soc. Am. Bull., 91, 147-155, 1980.
- Ramanantoandro, R., and M. H. Manghnani, Temperature dependence of the compressional wave velocity in an anisotropic dunite: Measurements to 500°C at 10 kbar, Tectonophysics, 47, 73-84, 1978.
- Richards, T. C., and D. J. Walker, Measurement of the thickness of the earth's crust in the Albertan plains of western Canada, Geophysics, 24, 262-284, 1959.
- Roller, J. C., Crustal structure in the vicinity of Las Vegas, Nevada, from seismic and gravity observations, U.S. Geol. Surv. Prof. Pap., 475-D, D108-D111, 1964.
- Roller, J. C., Crustal structure in the eastern Colorado plateaus province from seismic-refraction measurements, Bull. Seismol. Soc. Am., 55, 107-119, 1965.
- Roller, J. C., and J. H. Healy, Seismic-refraction measurements of crustal structure between Santa Monica Bay and Lake Mead, J. Geophys. Res., 68, 5837-5849, 1963.

- Roller, J. C., and W. H. Jackson, Seismic-wave propagation in the upper mantle: Lake Superior Wisconsin, to Denver, Colorado, in The Earth Beneath the Continents, Geophys. Monogr. Ser., Vol. 10, edited by J. S. Steinhardt and T. J. Smith, pp. 270-275, AGU, Washington, D.C., 1966.
- Romney, C., B. G. Brooks, R. H. Mansfield, D. S. Carder, J. M. Jordan, and D. W. Gordon, Travel times and amplitudes of principal body phases recorded from Gnome, Bull. Seismol. Soc. Am., 52, 1057-1074, 1962.
- Ryall, A., and D. J. Stuart, Travel times and amplitudes from nuclear explosions, Nevada test site to Ordway, Colorado, J. Geophys. Res., 68, 5821-5835, 1963.
- Rybach, L., and G. Buntebarth, Relationship between the petrophysical properties density, seismic velocity, heat generation and mineralogical constitution, Earth Planet. Sci. Lett., 57, 367-376, 1982.
- Sass, J. H., W. H. Diment, A. H. Lachenbruch, B. V. Marshall, R. J. Munroe, T. H. Moses, Jr., and T. C. Urban, A new heat-flow contour map of the conterminous United States, U.S. Geol. Surv. Open File Rep., 76-756, 1976.
- Shor, G. G., Jr., Seismic refraction studies off the coast of Alaska: 1956-1957, Bull. Seismol. Soc. Am., 52, 37-57, 1962.
- Shor, G. G., Jr., P. Dehlinger, H. D. Kirk, and W. S. French, Seismic refraction studies off Oregon and Northern California, J. Geophys. Res., 73, 2175-2194, 1968.
- Sinno, Y. A., G. R. Keller, and M. L. Sbar, A crustal seismic refraction study in west-central Arizona, J. Geophys. Res., 86, 5023-5038, 1981.
- Slichter, L. B., Crustal structure in the Wisconsin area, Rep. M9, ONR 86200, Office of Naval Research, Arlington, Virginia, 1951.
- Smith, R. B., M. M. Schilly, L. W. Braille, J. Anson, J. L. Lehman, M. R. Baker, C. Proehl, J. H. Healy, St. Mueller, and R. W. Greensfelder, The 1978 Yellowstone-Eastern Snake River plain seismic profiling experiment: Crustal structure of the Yellowstone region and experiment design, J. Geophys. Res., 87, 2583-2596, 1982.
- Sparlin, M. A., L. W. Braille, and R. B. Smith, Crustal structure of the Eastern Snake River plain determined from ray-trace modeling of seismic refraction data, J. Geophys. Res., 87, 2619-2633, 1982.
- Stauber, D. A., and D. M. Boore, Crustal thickness in northern Nevada from seismic refraction studies, Bull. Seismol. Soc. Am., 68, 1049-1058, 1978.
- Steinhart, J. S., and R. P. Meyer, Explosion studies of continental structure, Carnegie Inst. Washington Publ., 622, 1961.
- Steinhart, J. S., Z. Suzuki, T. J. Smith, L. T. Aldrich, and I. S. Sacks, Explosion seismology, Year Book Carnegie Inst. Washington, 63, 311-319, 1964.
- Stewart, S. W., Crustal structure in Missouri by seismic-refraction methods, Bull. Seismol. Soc. Am., 58, 291-323, 1968a.
- Stewart, S. W., Preliminary comparison of seismic travel times and inferred crustal structure adjacent to the San Andreas Fault in the Diablo and Gabilan Ranges of Central California, in Geologic Problems of San Andreas Fault System Conference Proceedings, edited by W. R. Dickinson, pp. 218-230, Publ. Geol. Sci., 11, Stanford Univ., Stanford, Calif., 1968b.
- Topozada, T. R., and A. R. Sanford, Crustal structure in central New Mexico interpreted from the Gasbuggy explosion, Bull. Seismol. Soc. Am., 66, 877-886, 1976.
- Tuve, M. A., The earth's crust, Year Book Carnegie Inst. Washington, 50, 69-73, 1951.
- Tuve, M. A., The earth's crust, Year Book Carnegie Inst. Washington, 52, 103-108, 1953.
- Tuve, M. A., The earth's crust, Year Book Carnegie Inst. Washington, 53, 51-55, 1954.
- Verhoogen, J., F. Turner, L. Weiss, C. Wahrhaftig, and W. Pyfe, The Earth, 748 pp., Holt, Rinehart, and Winston, New York, 1970.
- Warren, D. H., Transcontinental geophysical survey (35°-39°N) seismic refraction profiles of the crust and upper mantle, U.S. Geol. Surv. Maps I-532-D, I-533-D, I-534-D, and I-535-D, 1968.
- Warren, D. H., and J. H. Healy, Structure of the crust in the conterminous United States, Tectonophysics, 20, 203-213, 1973.
- Warren, D. H., Seismic-refraction survey of crustal structure in central Arizona, Geol. Soc. Am., 80, 257-282, 1969.
- Warren, D. H., and W. H. Jackson, Surface seismic measurements of the project Gasbuggy explosion at intermediate distance ranges, U.S. Geol. Surv. Open File Rep., 1023, 1968.
- Warren, D. H., J. H. Healy, and W. H. Jackson, Crustal seismic measurements in southern Mississippi, J. Geophys. Res., 71, 3437-3458, 1966.
- Warren, D. H., J. H. Healy, J. Bohn, and P. A. Marshall, Crustal calibration of the large aperture seismic array (LASA), Montana, U.S. Geol. Surv. Open File Rep., 1671, 1972.
- White, W. R. H., and J. C. Savage, Seismic refraction and gravity study of the earth's crust in British Columbia, Bull. Seismol. Soc. Am., 55, 463-486, 1965.
- Willden, R., Seismic-refraction measurements of crustal structure between American Falls Reservoir, Idaho, and Flaming Gorge Reservoir, Utah, U.S. Geol. Surv. Prof. Pap., 525-C, C44-C50, 1965.
- York, D., Least-squares fitting of a straight line, Can. J. Phys., 44, 1079-1086, 1966.
- York, D., The best isochron, Earth Planet. Sci. Lett., 2, 49-482, 1967.

(Received December 8, 1981;  
revised July 16, 1982;  
accepted July 21, 1982.)

SEISMOGRAMS OF EXPLOSIONS AT REGIONAL DISTANCES IN THE WESTERN  
UNITED STATES: OBSERVATIONS AND REFLECTIVITY METHOD MODELING

K. H. Olsen<sup>1</sup> and L. W. Braille<sup>2</sup>

<sup>1</sup> Geosciences Division, Los Alamos National  
Laboratory, Los Alamos, New Mexico 87545, U.S.A.

<sup>2</sup> Geoscience Department, Purdue University,  
West Lafayette, Indiana 47907, U.S.A.

**ABSTRACT.** Seismic energy propagating through vertically and laterally varying structures of the earth's crust and lower lithosphere-uppermost mantle is responsible for the numerous and complex seismic phases observed on short-period seismograms at regional distance ranges (100 to 2000 km). Recent advances in techniques for computing synthetic seismograms make it practical to calculate complete seismograms that realistically model many features of regional phases. A modified reflectivity method program is used to interpret some details of record sections of Nevada Test Site (NTS) underground explosions that were observed 700 to 800 km from the sources.

I. INTRODUCTION

Regional seismic phases recorded by high-gain, short-period or broadband instruments are likely to play an increasingly important role in seismic source location and identification as acceptable magnitude thresholds are pushed to lower levels. From the standpoint of complexity of seismograms, the epicentral distance range between ~200 km and the transition to simpler teleseismic waveforms around 2000 km presents many challenges to the seismic analyst. In this range, propagation paths can traverse the crust, the lower lithosphere, and the uppermost mantle where both vertical and lateral heterogeneities strongly influence waveform characteristics. Good observational data are rare for testing analysis techniques developed for regional problems. In contrast to the numerous detailed crustal refraction/reflection profiles that have been obtained from many parts of the world out to distances ~200 km, relatively few long-range

453

*E. S. Husebye and S. Mykkeltveit (eds.), Identification of Seismic Sources - Earthquake or Underground Explosion, 453-466.  
Copyright © 1981 by D. Reidel Publishing Company.*

profiles exist where station spacing is sufficiently tight to facilitate a clear interpretation of the onset, development, and amplitude vs. distance behavior of the many observable phases. Thus, although signals from sources of interest may be easily observable at regional distances, derivation of source parameters from observations at sparsely located observatories or arrays will require careful analysis and modeling of the intricacies of wave propagation at these scales.

Phases of interest in regional identification studies fall into two main categories: large amplitude, long duration, but somewhat indistinct wave groups such as Lg and  $\bar{P}$ ; and body waves (mainly compressional) that appear either as first arrivals or closely following as possible wide angle reflections/near-critical refractions from interfaces and/or steep velocity gradients in the deep crust, lower lithosphere, and uppermost mantle. The Lg and  $\bar{P}$  phases are often the largest amplitude features on regional short-period seismograms, but a clear explanation of how Lg and  $\bar{P}$  propagate is still lacking [1]; this lack perhaps is reflected in the fact that seismologists frequently use the notations  $\bar{P}$  or  $P_g$  interchangeably in reference to a broad, large amplitude phase following  $P_n$ . We adopt the  $\bar{P}$  notation here. The phase in question propagates very well in the western United States, but attenuates rapidly in the eastern U.S. A group velocity around 6 km/s implies  $\bar{P}$  propagates as compressional waves multiply reflected within the crust—which may thus act as a waveguide. Similarly, the ~3.5 km/s group velocity for Lg suggests shear waves multiply reflecting within the crustal layers. Some authors [2] prefer to treat Lg as a superposition of higher mode Love and Rayleigh waves propagating in a nearly laterally homogeneous, vertically layered crust. In any case, the propagation physics is complicated and will require quite sophisticated synthetic seismogram codes to properly model and interpret observed waveforms.

Record sections of long-range seismic refraction profiles often show one or more nearly parallel travel time (T) vs. distance ( $\Delta$ ) branches following within several seconds of first arrivals [3, 4, 5]. Each secondary branch may be traceable only over a distance interval of 50 to 200 km before being replaced in a "shingle-like" fashion with another branch or set of arrivals [5, 6, 19]. These are usually interpreted as parts of cusp phases arising from critical refractions and/or wide-angle reflections from first order discontinuities or steep velocity gradients in the upper mantle. Archambeau et al. [7] and Burdick and Helmberger [8], for example, have derived velocity vs. depth models for the major features of the upper mantle beneath the U.S. by a joint analysis of travel times, amplitude vs. distance variations, and waveform fitting of the first few compressional arrivals observed at widely separated seismograph

stations throughout the U.S. These and similar models by others are most valid for depths greater than about 250 km. Although these analyses suggest that the main features of mantle structure at depths below about 300 km (corresponding to compressional first arrivals at epicentral ranges beyond ~1500 km) may be more uniform over a global scale [8], it is known that significant lateral variations in lower lithosphere and uppermost mantle properties occur beneath the continents on regional and perhaps even finer scales [8, 9, 10, 11]. In the depth range between the Moho and ~300 km, several types of structural variations have been suggested in the literature that would give rise to wide angle reflections, converted phases, and similar closely spaced arrivals on seismograms at regional ranges. These include the presence or absence of the S-wave and/or the P-wave low velocity zone (LVZ) in the asthenosphere, high velocity mantle lids [12, 13], alternating lamellae of positive and negative velocity gradients [6, 19], etc. These early arriving phases often have better defined onsets than the  $\bar{P}$  and  $L_g$  phases and, since they are observed at distances beyond that where a true head wave  $P_n$  arrival can be expected, they may be useful in regional source location and identification. In order to make use of the information contained in these arrivals (especially the amplitude vs. distance behavior for particular paths of interest), it will be necessary to use modern sophisticated synthetic seismogram techniques to derive localized fine scale details from generalized crust-mantle models.

The purpose of this paper is to explore a few of the problems in modeling regional short-period seismograms by means of a modified reflectivity method [14] computer program developed by R. Kind [15]. This numerical program accounts for the effects of a buried source and is thus capable of computing 'complete' seismograms—including refracted waves, surface reflected body waves such as the  $pP$  phase, and surface waves. The effects of anelastic attenuation ( $Q$ ) for each layer are included as an integral part of the method [15]. The most severe limitation of the technique for studies of regional seismograms is the assumption of lateral homogeneity (this is also a limitation for normal modes summation techniques). An item of interest will be the extent synthetics can be made to match observed waveforms under this restriction.

Two problems are considered. The first, labeled the B-3 model for brevity, employs a simple model consisting of three layers in the crust without velocity gradients and an almost uniform velocity mantle. A large range of apparent surface phase velocities is used in order to display S phases and surface waves. The second calculation, the A-10 model, treats the mantle structure in detail, but confines attention to compressional phases near their start of the seismogram. The more

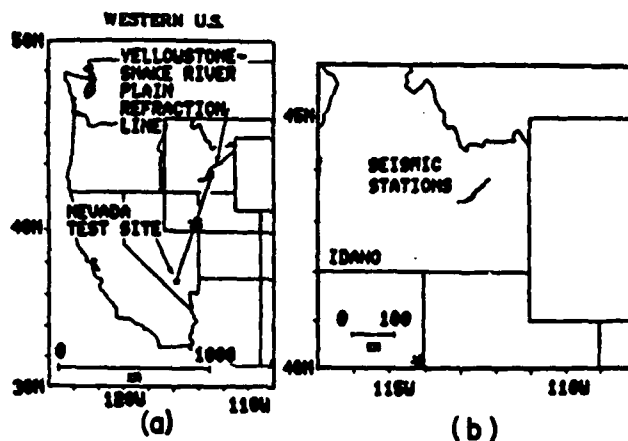


Fig. 1. (a) Location map of the western United States with relative positions of the Nevada Test Site and the Y-ESRP recording line. (b) Enlargement showing positions of stations that recorded the 27 September 1978 RUMMY explosion. Asterisk denotes approximate area for mantle ray turning points from NTS explosions.

important conclusions of the A-10 model are summarized here—a fuller discussion of this calculation and the implications for uppermost mantle structure beneath the western U.S. can be found in a previous publication [16]:

A comparison of the synthetic seismogram calculations has been made with a 100-km-long record section of short-period vertical component seismograms obtained in eastern Idaho during the 1978 Yellowstone-Eastern Snake River Plains (Y-ESRP) seismic profiling experiment. For these observations, the sources were underground nuclear explosions at the Nevada Test Site (NTS) at distances between 720 and 820 km from the nearly radially oriented linear station array (Fig. 1). Only the records from the largest NTS explosion, the  $m_b = 5.7$  RUMMY event at 1720:00.076 GMT, 27 September 1978, are reproduced here since they have the best signal-to-noise ratio of the three NTS explosions observed during the experiment. Additional details of the Y-ESRP instrumentation, experiment, and data can be found elsewhere [16].

## 2. COMPUTATIONAL TECHNIQUE

As discussed by Kind [15] and by Fuchs and Müller [14], the reflection coefficient and time shift calculations in the reflectivity method are carried out in the frequency domain and then Fourier transformed to plot seismograms. We included Müller's [17] earth flattening approximation in both of our problems to account for earth curvature effects. Both P and S velocities are independently specified in all calculations, since the reflection coefficients are functions of both P and S velocity contrasts at non-normal incidence angles and are required even when only computing P phases over a narrow time window. In the A-10 calculation, for example, the departure of the P/S velocity ratio in a layer from that given by Poisson's ratio = 1/4 is an important factor in our interpretation [16]. Densities are given by a Birch's Law relation (density =  $0.252 + 0.3788 * P$  velocity). The attenuation factor  $Q_\alpha$  for P waves was chosen as 25 in the source layers, 200 in the upper crust, and 1000 in the lower crust and the uppermost mantle layers; for the LVZ modeling of the A-10 model,  $Q_\alpha$  in the asthenospheric layers was adjusted as part of the fitting procedure (see Fig. 5). The attenuation factor for S waves was always assumed to be  $4Q_\alpha/9$  [20]. The explosive source algorithm [16] was used with the source buried at a depth of 0.640 km in a layer of P velocity = 3.55 km/s. These were close to actual field values for the NTS RUMMY explosion. Time intervals, number of samples, and computed lengths of seismograms were chosen so that the dominant frequency of the source spectrum was 1.6 Hz for the A-10 calculation—again close to the observed value. In order to save computer time for the extended duration B-3 seismogram sections, the parameters were chosen so that the dominant frequency of the source was shifted to 0.25 Hz; although this was low compared to observed frequencies, we felt it was adequate for the purposes of this initial study. To avoid long computer runs, the wave field was only computed within a limited phase velocity window: 1 km/s to 20 km/s for B-3, and 6.5 km/s to 1000 km/s for A-10. These integration limits sometimes introduced spurious single cycle "phases" at these apparent velocities in the computed record sections. The limit velocities were chosen so as to not overlap or interfere with arrivals of interest in the observations. In the record section plots, the amplitudes of each trace have been multiplied by station distance to maintain a convenient scaling of the amplitudes of the phases which are subject to geometrical spreading and attenuation due to anelasticity.

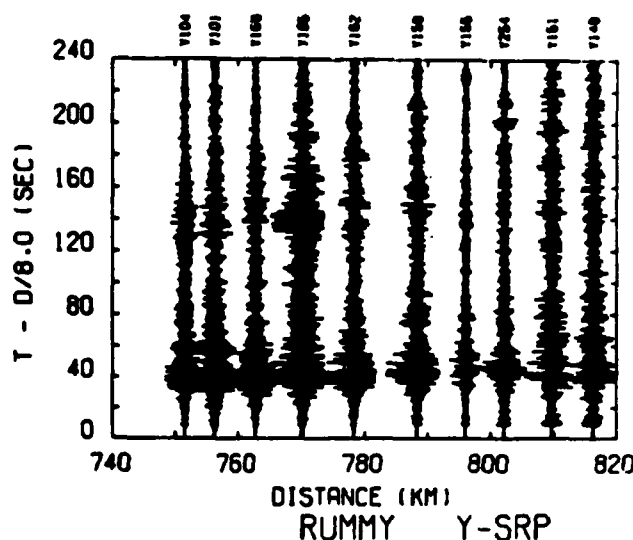


Fig. 2. Vertical component low time resolution seismic record section of the RUMMY explosion as recorded at Snake River Plains stations. The time scale is compressed to show envelope behavior; individual waveforms not readily seen. The  $\bar{P}$  phase is the broad feature at reduced times between 30 and 60 s. Upward ground motion to the left.

### 3. DISCUSSION

#### 3.1 The Extended Time Seismograms: B-3 Model

Figure 2 is a true relative amplitude vertical component record section of the RUMMY explosion recorded on ten matched short-period (1<sup>1</sup>/2 Hz natural frequency) instruments deployed in the eastern Snake River Plains (Fig. 1). Although the time scale is too compressed to reveal many details of the waveforms, several important overall features can be noted. The broad (~40-second-long) envelope of the  $\bar{P}$  phase appears at reduced times between approximately 30 to 60+ seconds, and is the largest amplitude feature on the record. In contrast, the Lg phase expected at reduced times of ~130+ seconds (an average velocity of about 3.5 km/s) is poorly developed on these unfiltered records; it is only obvious at the 770-km station. A few impulsive arrivals can be seen (such as the first arrivals at reduced time ~10 seconds, which will be discussed in Sec. 3.2, and perhaps an Sn (?) phase at  $t_{red}$  ~80 seconds and ~780 km), but the

impression one gets by viewing this observed section is that the correlations seem to be better described as broad energy correlations rather than phase correlations. A similar conclusion is suggested by seismograms from central Asia shown in the paper of Ruzaikin et al. [1]. A coherent structure in the  $\bar{P}$  and  $L_g$  phases is difficult to trace from station to station even though the stations are only separated by 8 km on the average.

The results of an attempt to model late time arrivals over a regional distance range is shown in Fig. 3. A rudimentary, almost trivial, crust/mantle velocity structure was assumed that consisted of three constant velocity layers in the crust overlying a nearly constant velocity halfspace. (A slight negative gradient in  $P$  velocity was introduced just below the Moho in order to suppress the  $P_n$  amplitudes as required by the observations; see Sec. 3.2.) We note several points.

- (a) The seismogram section from 100 to 900 km and the enlarged individual record for 800 km shows a surprising amount of complexity at times beyond the first arrivals even though an extremely simple earth model and source function is used. Groups corresponding to the  $\bar{P}$  and  $L_g$  phases can be identified.
- (b) There appears to be a considerable amount of  $S$ -wave energy although none is present in the explosion source algorithm. This is probably due to  $P$ -to- $S$  and  $S$ -to- $P$ , etc., conversions at interfaces and to multiples which the program adequately includes.
- (c) The calculated dispersed fundamental mode Rayleigh wave is very large. There are at least two reasons this Rayleigh wave is not representative of the observations. First, no corrections for the short-period bandpass response of the seismometers were included in the synthetics. Second, the assumed source spectrum has too much energy at the longer periods as compared with a near point-source representative of a NTS explosion, thus over enhancing the Rayleigh waves. Long-period Rayleigh waves from actual underground explosions are probably generated or modified and enhanced by mechanisms such as spall closure and/or tectonic strain release; these mechanisms are not adequately treated by the explosion algorithm used for the present calculation.
- (d) Because the calculated seismogram sections are quite complicated even for this simple earth model, they give the impression that broad "packets of energy" can be more readily correlated than any well defined phases--for at least the  $\bar{P}$  and  $L_g$  phases. This was the case with the observations in Fig. 2. In order to better understand the gross behavior of these phases with distance and to identify the origin of obscure features, it will be necessary to include calculations of the horizontal

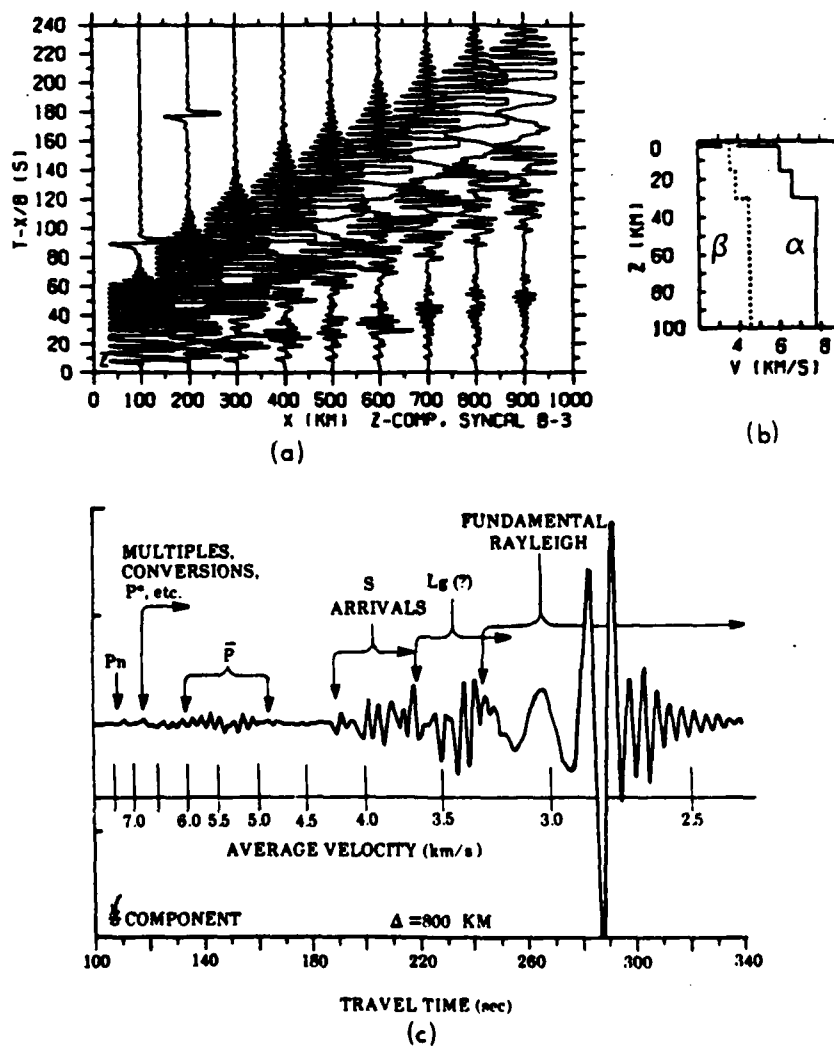


Fig. 3. (a) Synthetic seismogram vertical component record section calculated from the P and S velocity vs. depth structure (Model B-3) shown in (b). (c) Expanded plot of the synthetic seismogram at the 800-km distance. Approximate arrival time and average velocity windows for different phases or groups are indicated; the phase velocities of the different wave types are equal to or slightly greater than the average velocities. The Rayleigh waves on plot (a) are arbitrarily clipped in plotting to avoid large overlays in the seismograms.

(radial) component and to perform calculations at small station separation to increase recognizability of phase correlations.

These results suggest that the modified reflectivity method, even with the restrictive assumption of lateral homogeneity, can be a useful technique in understanding the intricacies of Lg and P phases and the types of earth structures that most affect them. In addition, these studies suggest that observations of complex and apparently-incoherent seismic phase arrivals--even over short distances--do not necessarily imply strong lateral heterogeneity in crustal structure. Parameter studies would help identify those aspects where refinements due to lateral heterogeneity and/or scattering need to be considered in order to better match observations.

### 3.2 Early Time Arrivals: A-10 Model

Figures 4a and 4b are enlarged portions of the first few seconds of the digitized RUMMY vertical component seismograms (see also Fig. 2) that show details of the earliest arrivals. We have interpreted [16] this record section in terms of three different compressional phases, all having apparent velocities close to 8 km/s: (a) an extremely weak leading arrival labeled P<sub>n</sub>, which was lost in the background noise for the two other, lower yield, NTS shots that were also recorded during the Y-ESRP experiments; (b) a stronger phase labeled P<sub>1id</sub> follows P<sub>n</sub> by about two or three seconds for epicentral distances between 700 and 780 km; (c) beyond 780 km, the P<sub>1id</sub> phase appears to be overtaken and overwhelmed by a low-frequency phase, P<sub>1</sub>, whose amplitude increases rapidly with distance out to at least the farthest station of the linear array. The detailed reasons for these labels and identifications are discussed in [16]; they can be summarized as follows.

The phase labeled P<sub>n</sub> could be a wide angle reflection from a weak P-velocity contrast in the lower lithosphere below the Moho rather than a true headwave (in the strict sense of the mathematical definition) that travels along the M-discontinuity interface over the entire 800-km path. However, the sub-Moho P velocity (7.7 to 7.9 km/s) in this region of the Great Basin is known to be close to both the average and the apparent velocity observed in Figs. 2 and 4. This, plus the fact that other travel time arguments [16] suggest there is no evidence for mantle lids or other thin but fairly high gradient zones down to a depth of about 100 km, argues that the most straightforward explanation for this arrival is that it is a P<sub>n</sub>-type phase. We calculate that the energy at 800 km is greatly reduced because the wave travels in a region beneath the Moho that has a slight negative velocity gradient.

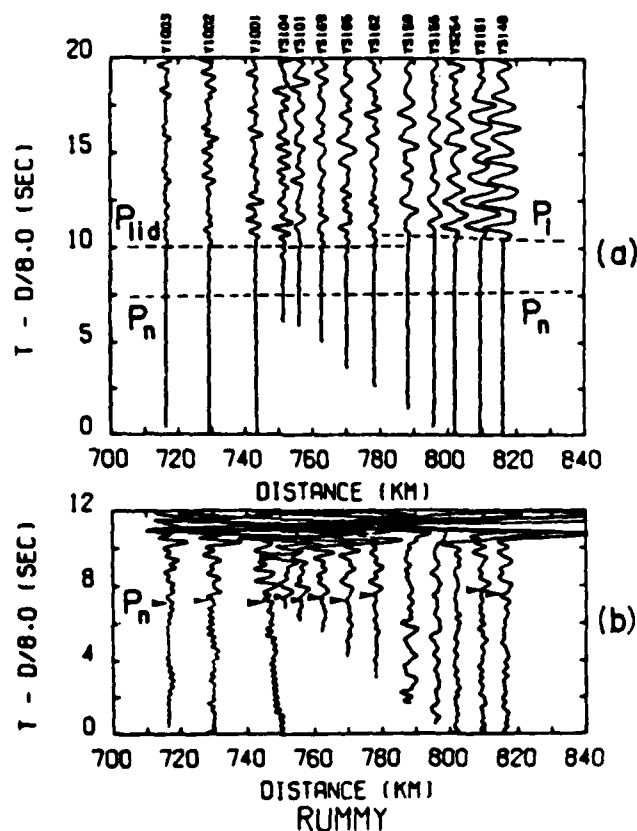


Fig. 4. (a) True relative amplitude record section of early compressional arrivals from the RUMMY explosion. (b) Same as (a) with increased amplitudes to show weak  $P_n$  phase. Upward motion to the left. All traces low pass filtered at 3 Hz.

The sudden onset at about 780 km and subsequent rapid amplitude growth of the  $P_1$  phase indicates it is the cusp of the critically refracted P-waves from the steep velocity gradient at the base of the asthenospheric low velocity zone. The observed dominant low frequency content is then explained by the attenuation of the high frequency components as the energy travels first downward and then back up through the very low-Q region of the LVZ. The notation of  $P_1$  for this phase follows the convention established by Archambeau et al. [7].

The travel times, moderate amplitudes, and relatively high frequency content imply the phase identified as  $P_{lid}$  is a wide angle reflection from a discontinuity near the base of the mantle lid (= top of LVZ) in this area.

The conclusions concerning these three early arriving compressional phases summarized above were confirmed by using the modified reflectivity program to quantitatively model the arrival times, amplitudes, and waveforms in the first 15 seconds of the record sections. The procedure was to begin with a generic P-velocity vs. depth model for the western U.S. (the T-7 model) derived from a wider data set by Burdick and Helmberger [8] and then to perturb the model to achieve a better fit [16]. Because of the influence of S-velocity contrasts on the P-wave reflectivity calculations, an S-velocity vs. depth model derived by Priestly and Brune [18] from an analysis of Rayleigh and Love wave dispersion on paths crossing the area of interest in the Great Basin of Eastern Nevada was incorporated into the synthetic seismogram modeling. The starting T-7 and Priestly-Brune (P/B) velocity models are shown by dotted lines in Fig. 5. The generic T-7 P-wave model has a pronounced mantle lid with a strong positive P-velocity gradient beneath the Moho for depths from 33 to 65 km. Calculation of synthetics for this lid structure gave very large amplitudes for the " $P_n$ " arrival, which was superimposed on a strong reflection from the base of the lid at 65 km [16]. Thus, the T-7 + P/B starting model gave results very different from observations. However, as seen in Fig. 5, only small changes to the initial model were necessary to match the observations. To bring the calculated synthetic seismograms into agreement with observations, the gradient at the base of the LVZ had to be raised to shallower depths and the positive gradient lid replaced with a smooth but gradual negative gradient starting at the M-discontinuity. The final model, A-10, that matches observations is shown by the solid lines in Fig. 5. Figure 6 is the comparison between the observed and synthetic record sections. Interestingly, no discontinuity in P-velocity is necessary to explain the  $P_{lid}$  reflections; the reflections can be adequately modeled by a small negative step in S velocities at a depth of about 100 km. The synthetics, however, do not seem to adequately model the long oscillatory trains following the  $P_1$  phase onset. This is probably due to interference effects caused by fine structure in the lower LVZ velocity gradient that we have not yet modeled by thin enough layers in the calculation [16].

These calculations illustrate that synthetic modeling techniques can be helpful in phase identification and in quantitative calculations of amplitude vs. distance behavior and waveform characteristics. With a sophisticated reflectivity method calculation we were able to model several important features of

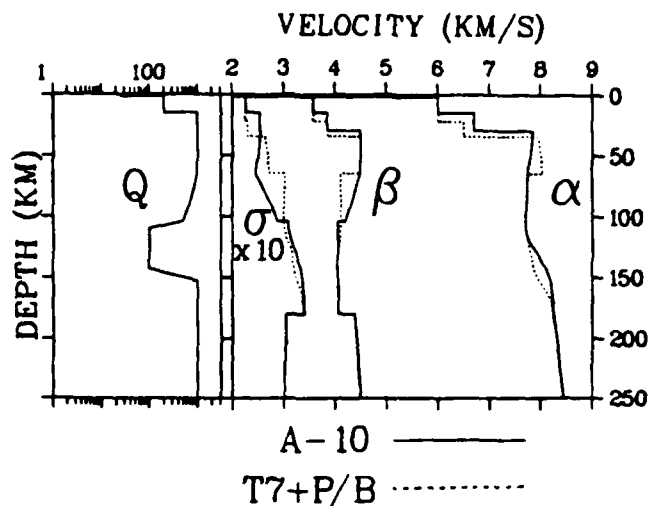


Fig. 5. P-velocity ( $\alpha$ ) and S-velocity ( $\beta$ ) vs. depth plots for the T-7/Priestly-Brune and A-10 models. Assumed Q structure at left:  $\sigma$  (dimensionless) is Poisson's ratio.

regional short-period seismograms. The technique appears promising in advancing knowledge of wave propagation and source identification at regional distance ranges.

#### ACKNOWLEDGMENTS

We especially thank Rainer Kind for making available to us the modified reflectivity method computer program that we have adapted for our analyses. Paul A. Johnson was responsible for the computer runs. We thank Terry C. Wallace and Mike Shore for discussions and for reviewing the manuscript. The calculational and data reduction efforts for this research were supported by the U.S. Department of Energy and partially by ONR Earth Physics Program grant N00014-75-C-0972 to L.W.B. The Snake River Plains data were collected during research partially funded by the U.S. National Science Foundation (grant EAR-77-23707 to the University of Utah and EAR-77-23357 to Purdue University) and by the U.S.G.S. Geothermal Research Program grant 14-08-0001-G-532 to Purdue.

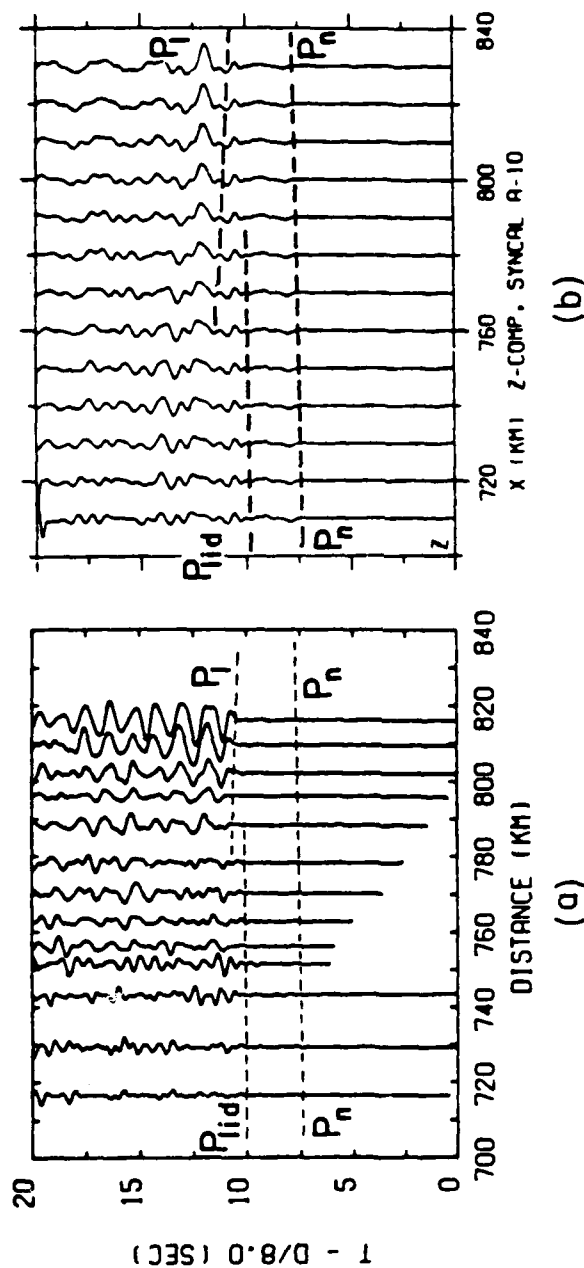


Fig. 6. Comparison of the observed (a) record section with the synthetic section calculated from the A-10 model (b).

## REFERENCES

1. A. I. Ruzaikin, I. L. Nersesov, V. I. Khalturin, and P. Molnar, *J. Geophys. Res.* 82, pp. 307-316, 1977.
2. L. Knopoff, P. Schwab, K. Nakanishi, and F. Chang, *Geophys. J. R. Astr. Soc.* 39, pp. 41-70, 1974.
3. V. Z. Ryaboi, *Izv. (Bull.) Acad. Sci. USSR, Geophys. Ser., AGU Trans.* 3, pp. 177-184, 1966.
4. R. P. Masse, *Bull. Seism. Soc. Am.* 63, pp. 911-935, 1973.
5. A. Hirn, L. Steinmetz, R. Kind, and K. Fuchs, *Z. Geophys.* 39, pp. 363-384, 1973.
6. R. Kind, *J. Geophys.* 40, pp. 189-202, 1974.
7. C. B. Archambeau, E. A. Flinn, and D. G. Lambert, *J. Geophys. Res.* 74, pp. 5825-5865, 1969.
8. L. J. Burdick and D. V. Helmberger, *J. Geophys. Res.* 83, pp. 1699-1712, 1978.
9. J. E. York and D. V. Helmberger, *J. Geophys. Res.* 78, pp. 1883-1886, 1973.
10. M. Cara, *Geophys. J. R. Astr. Soc.* 57, pp. 649-670, 1979.
11. B. A. Romanowicz and M. Cara, *Geophys. Res. Lett.* 7, pp. 417-420, 1980.
12. A. L. Hales, *Earth and Planet. Sci. Lett.* 7, pp. 44-46, 1969.
13. D. P. Hill, *Geol. Soc. Am. Bull.* 83, pp. 1639-1648, 1972.
14. K. Fuchs and G. Müller, *Geophys. J. R. Astr. Soc.* 23, pp. 417-433, 1971.
15. R. Kind, *J. Geophys.* 44, pp. 603-612, 1978.
16. K. H. Olsen, L. W. Braile, and P. A. Johnson, *Geophys. Res. Lett.* 7, pp. 1029-1032, 1980.
17. G. Müller, *J. Geophys.* 42, pp. 429-436, 1977.
18. K. Priestly and J. Brune, *J. Geophys. Res.* 83, pp. 2265-2272.
19. K. Fuchs, *Tectonophysics* 56, pp. 1-15, 1979.
20. L. Knopoff, *Rev. Geophys.* 2, pp. 625-660, 1964.

SEISMIC VELOCITY AND Q-STRUCTURE OF THE UPPER MANTLE LID  
AND LOW VELOCITY ZONE FOR THE EASTERN GREAT BASINK. H. Olsen,<sup>1</sup> L. W. Braille,<sup>2</sup> and P. A. Johnson<sup>1</sup><sup>1</sup>Geosciences Division, Los Alamos Scientific Laboratory, Los Alamos, New Mexico 87545<sup>2</sup>Department of Geosciences, Purdue University, West Lafayette, Indiana 47907

**Abstract.** A 100-km-long record section of NTS explosions recorded in the eastern Snake River Plains ( $70^\circ < \Delta < 80^\circ$ ) shows the cusp of critical refractions from the steepened P velocity gradient at the bottom of the upper mantle LVZ. Synthetic seismograms calculated with a modified reflectivity program have been used to derive a regional velocity model of the upper mantle beneath the eastern Great Basin. The model suggests that observed very weak  $P_n$  arrivals are due to a slight negative velocity gradient below the Moho and that no high velocity mantle lid exists in this region.

## Introduction

The seismic velocity versus depth structure of the upper mantle and lower crust beneath tectonically active areas of the western United States has been studied extensively for nearly 20 years. This has been possible because Nevada Test Site (NTS) underground explosions and western U.S. and Mexican earthquakes provide frequent seismic sources in an area well covered by seismograph stations. Compressional velocity distributions have mainly been determined by integrating the slope of the travel time curve,  $dT/d\Delta$ , using the Herglotz-Wiechert method. The required travel time (T) versus distance ( $\Delta$ ) data have been analysed from short-period recordings obtained along long-range profiles (Archambeau et al., 1969; Masse et al., 1972) and/or from apparent velocities measured directly across large seismic arrays (Johnson, 1967). Recently, availability of high speed computers and development of sophisticated synthetic seismogram modeling techniques make it practical to fit the travel time and amplitude data by a trial and error procedure (Burdick and Helmberger, 1978; Wiggins and Helmberger, 1973). The important advantage of the synthetic seismogram method is that it makes optimum use of amplitude data and detailed waveform fitting to derive P velocity structure.

Many compressional and shear wave studies show that a major feature of the mantle structure beneath the western U.S. is a low velocity zone (LVZ) in the depth range between 60 and 300 km. It is well known that significant lateral variations in LVZ properties (thickness, depth, values of minimum S and P velocities, presence or absence of a lithospheric "lid," etc.) occur over distances of several hundred kilometers and perhaps to even finer scales (Burdick and Helmberger, 1978; York and Helmberger, 1973; Romanowicz and Cara, 1980). On the other hand, Burdick and Helmberger (1978) suggest mantle structure deeper than about 300 km is more uniform over a global scale and therefore amenable to modeling using widely spaced sources and seismograph stations if emphasis is placed on long period body wave arrivals at distances beyond  $10^\circ$ . Here we report on a record section of NTS explosions taken with matched short-period instruments having a sufficiently small station spacing

(8 km) and yet long enough ( $\sim 100$  km) to identify at least three distinct (T,  $\Delta$ ) branches for P waves whose raypaths bottom in the uppermost mantle beneath a small area in east-central Nevada. Modeling of the arrival times, amplitudes, and waveforms using a reflectivity method synthetic seismogram program (Kind, 1978; Fuchs and Müller, 1971) enables us to perturb the generic western U.S. models into a crust-upper mantle model which gives fine details of the LVZ transition in this region.

## Observations

Our observations are recordings of two NTS nuclear explosions obtained while our equipment was deployed in eastern Idaho during the Yellowstone-Snake River Plains (Y-SRP) cooperative seismic profiling experiment (Braille et al., 1979). Twelve special high-explosive shots plus blasts at two quarries were used as sources for crustal profiles in eastern Idaho and Yellowstone Park. Figure 1a shows the area of the Y-SRP experiment; Figure 1b indicates those stations that were recorded on an approximate radial line to two NTS explosions on September 27, 1978 (Table 1). Because RUMMY and DRAUGHTS explosion sites were within 3 km of each other, our observed record sections are nearly identical except DRAUGHTS amplitudes are about 1/4 RUMMY amplitudes. We discuss only the better signal-to-noise RUMMY seismograms.

Instrumentation consisted of 13 vertical component short-period (1 Hz natural frequency) seismometers. Ten of these were telemetered to a centrally located site and recorded on analog magnetic tape; the three southernmost instruments were recorded on portable smoked paper units and FM tape recorders. All records were digitized at 100 samples per second and filtered (0-3 Hz) for this analysis.

The reduced-time, true relative amplitude record section for the RUMMY explosion is displayed in Figure 2. Three separate compressional phases within the first four seconds are marked on Figure 2a; our reasoning in so identifying these arrivals is as follows:

(1) The very first arrivals with an apparent velocity of 7.8-7.9 km/s are so weak that they could easily be missed on initial inspection. From the Y-SRP refraction data, we determined that the M-discontinuity is 40 km below these stations and the mantle  $P_n$  velocity is close to 7.9 km/s. An enlarged view of the first 12 seconds is shown in Figure 2b where the consistency of the  $P_n$  arrivals across the spread is more apparent. These Snake River Plains seismic stations had quite low background noise so the implication is that a true headwave  $P_n$  arrival will rarely be seen at distances beyond 600 km in the western U.S., except from events of  $m_b \geq 6$ . In these SRP seismograms the ratio of the amplitudes of the  $P_n$  arrivals to those of the  $\bar{P}$  phase is smaller than 0.005. (The  $\bar{P}$  energy arrives at reduced times greater than 32 seconds so is not shown in Figure 2a). Other investigators (e.g., Hill, 1972, 1973) have commented that  $P_n$  energy at these distances is probably very

This paper is not subject to U.S. copyright. Published in 1980 by the American Geophysical Union.

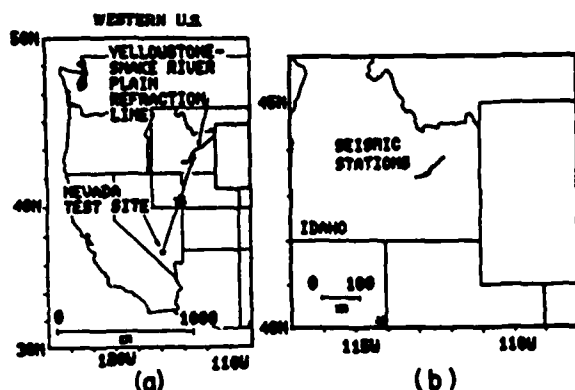


Figure 1. (a) Location map of the western U.S. with relative positions of the Nevada Test Site and the Y-SRP refraction line. (b) Enlargement showing seismic stations in Idaho used for the September 27 observations. Asterisk denotes the approximate area in the Great Basin for mantle ray turning points from NTS explosions.

weak and that care must be taken when attempting to extend the  $P_n$  branch during long range refraction profiling.

(2) Following  $P_n$  by about three seconds are stronger arrivals also having apparent velocities close to 8 km/s. A striking feature of Figure 2a is that beyond 780 km the amplitude of the second arriving phase increases rapidly with distance and the dominant frequency is noticeably lower ( $\sim 0.6$  Hz) than the frequencies for  $\Delta < 780$  km and for the  $P_n$  phase (both  $\sim 1.6$  Hz). This qualitative observation strongly suggests that the rapid increase of the low frequency phase for  $\Delta < 780$  km is a manifestation of a critical distance effect and that the high frequency energy has been attenuated along the travel path. The obvious place for this to occur is during the two-way transit of energy through the mantle LVZ (which also has a high anelasticity, i.e., low Q). These critical refractions are shown schematically in the ray diagram of Figure 3; we follow the convention of Archambeau et al. (1969) in labeling this cusp phase  $P_1$ .

(3) The higher frequency second arrivals for  $\Delta < 780$  km we attribute to large angle reflections from an interface lying mainly above the LVZ. These reflections are overtaken and overwhelmed by  $P_1$  for  $\Delta < 780$ . Because of the apparent velocity near 8 km/s, the high frequency content, and travel time just longer than  $P_n$ , the synthetic seismogram modeling discussed below suggests this reflection occurs at the base of the mantle lid and hence our notation of  $P_{lid}$ .

#### Modeling

Our technique in modeling the record section was to first use a fast asymptotic ray theory computer program (Červený, 1979) to fit travel times and approximate amplitudes. For more exact modeling we

then used a reflectivity method program developed by Kind (1978), which properly accounts for the effects of a buried source and thus allows computation of complete seismograms. One advantage of the reflectivity method over Cagniard-de Hoop techniques (Helmberger, 1973; Helmberger and Burdick, 1979) is that Q values can be individually assigned to each model layer rather than distributed over the entire path as part of a linear operator.

Burdick and Helmberger's (1978) T-7 model was adopted as the starting model for compressional wave velocities in the crust and mantle. The generic T-7 model was constructed mainly from long period data to the NW and SE of NTS—with emphasis on velocity structure below 200 km (arrivals for  $\Delta \geq 10^\circ$ ). Since our observations are in the range  $70^\circ < \Delta < 80^\circ$ , we perturbed the initial model only at depths above 250 km. The T-7 model has a  $P_n$  velocity of 7.95 km/s with a positive gradient below the M-discontinuity to 8.05 km/sec at the bottom of the lid at 65 km. A substantial LVZ for P-velocities is included below 65 km (Figure 5).

We did not calculate synthetics for shear wave phases but were required to include a realistic S-velocity structure because shear wave velocity contrasts can have a major influence on P-wave reflection coefficients—especially for large angles of incidence. Priestly and Brune (1978) used dispersion of fundamental mode Rayleigh and Love waves to derive a shear velocity model in the eastern Great Basin very close to the area of the mantle turning points of this study. The combined P- and S-velocity model, T-7/PB, is shown in Figure 5 along with Poisson's ratio ( $\sigma$ ) calculated from the tabulated velocities.

The modified reflectivity synthetics for the T-7/PB velocity model are shown in Figure 4a for an extended range from 600 km to 960 km. The  $P_1$  phase can be seen only for distances beyond 840 km and reduced times greater than 13 seconds. In order to bring the synthetic  $P_1$  phase into agreement with the observed arrival times and to shift the cusp from  $\sim 820$  km back to  $\sim 780$  km it was necessary to bring the gradient at the

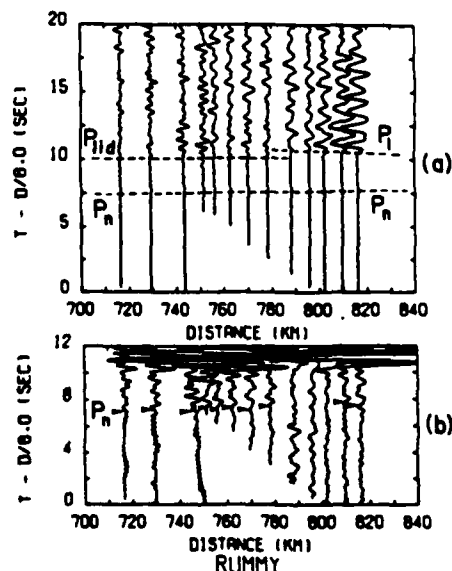


Figure 2. (a) True relative amplitude record section of P-wave arrivals from RUMMY. (b) Same as (a) with increased amplitudes to show weak  $P_n$  phase.

TABLE 1. NTS Explosions of September 27, 1978

Name	Origin Time (GMT)	Coordinates Lat. Long.	Depth (m)	Surf. Elev. (m)	Magnitude ( $m_b$ )
DRAUGHTS	1708:00.071	37.074°N 116.020°W	442	1262	5.6
RUMMY	1720:00.076	37.060°N 116.051°W	640	1253	5.7

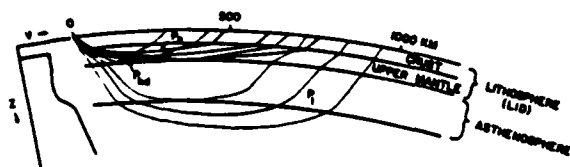


Figure 3. Schematic ray diagram showing the head wave phase  $P_n$ , the  $P_1$  phase critically refracted from the gradient near the bottom of the LVZ, and the  $P_{1d}$  phase reflected from the base of the mantle lid.

bottom of the LVZ to shallower depths and to make slight adjustments to its curvature. Also note from Figure 4a that the T-7/PB model gives too large amplitudes for  $P_n$  arrivals, and the  $P_{1d}$  phase from the discontinuity at 65 km depth arrives about 2.5 seconds too early so is superimposed on the  $P_n$  phase throughout much of the 600–960 km range. The result of perturbing the T-7/PB velocity model to better match the observations of Figure 2 is model A-10 shown in Figure 5. The A-10 synthetics are compared with the original T-7/PB model in Figure 4b and with the more limited distance range observations in Figure 6.

#### Discussion

We can summarize the nature and reasons for the various model perturbations as follows:

(1) The steepened positive P-velocity gradient in the lower part of the LVZ has been raised in order to fit the arrival times and cusp distance of the  $P_1$  phase.

(2) In order to match the observed weak  $P_n$ , a slight negative gradient just below the M-discontinuity is required instead of the positive gradient of the generic T-7 model. In fact, our A-10 P-velocity model suggests that, beneath this part of the Great Basin, the LVZ may be in contact with the crust at the M-discontinuity. Similar indications of the absence of a high velocity lid in parts of the western U.S. have been cited by Archambeau et al. (1969) (especially for their SHOAL-FALLON SE profile).

(3) The large negative discontinuity at a depth of 65 km present in both the T-7 P-velocities and the Priestly-Brune model appears to be too shallow to properly match the observed  $P_{1d}$ - $P_n$  travel time delay. The observed delay is better reproduced if the discontinuity is at about 100 km depth.

(4) The calculated amplitudes of the  $P_{1d}$  reflection are much too large if the T-7/PB velocity

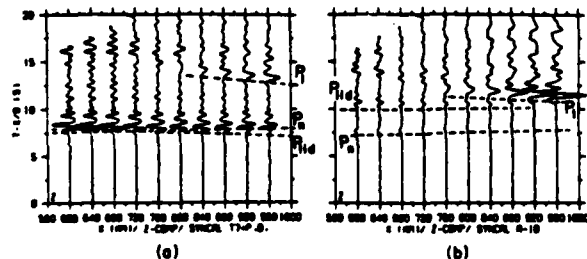


Figure 4. Synthetic seismograms (Z-component) of early compressional phase arrivals from (a) the generic T-7/PB model and (b) the A-10 mantle model (Figure 5) which match the observations in the 720 to 820-km range. Travel time curves calculated from the Cerveny program. Amplitude multiplied by distance for convenient plotting.

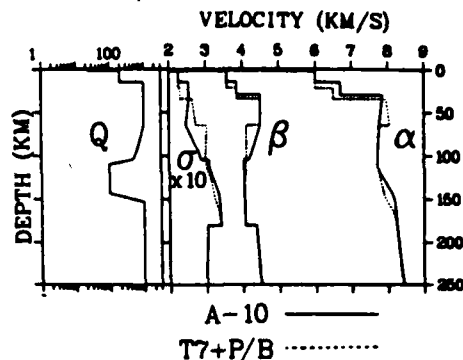


Figure 5. P-velocity ( $\alpha$ ) and S-velocity ( $\beta$ ) versus depth plots for the T-7/PB and A-10 models. Assumed Q-structure for both models shown at left.  $\sigma$  is Poisson's ratio.

contrasts ( $-0.3$  km/s for P,  $-0.39$  km/s for S) are used at a depth of  $\sim 100$  km. In fact, by including the effect of S-velocity contrasts on the P-wave reflection coefficients, we can match observed  $P_{1d}$  amplitudes by keeping the P-velocity contrast at zero and relying entirely on an S contrast of  $-0.15$  km/s to produce the effect on these wide angle reflections. In moving the bottom of the S-velocity lid from a depth of 65 km proposed by Priestly and Brune to the  $\sim 100$  km required in our A-10 model, we introduced a negative gradient in the S-velocities between these two depths; a similar negative gradient can be seen in the higher mode inversions by Cara (1979), but these are not plotted in Figure 5. Hill (1972) and Hales (1969) previously reported arrivals following  $P_n$  by two to three seconds at distances of  $\sim 600$  km in sections from long range refraction experiments in the Columbia Plateau (EDZOE experiment) and the central U.S. (EARLY RISE), respectively. Their interpretations—using travel time information only—suggest a thin ( $\sim 10$  km), sharp, but high velocity (8.0 to 8.4 km/s) lid at depths of 90–100 km is present in those regions. Our Great Basin data agrees in placing a discontinuity (which is perhaps the "boundary" between the lithosphere and the asthenosphere) at  $\sim 100$  km but our P-velocity contrast cannot be as pronounced as those implied by Hill and Hales and still give rise to the comparatively weak amplitudes that we observe in the 750 km range.

(5) the Q-structure (for P-waves) used for the A-10 model was a generalization of proposed values that have appeared in recent literature. The most important segment is the low value centered in the LVZ. A  $Q_0$  value in the range between 50 and 100 appears to adequately attenuate the higher frequency components

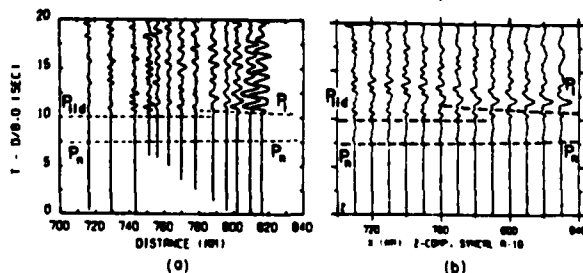


Figure 6. Comparison of observed (a) and synthetic (b) seismogram record sections for the 720 to 820-km distance range.

of the  $P_1$  phase.  $Q_\alpha > 100$  in the LVZ does not attenuate  $P_1$  enough, whereas  $Q_\alpha \sim 25$  completely obliterates the  $P_1$  phase in the synthetics. Our value of  $50 < Q_\alpha < 100$  is of the same order as that deduced by Helmberger (1973) from Cagniard-de Hoop techniques.

(6) One possible shortcoming of the A-10 model is the failure to reproduce details of the oscillations of the observed  $P_1$  phase. We do not believe this to be a result of an inadequately detailed source spectrum, since a comparison of the explosion source spectrum algorithm used in the modified reflectivity code is reasonably represented by the source spectrum plus instrument response function calculated from known physical parameters of these explosions (Mueller and Murphy, 1971). Archambeau et al. (1969) observed compressional wave energy spread out in long, rather complicated oscillatory wave trains near caustics and attributed this to interference between refracted and reflected components near the cusp. Our model layer thicknesses ( $\sim 5$  km) in the region of the lower depths of the LVZ (120–150 km) are of the same order as the wavelengths ( $\sim 10$  km) of the dominant short period energy. Thus, we believe the oscillatory  $P_1$  trains may be due to small details of fine structure in the transition zone which we have not yet attempted to model at the required resolution.

In conclusion, relatively minor adjustments in the T-7/PB model for the western U.S. yield an uppermost mantle structure that reproduces in detail the upper mantle arrivals and very weak  $P_n$  observed in the Great Basin.

**Acknowledgments.** We especially thank Rainer Kind for the modified reflectivity computer program used in our analysis. We appreciate the assistance of our LASL colleagues, E.F. Homuth and T.G. Handel with the observations and J.N. Stewart for computer advice. Cooperation of the Idaho National Engineering Laboratory during the field work is appreciated. K.H.O., P.A.J., and the LASL field team were supported by the U.S. Department of Energy. L.W.B. acknowledges support from NSF grants EAR-77-23351 and EAR-77-23707 and ONR grant N00014-75-C-0972. Field data were collected during research partially sponsored by the NSF grants and by USGS Geothermal Exploration Program grant 14-08-0001-G-532.

#### References

- Archambeau, C.B., Flinn, E.A., and Lambert, D.G., Fine structure of the upper mantle, *J. Geophys. Res.*, **74**, 5825–5865, 1969.
- Bräile, L.W., Smith, R.R., Ansorge, J., Baker, M.R., Prodehl, C., Healy, J.H., Mueller, S., Olsen, K.H., Priestly, K., and Brune, J., The Yellowstone-Snake River Plain seismic profiling experiment: eastern Snake River Plain (abs.), *EOS Trans. AGU*, **60**, 941, 1979.
- Burdick, L.J. and Helmberger, D.V., The upper mantle P velocity structure of the western United States, *J. Geophys. Res.*, **83**, 1699–1712, 1978.
- Cara, M., Lateral variations of S velocity in the upper mantle, *Geophys. J. Roy. Astron. Soc.*, **57**, 649–670, 1979.
- Červený, V., Accuracy of ray theoretical seismograms, *J. Geophys.*, **46**, 135–149, 1979.
- Fuchs, K. and Müller, G., Computation of synthetic seismograms with the reflectivity method and comparison with observations, *Geophys. J. Roy. Astron. Soc.*, **23**, 417–433, 1971.
- Hales, A.L., A seismic discontinuity in the lithosphere, *Earth and Planet. Science Letters*, **7**, 44–46, 1969.
- Helmberger, D.V., On the structure of the low velocity zone, *Geophys. J. Roy. Astron. Soc.*, **34**, 251–263, 1973.
- Helmberger, D.V. and Burdick, L.J., Synthetic seismograms, *Ann. Rev. of Earth and Planetary Sciences*, **7**, 417–442, 1979.
- Hill, D.P., Critically refracted waves in a spherically symmetric radially heterogeneous earth model, *Geophys. J. Roy. Astron. Soc.*, **34**, 251–263, 1973.
- Hill, D.P., Crustal and upper mantle structure of the Columbia Plateau from long range seismic-refraction measurements, *Geol. Soc. America Bulletin*, **83**, 1639–1648, 1972.
- Johnson, L.R., Array measurements of P velocities in the upper mantle, *J. Geophys. Res.*, **72**, 6309–6323, 1967.
- Kind, R., The reflectivity method for a buried source, *J. Geophys. Res.*, **44**, 603–612, 1978.
- Masse, R.P., Landisman, M., and Jenkins, J.B., An investigation of the upper mantle compressional velocity distribution beneath the Basin and Range province, *Geophys. J. Roy. Astron. Soc.*, **30**, 19–36, 1972.
- Mueller, R.A. and Murphy, J.R., Seismic characteristics of underground nuclear detonations: Part 1, seismic spectrum scaling, *Bull. Seismol. Soc. Am.*, **61**, 1675–1692, 1971.
- Priestly, K. and Brune, J., Surface waves and the structure of the Great Basin of Nevada and Western Utah, *J. Geophys. Res.*, **83**, 2265–2272, 1978.
- Romanowicz, B.A. and Cara, M., Reconsideration of the relations between S and P station anomalies in North America, *Geophys. Research Letters*, **7**, 417–420, 1980.
- Wiggins, R.A. and Helmberger, D.V., Upper mantle structure of the western United States, *J. Geophys. Res.*, **78**, 1870–1880, 1973.
- York, J.E. and Helmberger, D.V., Low-velocity zone variations in the southwestern United States, *J. Geophys. Res.*, **78**, 1883–1886, 1973.

(Received September 7, 1980;  
accepted October 7, 1980.)

# Modeling Short-Period Crustal Phases ( $\bar{P}$ , Lg) for Long-Range Refraction Profiles

K.H. Olsen<sup>1</sup>, L.W. Braile<sup>2</sup> and J.N. Stewart<sup>1</sup>

<sup>1</sup> Earth and Space Sciences Division, Los Alamos National Laboratory, Los Alamos, NM 87545 (U.S.A.)

<sup>2</sup> Department of Geosciences, Purdue University, West Lafayette, IN 47907 (U.S.A.)

The short-period seismic phases known as  $\bar{P}$  and Lg are often recorded at distances of 200–1000 km on long-range refraction profiles and are usually the largest-amplitude features on record sections for this distance range.  $\bar{P}$  and Lg propagate as multiply reflected compressional and shear waves in a crustal waveguide whose principal boundaries are the Moho and the free surface. Equivalently, they can be interpreted as the interference pattern produced by a superposition of higher-mode P, SV and SH wave propagating in a leaky waveguide. For compressional waves, the waveguide efficiency is a strong function of frequency and depends on the presence or absence of low-velocity layers within a few kilometers of the surface, such as deep sedimentary sections commonly found in active tectonic areas. Such low-velocity surface layers create constructive interference effects for upcoming P waves incident at near grazing angles at the free surface and lead to efficient  $\bar{P}$  propagation. Several good examples of strong  $\bar{P}$  phases can be found on long-range refraction profiles for the tectonically active western United States; the 550 km profile eastward from SHOAL to Delta, UT is analyzed here. We have used a modified reflectivity-method computer program to model crustal phases for the SHOAL–Delta profile. The reflectivity technique accounts for all body and surface waves contributing to the short-period seismograms. It is found that the synthetic waveforms realistically model the observed  $\bar{P}$  characteristics. In this case, the decay of  $\bar{P}$  amplitudes with distance appears to be dominated by surface-reflection leakage from the waveguide rather than by anelastic attenuation due to  $Q$  of crustal rocks.

## 1. Introduction

Until recently, the velocity structure of the Earth's crust was inferred mainly from travel-time studies of easily correlatable seismic phases (usually first arrivals) recorded in refraction profiling experiments. Amplitude and waveform information on seismic-record sections was used mainly in a qualitative way in phase identifications and as an indication of velocity gradients, transition zones, and attenuation properties. Since 1970, the increased availability of high-speed computers and the development of sophisticated synthetic-seismogram modeling techniques has made it possible to use amplitude and waveform data optimally to derive detailed velocity and  $Q$  structure (Müller and Fuchs, 1976; Braile, 1977). In particular, we employ here a modified reflectivity-method program developed by Kind (1978) that is capable of

computing "complete" seismograms, including all body and surface waves. Our objective is to investigate the possible utility of modeling rather complex short-period crustal phases (e.g.,  $\bar{P}$  and Lg) as an aid to the interpretation of crustal properties and structures. In this paper we attempt to describe the more important characteristics of the  $\bar{P}$  and Lg phases, investigate conditions for the generation and propagation of these phases, and determine which properties of the Earth structure influence this propagation. Because of the complexity and uncertainties about the theoretical details of the generation and propagation of these crustal phases, they have heretofore been little used in the interpretation of seismic refraction profiles — even though they are often the largest-amplitude features on record sections. We show one aspect of how modeling crustal phases with complete synthetic seismograms can improve our

knowledge of Earth structure. Because relatively few complete seismic-record sections for regional distances (200–2000 km) showing  $\bar{P}$  and Lg phases are available from observed data, we rely heavily on the analysis of  $\bar{P}$  and Lg waveforms by means of synthetic seismograms calculated using the modified reflectivity method for a variety of Earth models.

For clarity in both typography and context, we shall henceforth write “P-bar” in place of the  $\bar{P}$  notation.

## 2. Regional Crustal Phases (P-bar, Lg)

The P-bar and Lg phases are usually well recorded on short-period instruments at regional distance ranges (100–2000 km). They are commonly seen as broad ( $\Delta t > 20$  s), complex wave trains having group velocities of  $\sim 6.0$  km s<sup>-1</sup> for

P-bar and  $\sim 3.5$  km s<sup>-1</sup> for Lg (Olsen and Braile, 1981).

Both P-bar and Lg phases propagate efficiently in the continental crust and are often the largest-amplitude arrivals on short-period seismograms at regional distances (Fig. 1). In addition to the complex and long-duration character of both P-bar and Lg phases, these arrivals also display little coherence in waveform or even in the envelope of the complex wave packet over relatively short distances. These characteristics of P-bar and Lg wave propagation can be modeled qualitatively using synthetic-seismogram techniques. An example of a vertical-component synthetic-seismogram calculation resulting from a crustal model appropriate to the western United States or other tectonic areas is shown in Fig. 2. Both P-bar and Lg phases are prominent arrivals on the record sections, having durations of tens of seconds and relatively large amplitudes in the short-period range. Unlike the

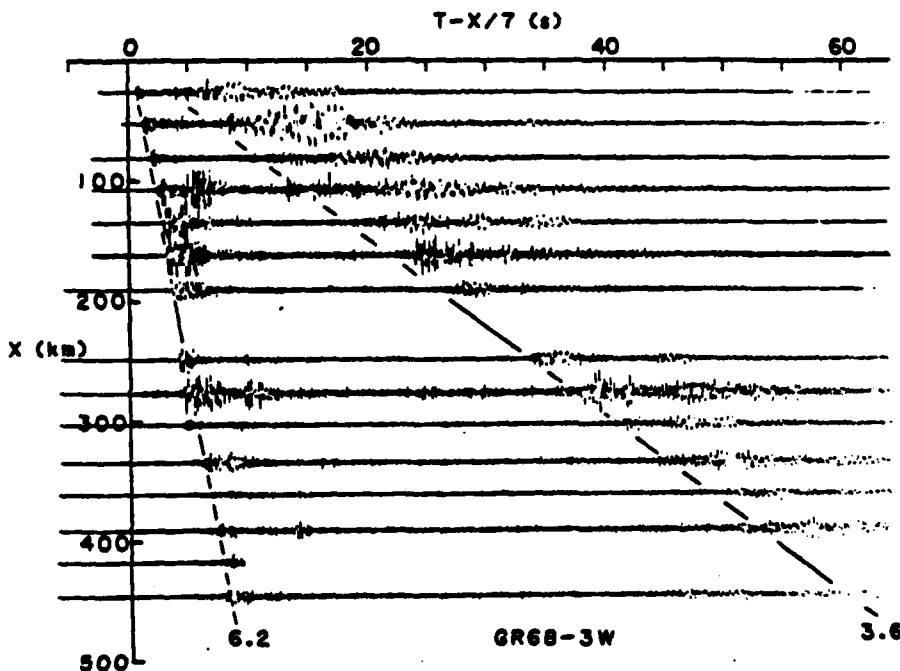


Fig. 1. Vertical-component record section recorded westward from the Schefferville shotpoint in the Superior Province of the Canadian shield showing examples of P-bar and Lg crustal phases. The broad P-bar and Lg phases approximately follow the average-velocity lines 6.2 km s<sup>-1</sup> and 3.6 km s<sup>-1</sup>, respectively, for ranges  $X$  beyond  $\sim 150$  km. Amplitudes have been multiplied by distance for convenient scaling. Adapted from Berry and Fuchs (1973).

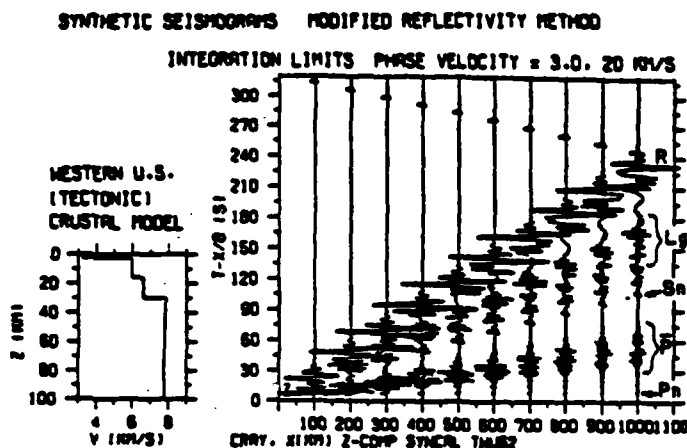


Fig. 2. Vertical-component synthetic-seismogram record section for a crustal model representative of a tectonically active region such as the western United States. The Pn, P-bar, Sn, Lg and fundamental-mode Rayleigh (R) wave groups are indicated on the  $X = 1000$  km seismogram.

primary waveforms, such as Pn and Sn, which display waveform coherence over long distances, the P-bar and Lg waveform characteristics change considerably with distance, and phase correlations are usually impossible. However, correlation of the energy represented by the group-velocity envelope is usually possible. An enlargement of one of the seismograms for the record section shown in Fig. 2

is illustrated in Fig. 3, indicating the waveform characteristics of the complex P-bar and Lg phases as a function of reduced time as well as their average or group velocity. It is seen for this model that the P-bar phase has average velocities in the range of  $6 \text{ km s}^{-1}$  and the Lg phase has group velocities near  $3.6 \text{ km s}^{-1}$ .

Observations and synthetic-seismogram analy-

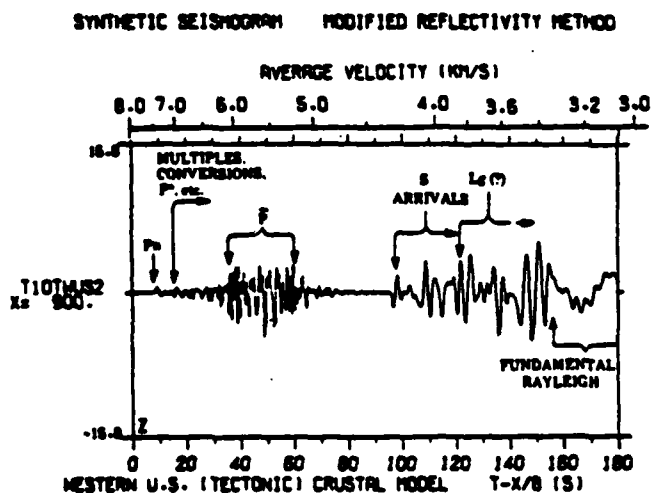


Fig. 3. Enlargement of the  $X = 900$  km synthetic seismogram from Fig. 2 showing more details of individual phases.

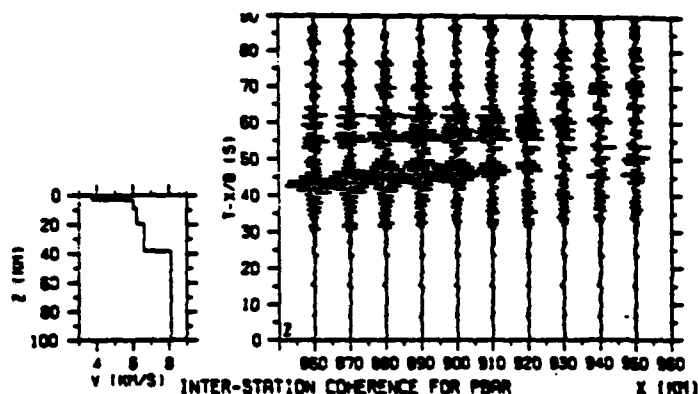


Fig. 4. Vertical-component synthetic-seismogram record section calculated using the modified reflectivity method for closely spaced (10 km) seismographs at distances between 860 and 960 km an explosion source. Note how rapidly the waveform coherence varies with distance in the P-bar window (reduced times 40–70 s). The P-velocity crustal model is shown at the left.

sis presented here and by Bouchon (1982) suggest that both P-bar and Lg propagate as multiply reflected compressional and shear waves within the crust, or, equivalently, they are the interference patterns produced by the superposition of a large number of leaky P- and S-modes respectively (Haskell, 1966). We have performed a parameter study of short-period propagation from explosion sources in continental crustal models, which shows that the modified reflectivity technique can reproduce many of the observed characteristics of these phases, such as envelope modulation, rapidly varying lateral-waveform coherence, etc. (Olsen *et al.* 1981).

For synthetic modeling of Lg using shallow explosion sources, the SV energy in the Lg group

window arises from P to S conversion. Once converted, SV energy is very efficiently confined in a waveguide whose principal boundaries are discontinuities or steep velocity gradients at the Moho and at the free surface. Although we have not here modeled the SH component of motion of the Lg phase, we expect that it also can be represented as a guided wave with the near surface and Moho as waveguide boundaries, as Bouchon (1982) has also suggested. The total channeled energy is relatively insensitive to fine-scale detail (a few km) of vertical velocity gradients near the waveguide boundaries, but the waveform coherence at surface seismometers can still vary appreciably over distances of ~10 km (Figs. 4 and 5). Undercritical and wide-angle reflections at the waveguide

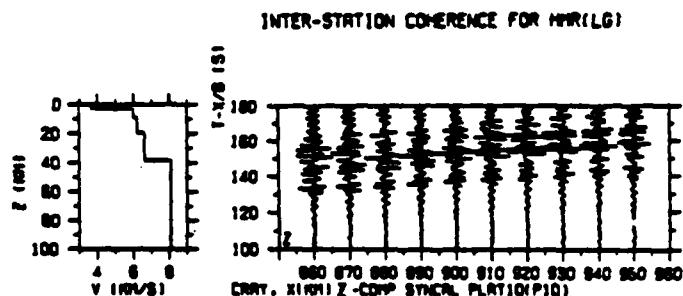
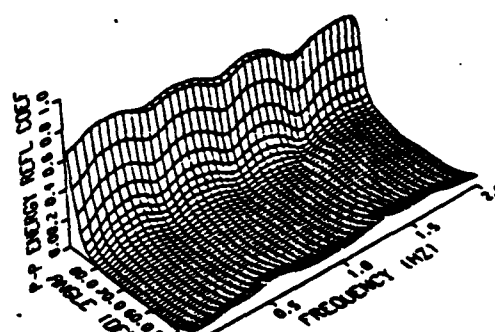


Fig. 5. Synthetic record section illustrating rapid lateral changes in waveform coherence in the Lg window (reduced times 130–170 s) for the same model and ranges as in Fig. 4.

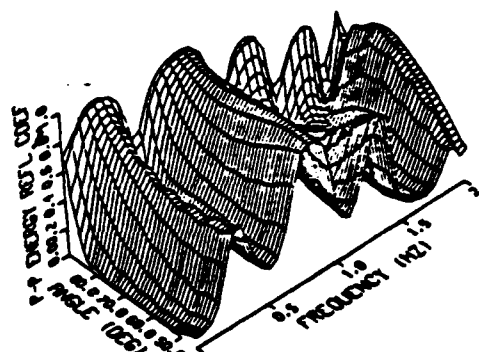
boundaries are nearly total, so attenuation and the frequency spectra depend almost entirely on  $Q$  of crustal materials. Thus  $L_g$  is a good measure of  $Q$ .

There is frequently a confusion or imprecision in the literature concerning the nomenclature for the P-bar phase, with the term  $P_g$  being applied to any phase following  $P_n$  and having an apparent velocity of  $\sim 6.0 \text{ km s}^{-1}$ . In the western United States where the complex P-bar phase can be very prominent at distances of 200–2000 km, the  $P_g$  phase — a head wave traveling along the top of the "granitic" basement — attenuates extremely rapidly and is usually unobservable beyond  $\sim 150 \text{ km}$  (Ryall and Stuart, 1963). So, although P-bar onsets fall on the extension of the  $P_g$  travel-time branch, the two phases have quite different propagation and attenuation characteristics. Similarly to  $L_g$ , the "true" P-bar phase propagates by multiple wide-angle reflection of  $P_mP$ , but the efficiency of the upper waveguide boundary is a complex function of frequency and is very sensitive to the presence of low-velocity layers at or near the surface. Our parameter studies (e.g., Figs. 6 and 7) confirm that a low-velocity surface layer — such as the thick sedimentary section in tectonic areas such as the Basin and Range and Colorado Plateau provinces of the western United States — is the key factor for efficient propagation of P-bar. The controlling factor is the nature of the free-surface reflection of upcoming P-waves previously reflected from the Moho and midcrustal discontinuities. In the absence of low-velocity surface layers (i.e., in shield areas) nearly all upward-traveling P energy is converted to SV upon free-surface reflection. Note the very small values of the P-P energy-reflection coefficient ( $R_{opp} \approx 0$ ) in Fig. 6(A); the energy fraction converted to SV at the free surface is  $R_{ops} = 1 - R_{opp}$  (Haskell, 1966). Thus, P-SV conversion is nearly complete and P-bar does not propagate efficiently in shields.

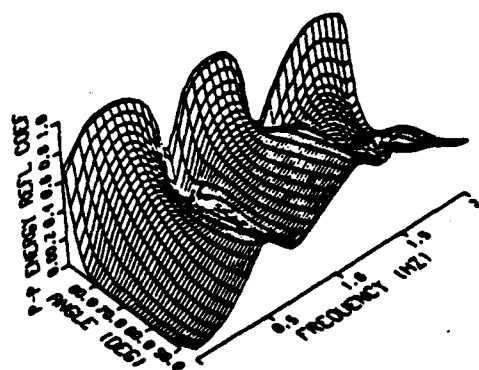
On the other hand, when a low-velocity near-surface layer is present,  $R_{opp}$  is a strong function of frequency (owing to constructive and destructive interference effects) but on the average is large (Figs. 6(B) and 6(C)). A relatively large amount of compressional energy is reflected back into the crust, and P-bar propagates with moderate efficiency. Figure 7 illustrates the effect of a



MODEL SD10, UPPER 6.7KM (A)



MODEL SD9, UPPER 6.7KM (B)



MODEL SD16, UPPER 6.7KM (C)

Fig. 6. Energy-reflection coefficient  $R_{opp}$  as a function of angle of incidence and frequency for the three Basin and Range crustal models shown in Fig. 14.  $R_{opp}$  is the fraction of incident P-wave energy reflected as P from the free surface. Note that, for the free surface, the fraction of P-wave energy converted to SV is  $R_{ops} = 1 - R_{opp}$ .

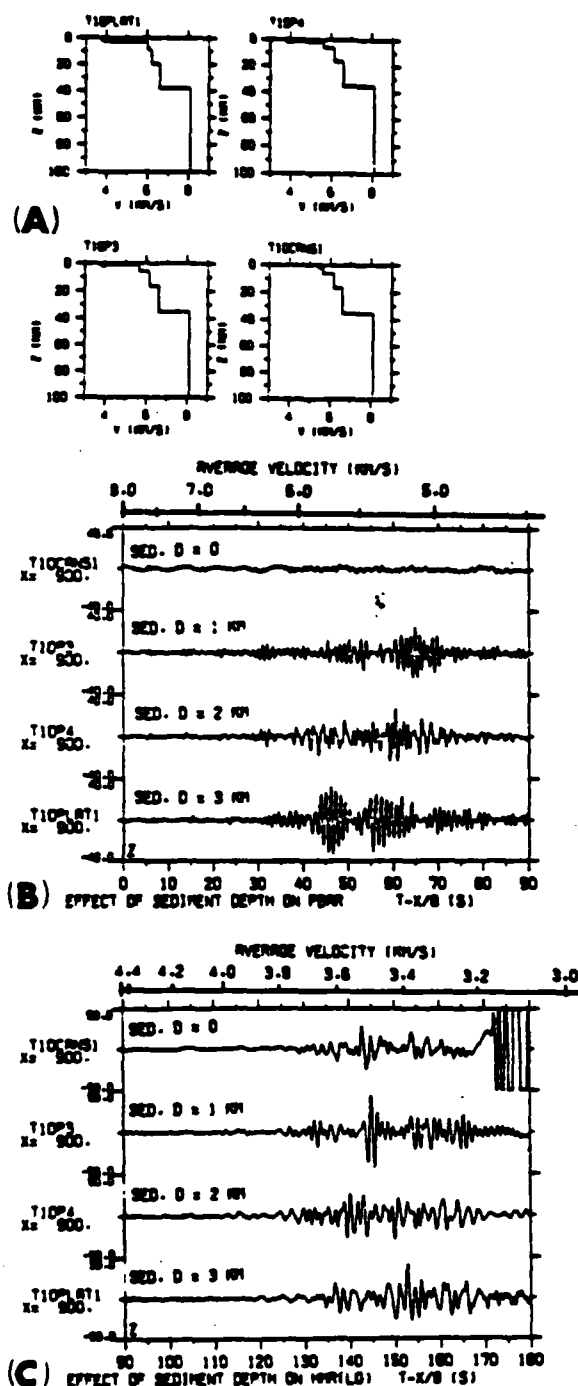


Fig. 7. (A) P velocity versus depth for crustal models with respectively 3 km (T10 PLAT1), 2 km, 1 km, and 0 km (T10

low-velocity surface layer on both P-bar and Lg propagation. Figure 7(B) illustrates that as the thickness of the low-velocity surface layer is increased, the efficiency of propagation of the P-bar phase increases. With no low-velocity sedimentary layer (Model T10CANS1), the P-bar arrivals are extremely small — having amplitudes of the same order as those of primary arrivals such as Pn and P\*. With the presence of a thin low-velocity surfacelayer, large-amplitude P-bar arrivals are present. Varying the thickness of the low-velocity surface layer does not change the peak amplitude of the P-bar phase appreciably, but does significantly affect the complex waveform characteristics of the phase. The exact waveform character of the P-bar phase cannot be predicted at any given distance, even for these laterally homogeneous models, because the lateral coherency (Fig. 4) varies rapidly owing to the constructive and destructive interference effects inherent in the propagation of P-bar. Barker et al. (1981) have emphasized that the P-bar and Lg phases are significantly affected by local geological structure (site-response conditions). They have shown that variations in amplitude, by a factor of as much as 10, and significant differences in the character and waveform of both P-bar and Lg may be caused by local geological conditions in the vicinity of the recording seismograph. However, these local effects must be distinguished from the waveform complexity which is due to constructive and destructive interference effects in the propagation of the P-bar and Lg phases. For example, in the very simple and laterally homogeneous models that we have shown here (Figs. 2, 4, 5, 7(B), (C)), the detailed characteristics of the P-bar and Lg phases are complicated because of propagation effects even though the possible contributions of local geological conditions have not been included.

Haskell (1966) has discussed the attenuation of P-bar amplitudes with distance due to P to SV conversion by multiple surface reflections, and

CANS1) low-velocity surface layers; (B) synthetic seismograms at 900 km range showing changes in amplitude and waveform characteristics in the P-bar time window; (C) same as (B) except for the Lg time window. Only vertical components are shown.

concluded that this leakage attenuation usually dominates over  $Q$ -effects even in the western United States where P-bar is often very strong on short-period seismograms. Our work on the SHOAL-Delta record section discussed below is in agreement that P-bar attenuation is a poor measure of  $Q$  for crustal rocks.

Shurbet (1960) observed P-bar phases from Nevada Test Site (NTS) explosions at Lubbock, TX (~1400 km range) and suggested (Shurbet, 1969) that a low-velocity ( $V_{\min} \sim 5.5 \text{ km s}^{-1}$ ) channel at depths between 5 and 10 km would explain several features of the P-bar phase on the Lubbock seismograms. Our reflectivity-method calculations show that such a low-velocity crustal channel is not uniquely required for P-bar propagation — low-velocity layers at the surface are sufficient to form a good P-bar waveguide. However, since P-bar is essentially an interference pattern produced by layers less than one seismic wavelength in thickness (analogous to thin-film coatings in optics), shallow low-velocity channels would affect the details of the P-bar coda. Thus, certain details of P-bar phases may in some instances lend support to suggested low-velocity channels in the crust.

Strong P-bar phases are often found on long-range refraction profiles for other parts of the world, as well as for the western United States. Good examples are the Eschelohe NW profile in southern Germany (Mueller, 1977), the 900 km Brest to Toulon profile in France (Hirn et al., 1973; Kind, 1974) and the 800 km EDZOE profile in the Canadian Rockies and foreland of Alberta (Meru et al., 1977). The Superior Province Canadian shield profiles discussed by Berry and Fuchs (1973) show fine examples of Lg as well as intermittent P-bar phases (Fig. 1). Peterschmitt (quoted by Mueller, 1977) has analyzed P-bar on several European profiles and also concluded that P-bar consists of a superposition of multiply reflected PmP waves, which are recorded only if the upper reflection point at the surface lies in sedimentary terrain.

As suggested by Haskell (1966) and Bouchon (1982), the lower boundary of the waveguide for P-bar and Lg propagation is the Moho (with possible contributions from other discontinuities within

the lower crust). Three observations provide evidence for the efficiency of P-bar and Lg propagation being due to a waveguide effect in which the lower boundary of the waveguide is the Moho discontinuity. First, Haskell (1966) has shown that the Moho velocity-transition zone (or discontinuity) is an effective reflector for wide-angle P and SV reflection (large reflection coefficients). Secondly, observed seismic refraction and wide-angle-reflection record sections for both shield and tectonic areas (Figs. 8–10) indicate that P-wave reflection from the Moho (phase PmP) not only is large, but multiple PmP arrivals can also be distinguished on the seismic-record section. These multiple PmP reflections (as well as other, more complicated paths) contribute to high-amplitude arrivals which have a complicated and long-duration wave character but which travel within an

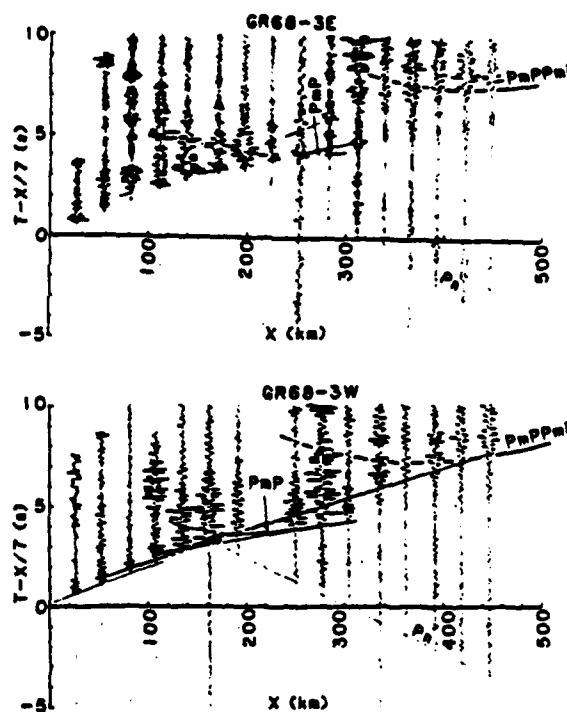


Fig. 8. Record section from the Canadian shield experiment (Berry and Fuchs, 1973) illustrating how multiple reflections of PmP (PmPPmP) merge at ranges beyond 400 km to form part of the P-bar wave group.

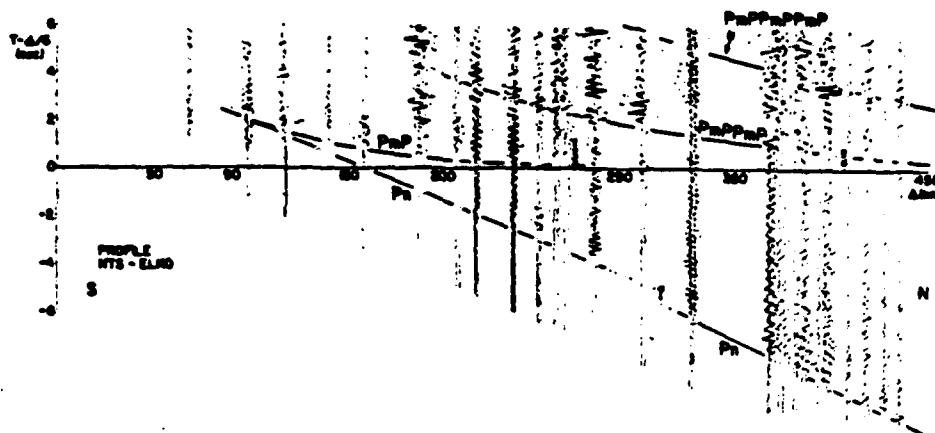


Fig. 9. Vertical-component record section from NTS to Elko, NV, illustrating merging of multiple PmP at distances beyond 300 km to form part of P-bar.

average velocity of  $\sim 6 \text{ km s}^{-1}$  across the record sections at ranges of several hundred kilometers or greater. Thirdly, our synthetic-seismogram model studies, as shown above and in the synthetic waveforms calculated for the SHOAL-Delta profile discussed below, as well as the results of Bouchon (1982), also indicate that the Moho discontinuity is an effective waveguide boundary for P-bar and Lg propagation. Thus, we view the generation and

propagation of the P-bar phase as illustrated schematically in Fig. 11. Multiple PmP reflections, as well as more-complex multiples within the low-velocity surface layer and possible P to S conversions and multiples at the Conrad discontinuity, contribute to wide-angle reflected energy having a complex interference waveform propagating at  $\sim 6 \text{ km s}^{-1}$  at distances of several hundred kilometers from a source. A low-velocity surface layer is

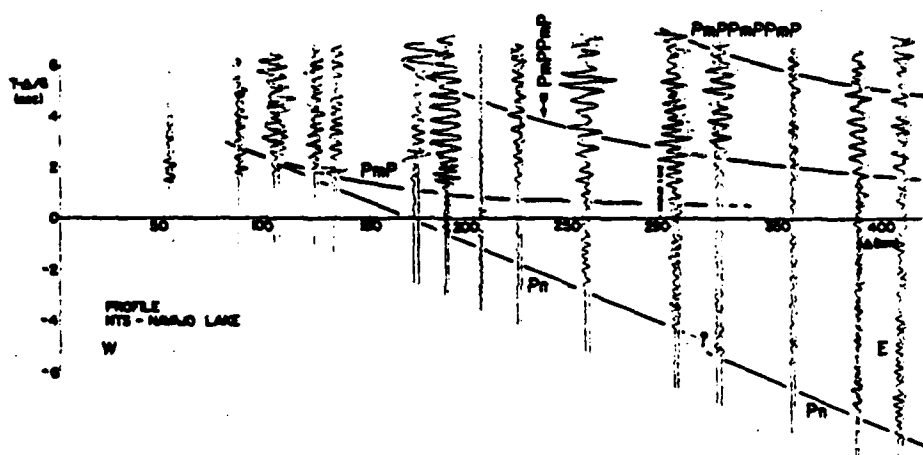


Fig. 10. Same effects as in Fig. 9 for the profile from NTS to Navajo Lake, NM.

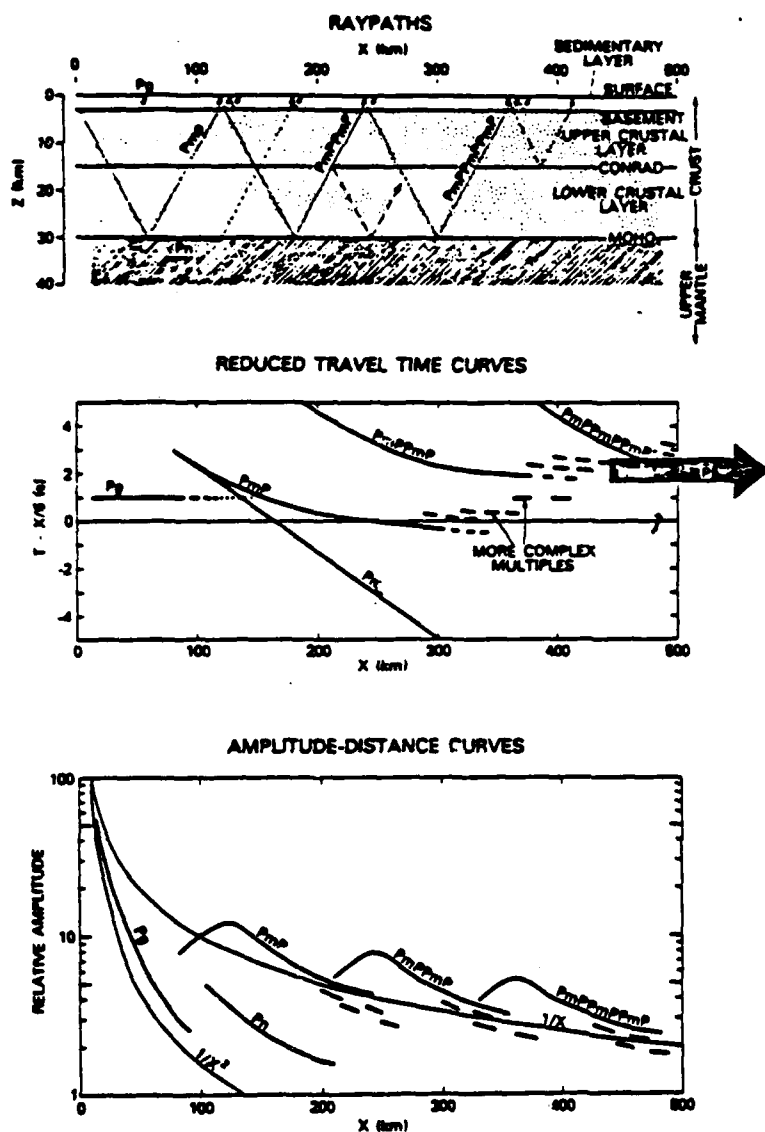


Fig. 11. Schematic diagram indicating how multiple reflections of PmP merge to form the crustal P-bar phase for ranges beyond  $\sim 200$  km. Except for details of interference effects in the near-surface low-velocity layers, the same general physical picture pertains to the SV component of Lg propagation, with PmP replaced by SmS, etc.

necessary for efficient propagation of the P-bar phase. If the surface low-velocity layer is not present, the majority of multiple PmP energy is eventually converted to SV motion as indicated by the reflection coefficients shown in Fig. 6 and the re-

sults of synthetic-seismogram calculations illustrated in Fig. 7. We expect that both the SV and SH components of Lg wave propagation are analogous to those shown in Fig. 11 for P-bar, except that the low-velocity surface layer is not required

in order to produce an efficient waveguide. The free surface and the Moho and other crustal discontinuities are adequate for producing a waveguide for the Lg phase.

### 3. Application to SHOAL-Delta profile

Figure 12 is a map of the western United States showing the locations of several refraction profiles that display examples of the P-bar phase. This paper discusses only the interpretation of the P-bar phase along the 550 km profile extending eastward from the nuclear explosion SHOAL to Delta, UT.

The long-range SHOAL profile was part of a network of refraction-profile recordings mainly in California, Nevada and Utah carried out between 1961 and 1963 by field parties from the U.S. Geological Survey (Prodehl, 1979). Approximately 31 different explosion and earthquake source sites were used; there were several explosions within the Nevada Test Site (shown as only one source location in Fig. 12). Many of the crustal models derived by Prodehl (1979) from the 1961-1963 profiles were obtained from 200-300 km profiles using chemical explosions in the Pacific Ocean, in lakes or in drill holes. Two of these segmented shorter-range reversed profiles (NTS-Boise, ID,

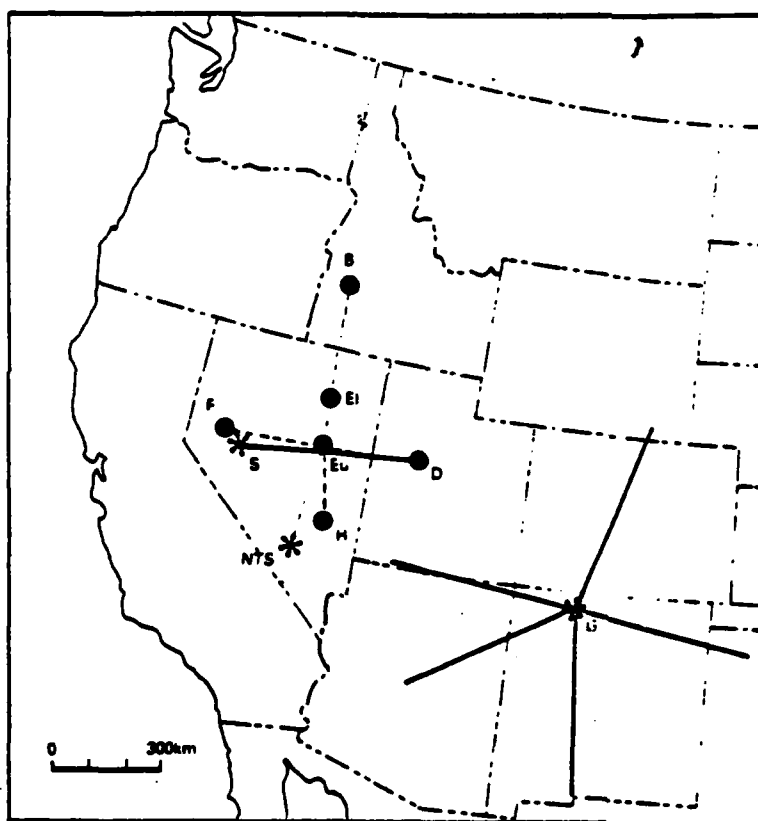


Fig. 12. Locations of some long-range seismic profiles (heavy lines) in the western United States which exhibit strong P-bar phases. Asterisks are nuclear explosion sites; dots are chemical shotpoints. Dashed lines are intersecting shorter-range profiles which were used for detailed crustal-structure studies. Nuclear shotpoints: S, SHOAL; G, GASBUGGY; NTS, Nevada Test Site. Other shotpoints: D, Delta, UT; Eu, Eureka, NV; El, Elko, NV; B, Boise, ID; H, Hiko, NV; F, Fallon, NV (earthquake). Simplified from Prodehl (1979).

and Fallon, NV-Delta, UT) intersect near Eureka, NV, which is near the midpoint of the SHOAL-Delta long-range profile.

The observed reduced-time vertical-component record section from the SHOAL shotpoint is given in Fig. 13(A) (Prodehl, 1979), where the onset times of the Pn, PmP and P-bar phases have been marked. For the ~200 km profiles used for detailed crustal-structure studies, ten ~2.5 km (six-seismometer) spreads were separated by distances of ~10-15 km (Prodehl, 1979). In contrast, as shown in Fig. 13(A), the long-range SHOAL profile had ~50 km station separations, so the inter-

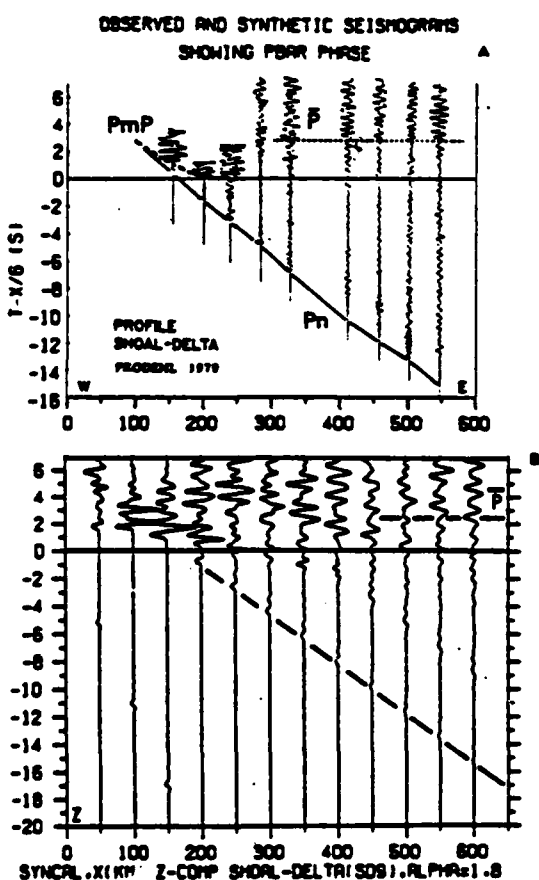


Fig. 13. Comparison of observed (upper) and synthetic (Model SD9) (lower) seismic record sections for the SHOAL-Delta long-range refraction profile. Approximate onset times for Pn, PmP and P-bar are indicated by dashed lines.

station coherence (or lack thereof) of the different compressional phases is not apparent. Our synthetic-seismogram modeling shows rapid changes in interstation coherence for the P-bar phase over distance intervals sometimes less than 10 km. Such rapid coherence variation is one of the more distinctive characteristics of P-bar and Lg interference-pattern-type phases, as discussed above. However, the P-bar phases from SHOAL (Fig. 13) well illustrate another characteristic of these phases — the long oscillatory trains following emergent onsets. In Fig. 13(A), the P-bar trains become identifiable at ranges between 300 and 400 km.

Our procedure for modeling the SHOAL-Delta seismograms was to accept the basic Basin and Range crust/upper-mantle velocity model interpreted by Prodehl (1979) from several short (150-250 km) refraction profiles in the vicinity of Eureka, NV (Fig. 12) involving shotpoints at Eureka, NV; Delta, UT; Hiko, NV; Elko, NV; and NTS. This is the crustal model given in Prodehl's (1979) Table 2 and shown here in Fig. 14.

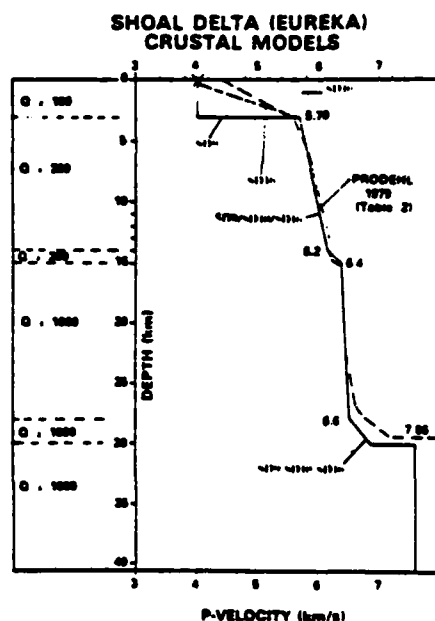


Fig. 14. P-velocity and Q structure models near Eureka, NV. The SD9/SD10/SD16 Models used for the synthetic-seismogram calculations differ only in the top 3 km. Assumed explosion source at 0.3 km depth for all calculations.

We then adjusted the details of the P-velocity model *only* for the uppermost 3 km (Models SD10, SD9 and SD16, shown in Fig. 14). Our purpose here is not to make a complete reinterpretation of the SHOAL-Delta profile, but only to demonstrate how the presence or absence of low-velocity surface layers determines the corresponding presence or absence of P-bar phases on Basin and Range record sections. Our synthetic modeling indicates that we could continue improving the fit to the relatively sparse SHOAL-Delta observations by adjusting deeper crustal velocity discontinuities and/or gradients as well as the near-surface velocity structure. However, we feel that these other model adjustments might unduly confuse the key physical issue of the P-bar/low-velocity surface-layer relation that we want to emphasize here. For all SD-series Models the source depth was held constant at 0.3 km — the approximate SHOAL explosion depth. Poisson's ratio was assumed to be 0.25 ( $V_s = V_p/\sqrt{3}$ ), and a Nafe-Drake velocity-density relationship was assumed (Olsen and Braile, 1981). The assumed variation of  $Q$  with depth is also shown in Fig. 14. The assumed peak frequency for the source spectrum with 1.2 Hz.

The crustal model that gives the better agreement with the observed record section is SD9, which has a pronounced low-velocity layer ( $V_p = 4.0 \text{ km s}^{-1}$ , 3 km thick) at the surface. The observed and synthetic record sections are compared in Fig. 13.

#### 4. Discussion

The key role of near-surface layers in controlling the amplitude and character of the P-bar phase can be followed by comparing Figs. 6, 13 and 15. Figure 6 is a comparison of the reflection coefficients (square root of energy) for near-surface P to P reflection ( $R_{pp}$ ) for near-critical to grazing angles of incidence of upward-traveling P-waves. These plane-wave reflection functions were calculated using a Thomson-Haskell layer matrix method (Haskell, 1966), which is the same algorithm used in the reflectivity program (Kind, 1978). Although the details of the interference fringes are

somewhat different, both the SD9 Model (uniform 3 km layer of  $4 \text{ km s}^{-1}$  sediment) and the SD16 Model (uniform gradient from  $V_p = 4.0 \text{ km s}^{-1}$  at 0.6 km depth to  $V_p = 5.7 \text{ km s}^{-1}$  at 3.0 km) show appreciable P energy returned to the crust for energy in the  $\sim 60^\circ$  incidence angle and 0.5–1.5 Hz range, which are the ranges in which most of the energy is transmitted for these models. Figures 15(B) and (C) show that the integrated result of such multiple reflections is a well-developed P-bar phase in both cases. Conversely, the SD10 Model with no low-velocity surface layer (Fig. 6(A)) has nearly zero P-P conversion and completely suppresses P-bar propagation (Fig. 15(A)). Since there are, undoubtedly, lateral variations in the near-surface layer structure and velocity, waves propagating in the real Earth will "average" minor variations, and a detailed matching of P-bar waveform and modulation characteristics is not justified. However, the total energy in the P-bar phase as represented by the RMS amplitudes over the several-second duration of the P-bar phase is a quantity that depends on the presence of low-velocity surface layers over the propagation path, but this energy is relatively insensitive to assumed fine details in the synthetic models so long as some low-velocity layers are present (see also Fig. 7(B)).

In summary, the short-period regional crustal phases, commonly known as P-bar and Lg, propagate as multiple P-wave and S-wave reflections in a crustal waveguide whose principal boundaries are the Moho and the free surface, as shown schematically in Fig. 11. Near-surface low-velocity layers create constructive interference effects for upcoming P-wave energy at wide angles of incidence, which results in a large fraction of the P-wave energy being retained in the waveguide and hence in efficient propagation of the P-bar phase. For no surface low-velocity layers, nearly all upcoming P energy converts to SV and is lost to further P-bar propagation. Although the Moho and the free surface are also the principal waveguide boundaries for Lg, Lg propagation efficiency is little affected by near-surface low velocities.

Comparison of our synthetic modeling with the observations discussed by Barket et al. (1982) sug-

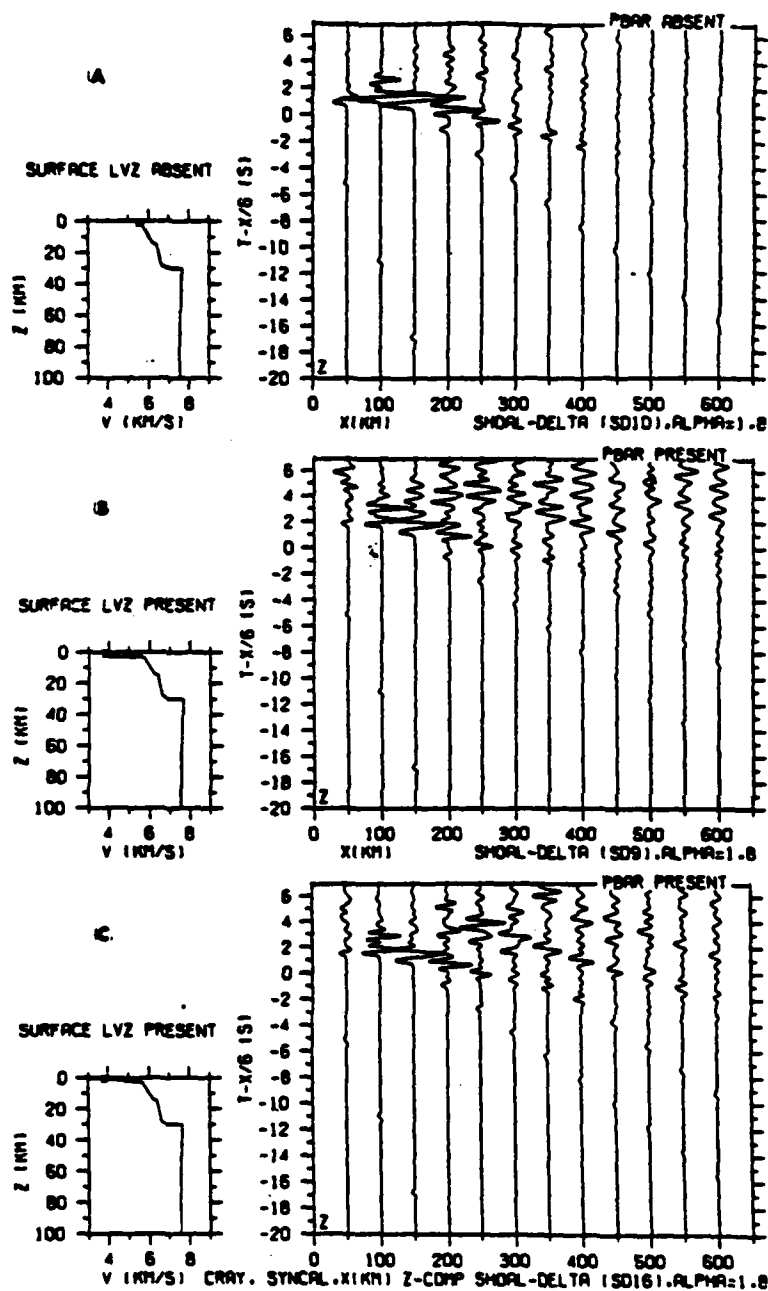


Fig. 15. Vertical-component synthetic seismograms calculated using the modified reflectivity method for the three crustal models of Fig. 14. P-bar phases (long oscillatory trains for ranges  $> 300$  km) are prominent whenever a surface low-velocity zone is present. Calculated amplitudes have been multiplied by distance to the 1.8 power for convenience in plot scaling. The three synthetic sections of (A), (B) and (C) are in the same order as the surface-reflection coefficients for the same models shown in Fig. 6(A)-(C).

gests that there are two important factors in the observed complexity of P-bar and Lg phases. The first is the complicated interference patterns of propagation, even for very simple laterally homogeneous crustal layers such as we have discussed here, and the second is the local geology or site-response effects. The first-order effect is that of laterally homogeneous layering; propagation within this structure is sufficient to produce very complex seismograms which display little lateral coherency, as we have shown. Consideration of the effects of local geological conditions, as discussed by Barker et al. (1982), leads to further waveform and amplitude complexities which are difficult to disentangle in single-station seismograms.

#### Acknowledgments

We thank Greg Elbring for the Thomson-Haskell computer program and for the reflection-coefficient plots. Carl Daudt assisted with computer work and illustrations. We are grateful to Dave Warren for collecting and making available to us unpublished amplitude-calibration data for the SHOAL-Delta profile and for GASBUGGY record sections from U.S. Geological Survey open files. We thank Mike Berry for the record sections in Figs. 1 and 8, and Claus Prodehl for those in Figs. 9 and 10. This work was supported by the U.S. Department of Energy.

#### References

- Barker, B.W., Der, Z.A. and Mrazek, C.P., 1981. The effect of crustal structure on the regional phases Pg and Lg at the Nevada Test Site. *J. Geophys. Res.*, 86: 1686-1700.
- Berry, M.J. and Fuchs, K., 1973. Crustal structure of the Superior and Grenville provinces of the northeastern Canadian shield. *Bull. Seismol. Soc. Am.*, 63: 1393-1432.
- Bouchon, M., 1982. The complete synthesis of seismic crustal phases at regional distances. *J. Geophys. Res.*, 87: 1735-1741.
- Braile, L.W., 1977. Interpretation of crustal velocity gradients and Q structure using amplitude-corrected seismic refraction profiles. In: J.G. Heacock (Editor), *The Earth's Crust*. American Geophysical Union, Geophysical Monograph 20, Washington, DC, pp. 427-439.
- Haskell, N., 1966. The leakage attenuation of continental crustal P waves. *J. Geophys. Res.*, 71: 3955-3967.
- Hirn, A., Steinmetz, L., Kind, R. and Fuchs, K., 1973. Long range profiles in western Europe. II. Fine structure of the lower lithosphere in France (southern Bretagne). *Z. Geophys.*, 39: 363-384.
- Kind, R., 1974. Long range propagation of seismic energy in the lower lithosphere. *J. Geophys.*, 40: 189-202.
- Kind, R., 1978. The reflectivity method for a buried source. *J. Geophys.*, 44: 603-612.
- Mereu, R.F., Majumdar, S.C. and White, R.E., 1977. The structure of the crust and upper mantle under the highest ranges of the Canadian Rockies from a seismic refraction survey. *Can. J. Earth Sci.*, 14: 196-208.
- Mueller, S., 1977. A new model of the continental crust. In: J.G. Heacock (Editor), *The Earth's Crust*. American Geophysical Union, Geophysical Monograph 20, DC, pp. 289-317.
- Müller, G. and Fuchs, K., 1976. Inversion of seismic records with the aid of synthetic seismograms. In: P. Giese, C. Prodehl and S. Stein (Editors), *Explosion Seismology in Central Europe*. Springer, Berlin, pp. 178-188.
- Olsen, K.H. and Braile, L.W., 1981. Seismograms of explosions at regional distances in the western United States: observations and reflectivity method modeling. In: E.S. Husebye and S. Mykkeltveit (Editors), *Identification of Seismic Sources — Earthquake or Underground Explosion*. Reidel, Dordrecht, pp. 453-466.
- Prodehl, C., 1979. Crustal Structure of the Western United States. Prof. Pap. 1034, U.S. Geol. Survey, Washington, DC, 74 pp.
- Ryall, A. and Stuart, D.J., 1963. Travel times and amplitudes from nuclear explosions. Nevada Test Site to Ordway, Colorado. *J. Geophys. Res.*, 68: 5821-5835.
- Shurbert, D.H., 1960. The P phase transmitted by crustal rock to intermediate distances. *J. Geophys. Res.*, 65: 1809-1814.
- Shurbert, D.H., 1969. A low-velocity layer in the Earth's crust. *Geol. Soc. Am. Bull.*, 80: 895-898.

## Amplitude Study of the *Pg* Phase\*

E. Banda<sup>1</sup>, N. Deichmann<sup>1</sup>, L.W. Braile<sup>2</sup>, and J. Ansorge<sup>1</sup>

<sup>1</sup> Institute of Geophysics, ETH-Hoenggerberg, CH-8093-Zürich, Switzerland

<sup>2</sup> Department of Geosciences, Purdue University, West Lafayette, Indiana 47907, USA

**Abstract.** The amplitude of the *Pg* phase, as recorded in explosion seismology studies, is analyzed with the aid of synthetic seismograms. Parameters such as source frequency, low-velocity cover above the crust (sediments or weathered layer), low-velocity layers within the upper crust, velocity gradients, thickness of the gradient zone, attenuation and Poisson's ratio strongly influence the amplitude-distance pattern of the *Pg* phase. A systematic study clearly shows that different models of the continental upper crust display distinct amplitude-distance characteristics. These models could not be distinguished by travel-time interpretation alone.

In the presence of gradient zones the amplitude-distance curve shows different patterns depending on the source frequency. The higher the frequency, the more pronounced are the relative maxima in the amplitudes. The presence of a low-velocity cover at the surface accentuates the character of the amplitude-distance curves even if the cover is thin (a few hundred meters). Moreover, a low-velocity cover produces *P* to *S* conversions and multiples following the *Pg* which obscure possible secondary crustal phases. The thickness of the velocity gradient zone influences the amplitude decay and the width of the relative maxima. Low-velocity layers within the upper crust cause a faster drop-off of the amplitudes than would be expected from ray theory. Detailed *Pg* amplitude studies are thus useful in improving the knowledge of the physical properties of the upper continental crust. The application of the derived criteria to two sets of real data allow us to determine fine details of the velocity-depth function which are of great importance for the understanding of the earth's crust.

**Key words:** Explosion seismology – Upper continental crust – Seismic amplitude – Source frequency – Low-velocity layer – Velocity gradient.

### Introduction

Understanding the fine structure and physical properties of the continental crust is one of the principle goals of explosion seismology. Interpretation of seismic refraction data using traditional travel-time methods gives only a

rough picture of the velocity-depth structure. The increasing use of the ray tracing interpretation techniques and methods derived from the Herglotz-Wiechert travel-time inversion (including  *$\tau$ - $p$*  methods) result in velocity models of the upper crust that include velocity gradients which are very often poorly defined. In fact, layers with constant velocity, the simplest model, fit the travel-time data equally well in most cases. Healy (1963) has shown that very different velocity-depth models, from homogeneous layers to continuous gradient zones can fit equally well the travel-time data for a particular phase. However, as will be shown below, the amplitude-distance character of these models may be significantly different. At present, either very detailed travel-time information or amplitude studies are the only techniques available for accurate determination of velocity gradients in the earth's crust.

In the following discussion, we use the term upper crust for the upper 10–15 km of the crystalline continental basement lying immediately beneath the surface sediments and above the lower crustal layer. The *P*-wave velocity of the upper crust normally varies between 5.7 and 6.3 km/s. These velocities are characteristic of sialic rocks at the appropriate upper crustal temperature and pressures. The compressional seismic wave critically refracted (head wave) in the upper crust is usually called *Pg*. In explosion seismic studies, the *Pg* phase is normally recognized as the first arrival in the distance range of about 10–100 km. The notation *Pg* is also used in earthquake seismology studies but in these cases it often refers to a different phase at larger distances.

Studies of the *Pg* phase recorded in refraction profiles (Müller and Fuchs, 1976; Müller and Mueller, 1979; Banda and Ansorge, 1980; Braile et al., 1982) have shown how amplitude information can be used to greatly reduce the range of models fitting the travel-time interpretation. As refraction surveys are becoming more detailed, with closely spaced recordings and improved amplitude control, we feel that the qualitative comparisons attempted so far in most amplitude studies are not enough, and that understanding the variation of *Pg* amplitudes as a function of various parameters will provide further insight into the velocity structure of the upper crust. In turn, this information will serve as a basis for comparison with laboratory measurements and petrological studies leading to a better knowledge of the physical properties of the basement.

In this paper we discuss, on the basis of synthetic seismograms, the *Pg* amplitude-distance curves and their vari-

\* Contribution No. 383 Institute of Geophysics ETH-Zürich, Switzerland

Offprint requests to: J. Ansorge

ation with parameters such as frequency content of the source, presence of low-velocity cover and of low-velocity layers within the upper crust, velocity gradients, thickness of the gradient zone, attenuation ( $Q^{-1}$ ) and Poisson's ratio. We also present examples of amplitude-distance modelling for observed  $P_g$  amplitude data from central Europe and western North America.

### Methods of Computation

Synthetic seismograms can at present be calculated by a variety of methods. For our purposes we have used the reflectivity method developed by Fuchs (1968) and Fuchs and Müller (1971) with the fundamental modification by Kind (1978) and the asymptotic ray method described by Červený et al. (1977). These two methods and others have been extensively discussed in the literature (see Chapman, 1978 and Spudich and Orcutt, 1980 for reviews).

Since the objective of this paper is to describe in detail the amplitude-distance behaviour of the  $P_g$  wave and to understand related later arrivals (multiply reflected, refracted and/or converted), we have used mainly the reflectivity method. The modification by Kind (1978) includes these secondary effects by taking into account the free surface and placing the source in the reflectivity zone. This technique requires velocity models consisting of laterally homogeneous and isotropic layers. Velocity gradients are approximated by a stack of thin layers with small velocity

contrasts. For our computations we have used thicknesses corresponding to less than one wavelength of the frequency range considered.

Record sections of the vertical component of ground displacement have been calculated for all the models with a distance interval of 5 km between 0 and 100 km (Fig. 1). Except where stated, the  $V_p/V_s$  ratio was assumed to be  $\sqrt{3}$  (Poisson ratio = 0.25) and the  $Q_p$  values were fixed at 100 for the sediments or weathered layer and at 500 for the basement with  $Q_s$  equal to  $4Q_p/9$ . The depth of the source was fixed at 100 m depth.

All record sections were plotted with a reduction velocity of 6.0 km/s and the amplitudes of each trace were multiplied by the distance for a more accurate reading of the amplitudes (Fig. 1). Amplitudes were read taking the maximum (peak-to-peak) of the first cycle (reading the first pulse has given identical results for theoretical seismograms). Finally the amplitude readings were plotted as function of distance, as shown in Fig. 1.

The phase velocity interval used to determine the range of angles of incidence over which the reflectivity program integrates was 0.2–0.4 km/s below the minimum velocity in the models and 1.0–2.0 km/s above the maximum. This range includes all of the compressional and shear waves of interest propagating in the upper crust. The large phase velocity range leads, especially for high frequencies, to very long computer runs (e.g. for the model in Fig. 1, 23.3 min CPU time on a Cyber M0722A). However, it is worthwhile

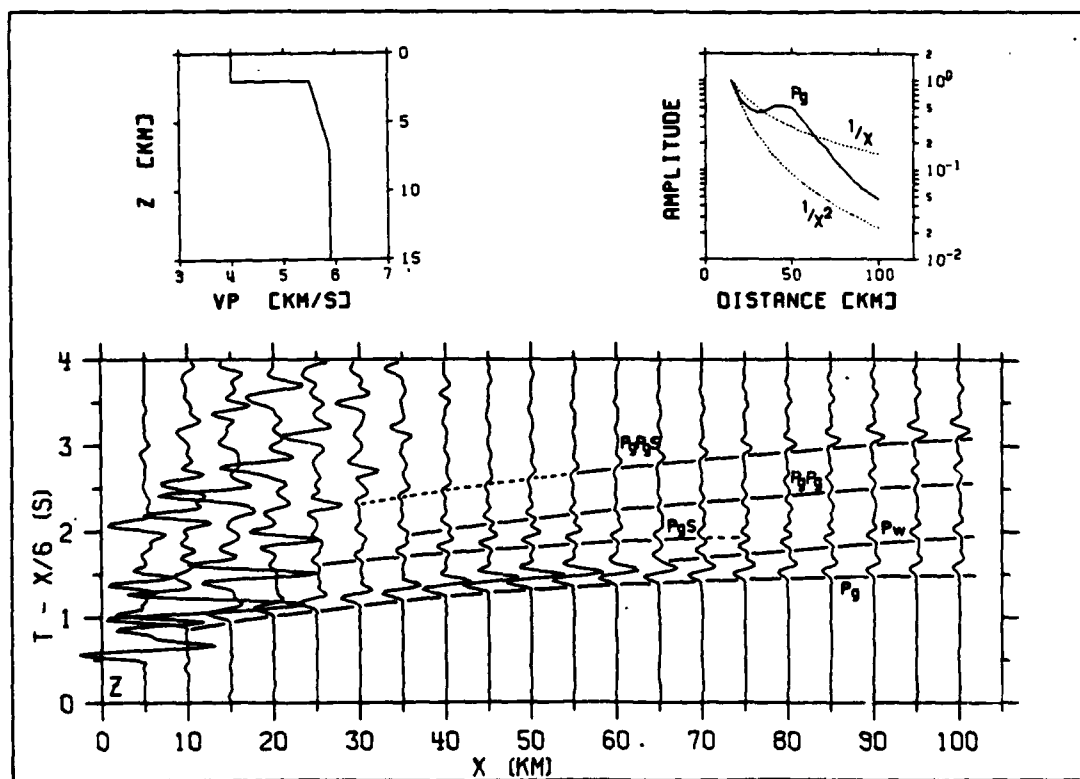


Fig. 1. Example of synthetic record-section calculated using the reflectivity method with a dominant frequency of 4 Hz for model PG11K, displayed in the left inset. The amplitude-distance curve (solid line) is shown together with the curves for  $1/x$  and  $1/x^2$  decays in the right inset. Note the prominent secondary phases: Pw, whispering gallery (see Červený et al., 1977),  $P_g(S)$ , direct  $P_g$  converted to S at the base of the sediments,  $P_gP_g$ ,  $P_g$  reflected once at the free surface,  $P_gP_g(S)$ , reflected  $P_g$  converted to S

Table 1. Model parameters

Model	Lower limit of layer (km)	Layer thickness (km)	$V_p$ (km/s)	Number of layers	Gradient (km/s/km)
PG1	2.0	2.0	4.0	2	0.0
	15.0	13.0	6.0	5	0.0
	20.0	5.0	6.5	2	0.0
PG3	2.0	2.0	4.0	2	0.0
	15.0	13.0	5.9-6.1	5	0.015
	20.0	5.0	6.1	2	0.0
PG6	2.0	2.0	4.0	2	0.0
	15.0	13.0	5.75-6.25	5	0.038
	20.0	5.0	6.25	2	0.0
PG11	2.0	2.0	4.0	2	0.0
	15.0	13.0	5.5-6.5	5	0.077
	20.0	5.0	6.5	2	0.0
PG11K	2.0	2.0	4.0	2	0.0
	7.0	5.0	5.5-5.885	5	0.077
	20.0	13.0	5.885	3	0.0
PG11KK	2.0	2.0	4.0	2	0.0
	10.0	8.0	5.5-6.12	10	0.077
	20.0	10.0	6.12	2	0.0
PG11L	2.0	2.0	4.0	2	0.0
	7.0	5.0	5.5-5.885	5	0.077
	12.0	5.0	5.5	1	0.0
	20.0	8.0	6.3	1	0.0
PG11LL	2.0	2.0	4.0	2	0.0
	10.0	8.0	5.5-6.12	8	0.077
	15.0	5.0	5.5	1	0.0
	20.0	5.0	6.3	1	0.0
PG12	2.0	2.0	4.0	2	0.0
	15.0	13.0	6.1-5.9	5	-0.015
	20.0	5.0	6.5	2	0.0
PG22	2.0	2.0	4.0	2	0.0
	15.0	13.0	5.3-6.7	5	0.108
	20.0	5.0	6.7	2	0.0
SULZ3	1.0	1.0	4.5	2	0.0
	1.3	0.3	4.8-5.6	1	2.67
	5.0	3.7	5.6-5.9	5	0.081
	10.0	5.0	5.9-6.1	7	0.04
	21.0	11.0	6.1	2	0.0
SULZ4	1.0	1.0	4.3	2	0.0
	1.3	0.3	4.8-5.6	1	2.67
	6.3	5.0	5.6-6.0	6	0.08
	17.0	10.7	6.0	2	0.0
SULZ6	1.0	1.0	4.6	2	0.0
	5.7	4.7	5.6-5.95	7	0.074
	8.2	2.5	5.95-6.0	4	0.02
	17.0	8.8	6.0	1	0.0
SULZ7	1.0	1.0	4.6	2	0.0
	5.7	4.7	5.6-5.95	7	0.074
	7.0	1.3	5.95-5.98	3	0.023
	17.0	10.0	5.98	1	0.0

performing these computations to reveal the influence of the sediments. Many tests were run before choosing the best illustrative models for the purpose of this paper, which are listed in Table 1.

To compare the performance of the reflectivity method

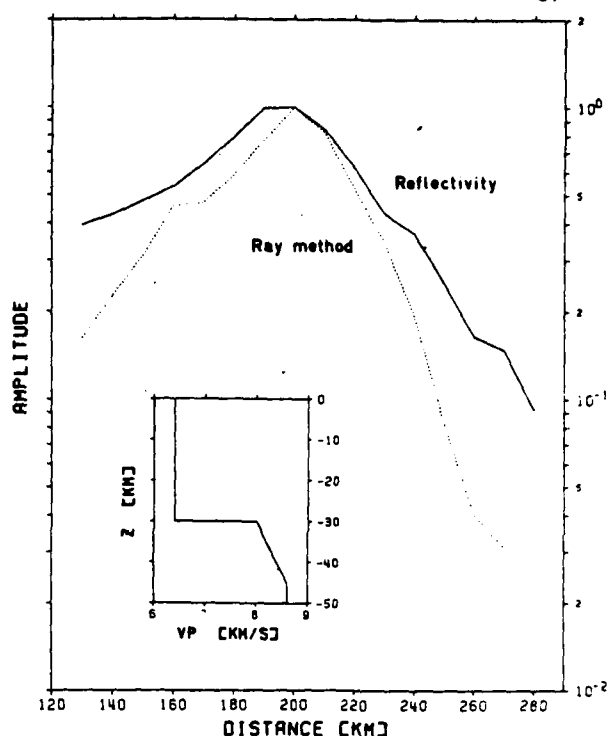


Fig. 2. Amplitude-distance curves (peak-peak) of  $P_n$  phase for model EC4 (Červeny, 1979) computed using reflectivity (continuous line) and using ray-method (dotted line)

with the asymptotic ray theory method, we started by determining the amplitude-distance curves for one of the models published by Červeny (1979) for which he used both methods (Fig. 2). Although this case deals with a gradient zone in the upper mantle, the situation is analogous to a gradient zone in the upper crust with a sedimentary layer above. The ray method obviously sharpens the peak of the amplitude-distance curve. This is because the asymptotic ray method represents a "high frequency approximation" to the wave equation (Červeny et al., 1977; Chapman, 1978). As is shown below, similar results were obtained from other computations in this study. The ray method is inexpensive and for much of the available data and some crustal models, which can also include lateral inhomogeneities, this approximation is accurate enough. For more detailed studies, in which the models can be approximated by flat homogeneous layers, the reflectivity method is more appropriate and has therefore been used in this paper.

The synthetic seismograms computed in this study represent ground displacements instead of ground velocities, as measured in observed seismograms. As shown in the example in Fig. 3, for which both velocity and displacement were calculated, the difference in the amplitude-distance behaviour is not significant. At least for the models presented here, the results from displacement can thus be applied directly to observed velocity data. Moreover, it should be noted that the dominant frequency used in displacement computations is increased when the displacement seismograms are differentiated to obtain velocity (see spectra in Fig. 3).

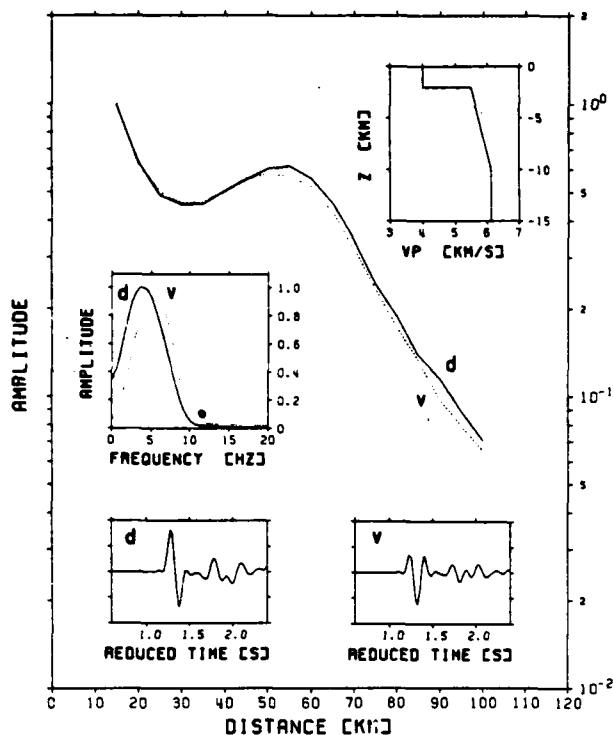


Fig. 3. Comparison of amplitude-distance curves of displacement (continuous line) and velocity (dotted line) seismograms for model PG11KK (upper right inset). The corresponding spectra show the frequency shift between displacement and velocity signals. The bottom insets show the signals (at 35 km) for displacement and velocity; the intervals used to calculate the spectra are marked by vertical bars

### Discussion of Model Parameters

#### Source Frequency

The frequency content of seismic refraction data varies from about 2 Hz to more than 20 Hz depending on the shooting technique, charge size, frequency response of the instrument and local geological environment. Comparison of the shape of the amplitude-distance curves for low frequency source signals ( $\sim 2$  Hz) with those for high frequency ( $\approx 8$  Hz) shows significant differences when velocity gradients are truncated at shallow depth or low-velocity layers are present in the model. For that reason we have computed most of the models for frequencies 2–8 Hz.

Figure 4 shows an example of the results for model PG11K computed for 2.5, 4, 6 and 8 Hz dominant frequencies. The fact that the velocity structure of the upper crust changes, from a positive gradient (0.077 km/s/km) to zero gradient at 7 km depth produces a different response of the medium depending on the source frequency. The variation of amplitude with distance is more pronounced at the higher frequencies. As discussed in more detail below, this is due to the fact that shorter wavelengths are affected mainly by the focusing effect of the gradient zone, thus producing strong relative amplitude-maxima at a distance of 45 km. At the same distance, longer wavelengths are already affected by the homogeneous layer beneath the gradient zone. Higher frequencies are thus more informative in amplitude studies.

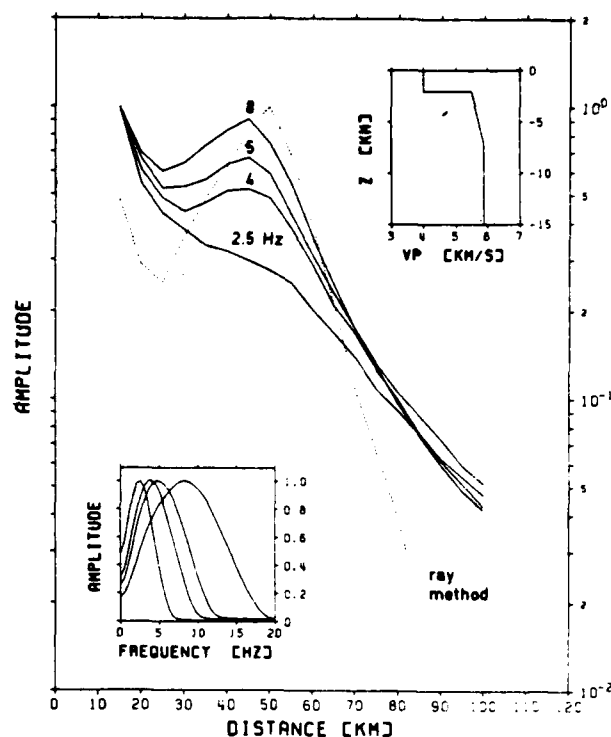


Fig. 4. Amplitude-distance curves for model PG11K (upper right inset) for frequencies of 2.5, 4, 5 and 8 Hz (Fourier spectra in the lower inset) computed using reflectivity method (continuous lines). Dotted line corresponds to ray-method computation with program SEIS4

For the same model, amplitudes were computed with the asymptotic ray theory and are also displayed in Fig. 4. As was to be expected, the ray method works reasonably well for high frequencies, although the slope of the amplitude decay is somewhat enhanced. Asymptotic ray theory accounts for the influence of different frequencies on the amplitudes of waves reflected at first order discontinuities (Červený et al., 1977) but not for waves refracted from a gradient zone (Banda, 1979). Therefore, if we are dealing with good quality data, suitable for amplitude studies, it is of fundamental importance to compute the theoretical seismograms using the reflectivity, or other wave theory method, with a source which has a dominant frequency similar to that of the experimental data.

#### Thickness and Velocity Structure of Sediments

Qualitative differences in the character of the wave field due to the presence of sediments are well known. Their influence was studied quantitatively with models which are identical except for the velocity structure of the sediments.

Figure 5 shows the results for models with 0, 0.2, 2 and 5 km of sediments overlying an upper crust containing a velocity gradient of 0.077 km/s/km. Beyond about 60 km the shapes of the amplitude-distance curves are essentially identical. The most important difference is that even for models with as little as 0.2 km of sediments, a relative maximum of the amplitude curve is observed which is missing

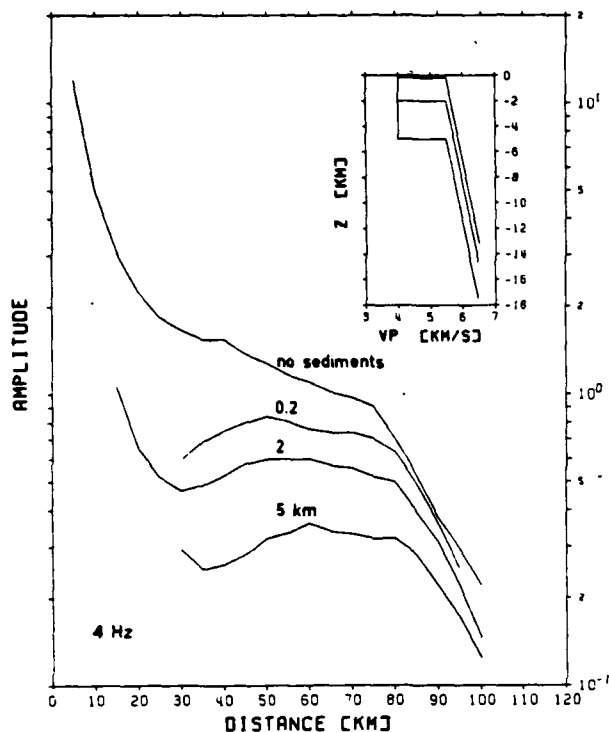


Fig. 5. Amplitude-distance curves for model PG11 with 0.0, 0.2, 2.0 and 5.0 km of low-velocity material (inset upper right) overlying the basement

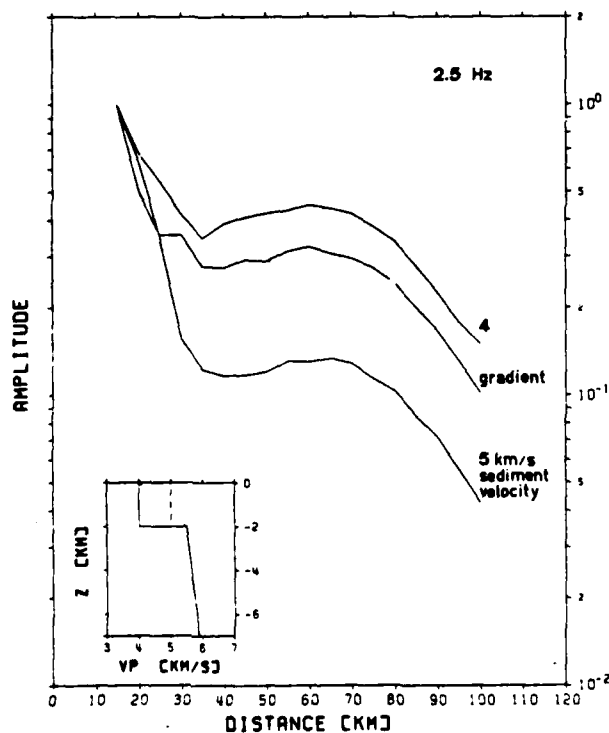


Fig. 6. Amplitude-distance curves for model PG11 (2.5 Hz) with different velocity structures of the low-velocity cover of the basement (inset lower left)

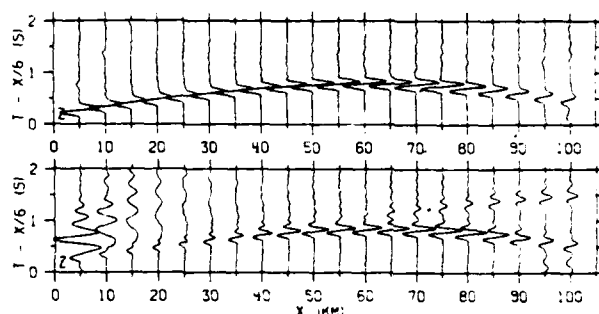


Fig. 7. Record-sections for model PG11 (4 Hz) with and without low-velocity cover (0.2 and 0.0 km, lower and upper sections respectively). Note the difference in the wave field of secondary arrivals (see also Fig. 1)

for the model without sediments. We interpret this as an effect of the change of the angle of incidence affecting the transmission coefficient. On the other hand, models with a low-velocity cover alone and without a gradient in the upper crust do not have a relative amplitude maximum.

Results for models with different velocity structures in the sediments are displayed in Fig. 6, which show that there is no significant difference in the overall shape of the  $P_g$  amplitude-distance curves. However, the level of the amplitudes at the local maximum around 60 km relative to the amplitudes at 15 km is lower for sediments with a velocity of 5 km/s than for those of 4 km/s or for sediments with a velocity gradient starting with 4 km/s at the surface. This again is due to the fact that the angle of incidence is steepened by the lower velocity at the surface, thus producing higher  $P$ -wave amplitudes on the vertical component seismograms studied here.

As a result, we can state that any influence of the thickness and velocity structure of the sedimentary layer on the amplitude-distance behaviour of the first cycle of the  $P_g$  phase is restricted to shorter distances. However, the total wave fields for models with and without sediments are radically different. Reverberations within the sediments and  $P$  to  $S$  conversions result in conspicuous seismic phases that appear after the  $P_g$  phase (Fig. 7, see also Fig. 1).

#### Thickness of Gradient Zone and Low-Velocity Layers

Significant differences in the amplitude-distance curves for models having the same gradient but different thickness of the gradient zone are shown in Fig. 8. The models include structures with a continuous gradient between 2 and 15 km (model PG11), 2 and 10 km (model PG11KK) and 2 and 7 km (model PG11K) on top of a half space. A decrease in the thickness of the gradient zone leads to a faster drop-off of the amplitudes with distance.

The introduction of a low-velocity layer below a gradient zone between 2 and 7 km and 2 and 10 km (models PG11L and PG11LL) show another interesting effect. A significant shift of the maximum and a change in the slope of the amplitude decay is evident when a low-velocity layer is present at the same depth at which the gradient is terminated (compare PG11K and PG11L in Fig. 8).

The influence of the frequency content of the source in the presence of a low-velocity layer is shown in Fig. 9. The main effects are to sharpen the maximum and to shift

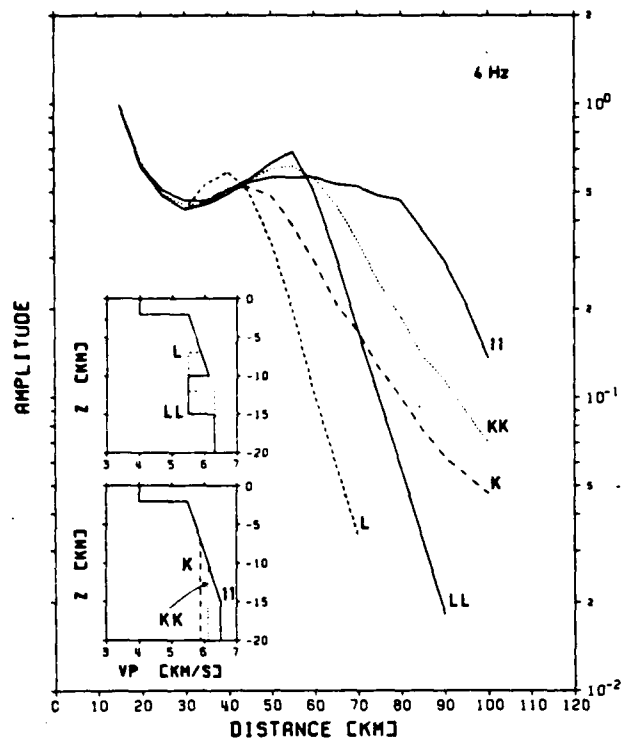


Fig. 8. Amplitude-distance curves for models PG11, PG11K, PG11KK with variable gradient zone thickness (continuous, dashed and dotted lines, respectively in the lower inset) and PG11L and PG11LL with low-velocity layer at different depths (dashed and continuous lines, respectively, in the upper inset) computed for a frequency of 4 Hz

it to larger distances as the frequency is increased. Model PG11L peaks very smoothly for 2.5 Hz at about 30 km whereas it peaks sharply at 40 km for the higher frequencies. The waves behave as if they "sense" the low-velocity layer well before this would be expected from ray considerations. To illustrate the effect of the truncated gradients, the ray tracing for model PG11K is shown in Fig. 10. Here, even though the gradient zone is terminated at a depth of 7 km, we observe rays emerging at distances out to 58 km, which is in disagreement with the results from these amplitude calculations. As stated above, a decrease in thickness of the gradient zone causes the Pg-amplitude drop-off to occur at smaller distances than expected. For models PG11K and PG11L, in which the gradient zone is terminated at 7 km depth, the amplitudes start deviating from those of model PG11, whose gradient extends down to 15 km, at distance as short as 45 km. As is shown in Fig. 10 rays arriving at this distance reach a maximum depth of only 4.9 km, which is well above the bottom of the gradient zone. In fact, the distance between the turning point of the ray and the bottom of the gradient zone is greater than one wavelength (about 1.5 km at 4 Hz). This phenomenon, which can not be explained by geometrical ray theory, is analogous to the Fresnel-zone effect in the case of electromagnetic waves: the energy arriving at a receiver is due not only to the ray propagating with minimal travel-time, but, as a consequence of Huyghens' principle, consists of diffractions interfering with each other, whose travel-times are greater than that of the direct wave (Born, 1933). Mod-

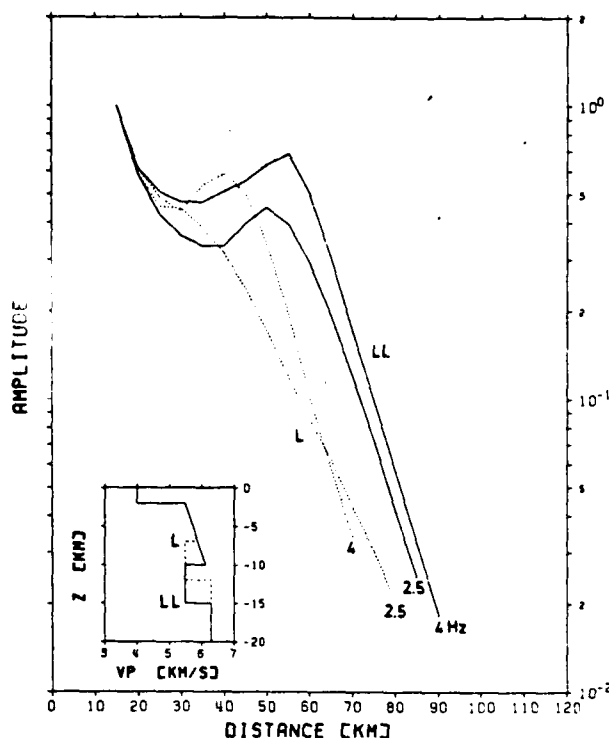


Fig. 9. Amplitude-distance curves for models PG11LL and PG11L (continuous and dotted lines respectively, in the inset) computed for 2.5 and 4 Hz

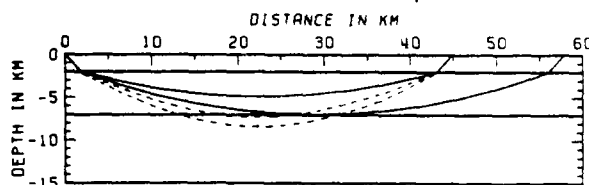


Fig. 10. Ray-trace for model PG11K, with the ray emerging at 45 km and the ray grazing the lower boundary of the gradient zone emerging at 58 km (solid curves). The lower dashed curve shows the edge of the first Fresnel-zone (corresponding to a phase shift of  $T/2$ ) while the upper dashed curve corresponds to a phase shift of  $T/4$  for a signal with 4 Hz dominant frequency

fications of asymptotic ray theory which take this effect into account have been introduced by various authors (see Spudich and Orcutt, 1980 for a review). In particular, Wiggins (1976) approximates the wave behaviour by envisaging the energy transported by a ray as being distributed over a disk travelling with that ray, and constructs a synthetic seismogram by summing the contribution of neighbouring rays as their disks intersect the surface at the distance of interest. As can be seen from the dashed ray-paths in Fig. 10, the first Fresnel zone, which contains the most significant contributions to the amplitude of the signal, extends to a depth beyond the limit of the gradient zone for energy arriving at a distance of 45 km. Thus, changes in gradient will influence the amplitudes of waves with longer periods at smaller distances than those with shorter periods. This is also the reason for the marked shift of the amplitude peak in models PG11L and PG11LL between

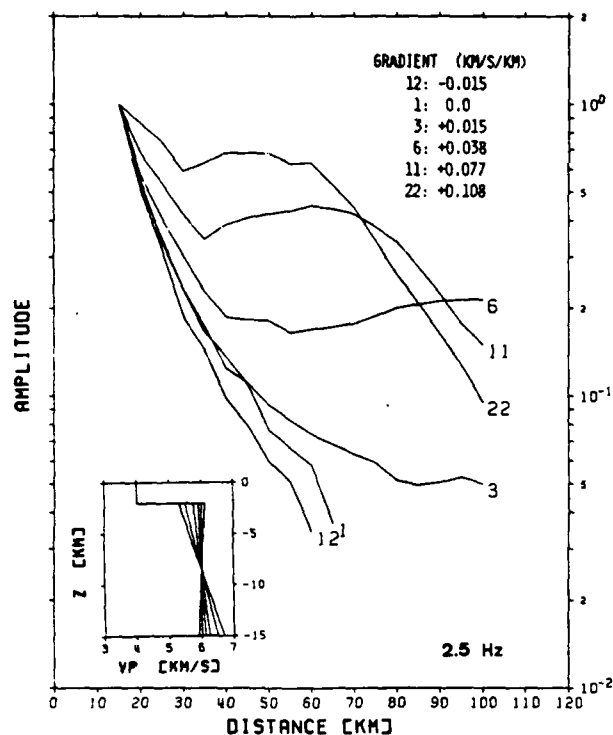


Fig. 11. Amplitude-distance curves for models PG12 (negative gradient), PG1 (no gradient) and PG3, PG6, PG11 and PG22 (positive gradients) for a frequency of 2.5 Hz (see Table 1 for model specifications)

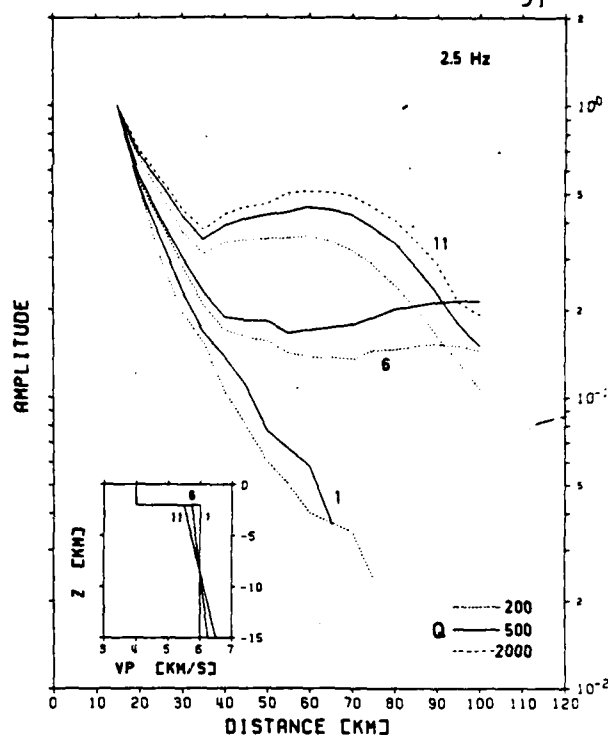


Fig. 12. Amplitude-distance curves for models PG1, PG6 and PG11 (see inset and Table 1) for  $Q=500$ , continuous lines,  $Q=200$ , dotted lines and  $Q=2000$  (dashed line for model PG11)

2.5 and 4 Hz, and for the frequency dependence shown in Fig. 4.

Reflections originating from the low-velocity layer have also been studied. Our results do not differ from those published by Braile and Smith (1975), Smith et al. (1975) and further modified by Banda (1979): the reflection from the top of the low-velocity layer will only be seen as a separate phase when the upper crust has a very small or zero gradient, the frequency is high enough and the transition is nearly a first order discontinuity. In this case the interference of  $P_g$  with the reflection changes the  $P_g$  amplitudes at larger distances (this has not been studied in detail in this paper). If the above mentioned conditions are not fulfilled the  $P_g$  amplitudes will barely be affected by the reflection from the top of the low-velocity layer.

#### Variation of Gradients

It is well known that even a slight positive velocity gradient greatly influences the amplitude of refracted phases (Červeny, 1966; Hill, 1971). Thus, we have tried to vary systematically the velocity gradient in the basement models in order to determine the corresponding amplitude-distance curves. We have arbitrarily chosen the gradient to be linear. Amplitudes for models with various gradients between  $-0.015$  and  $0.108$  km/s/km were computed and are shown in Fig. 11. From a comparison with a calculation for model GP11 at higher frequency and from the discussion in the previous section, it can be stated that, although these curves

were calculated for 2.5 Hz, they are also representative of higher frequencies as long as the gradient zones extend to sufficient depth. The results shown in Fig. 11 illustrate that small positive velocity gradients in the upper crust will be resolvable by amplitude measurements on reasonably good experimental data. For example, the amplitude-distance characteristics of Models PG1 and PG6 are significantly different although the velocity structure differs only by the presence of a small ( $0.038$  km/s/km) gradient in Model PG6.

#### Attenuation ( $Q$ )

We have tested models with  $Q$  values for compressional waves of 200, 500 and 2000 for the upper crust to investigate the influence of attenuation upon the amplitude of the  $P_g$  wave. The curves shown in Fig. 12 are not sufficiently distinct for us to infer apparent  $Q$  from  $P_g$  amplitude calculations. As already demonstrated by Hill (1971) a slight change in the gradient could make up for the differences shown in Fig. 12 without taking the attenuation into account. To estimate  $Q$  in the basement one could use the method proposed by Braile (1977) which requires that the  $P_g$  amplitudes be modelled simultaneously with the amplitudes of the reflection from the bottom of the upper crust. Alternatively, if the geometrical spreading factors are sufficiently well known, and the band-width of the source is broad enough, it is conceivable that spectral ratio methods (see Báth, 1974 for a review) might be adequate to infer  $Q$  in the upper crust.

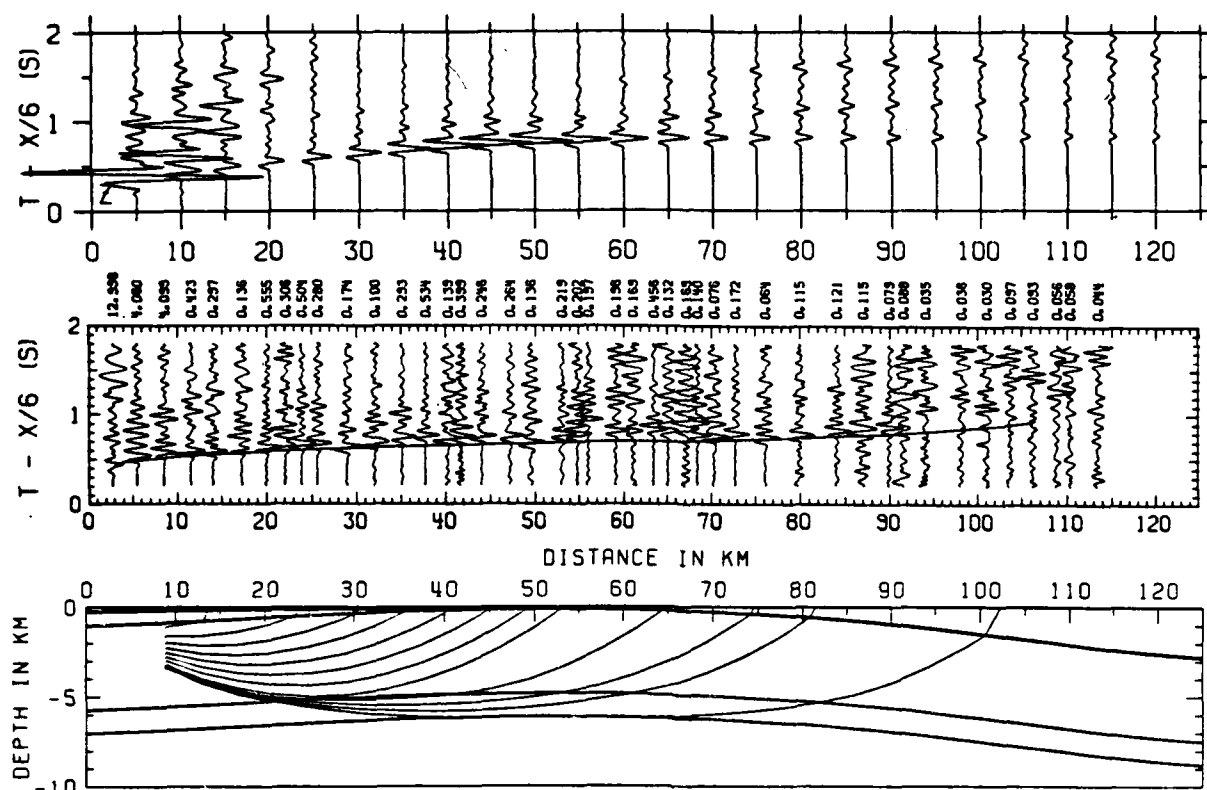


Fig. 13. Bottom: ray-trace for model Sulz-7. Note vertical exaggeration of model plot. Middle: record section of Sulz-south data, vertical component, bandpass filtered 8-16 Hz, trace normalized. Travel-time curve corresponds to ray-trace below. Top: synthetic record section of flat layer approximation of model Sulz-7 (see Fig. 14 and Table 1) vertical component velocity amplitude multiplied by distance

#### Poisson's Ratio ( $\sigma$ )

Seismic velocity studies of the crust show that a Poisson ratio of 0.25 is in general a good average. However, in some cases strong deviations from this value have been found. The influence of  $\sigma$  has been studied for a few models with values 0.2-0.35. The resulting amplitude-distance curves do not differ significantly from each other. Only curves for models involving a sudden change of  $\sigma$  at a discontinuity produce distinct features in the  $P_g$  versus reflection amplitude ratio as already shown by Olsen et al. (1979).

#### Examples of Data from the Black Forest (Germany) and the Basin and Range (U.S.A.)

Between 1974 and 1980 several quarry blasts near Sulz, southern Germany, were recorded along a 113 km long profile running south along the eastern margin of the Black Forest into the Swiss Alpine foreland. The first 2 s of the resulting seismic record-section are shown in Fig. 13 together with the travel-time curve corresponding to the ray-trace model in the lower part of the figure. The ray tracing was performed using the method of Gebrande (1976).

The velocity structure of the sediments (including a wedge of late Paleozoic and early Mesozoic sediments with  $P$ -velocity of 3.8 km/s between 0 and 40 km) and the shape of the basement/sediments boundary were modelled to fit the available bore-hole data (Buechi et al., 1965; Boigk and

Schoeneich, 1968; Lemcke et al., 1968). The velocity structure of the basement was then adjusted until the general shape of the travel-time data was matched. No attempt was made to model the local variations in sedimentary structure and basement depth which produce the small time discrepancies, limited to one or two consecutive records. This applies particularly to the local anomaly between 94 and 101 km which, because of the poor signal to noise ratio, cannot be resolved with these data alone.

For plotting convenience, the seismograms in Fig. 13 were trace normalized. The peak-to-peak amplitudes of the first cycle were multiplied by the scale factor marked above each seismogram to obtain the true particle velocity values in  $\mu\text{m/s}$ . The amplitude data for the  $P_g$  phase are plotted as crosses with corresponding shot and station numbers in Fig. 14.

The size of shot number 1 was only 700 kg while the others were around 2,000 kg, so that the corresponding amplitude values were multiplied by a correction factor of 1.4, equal to the cube root of the charge ratio, which seems to be appropriate for this specific quarry. The remaining scatter seems to be independent of the shots, and although it amounts to about a factor of two, the data define an amplitude-distance behavior characterized by a rapid decrease in the first 20 km, a local maximum at about 40 km and a smooth decay out to about 100 km.

In order to be able to apply the reflectivity method to the data, the curved layers derived from the ray-tracing technique were approximated by flat layers in model

AD-A128 305

SYNTHETIC SEISMOGRAM MODELING(U) PURDUE UNIV LAFAYETTE  
IN DEPT OF GEOSCIENCES L W BRAILE 15 NOV 82  
TR-1-82-ONR N00014-75-C-0972

2/2

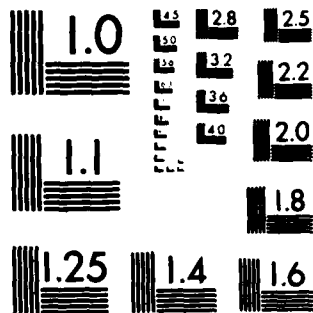
UNCLASSIFIED

F/G 8/11

NL



END  
DATE  
FILMED  
6 83  
DTIC



MICROCOPY RESOLUTION TEST CHART  
NATIONAL BUREAU OF STANDARDS-1963-A

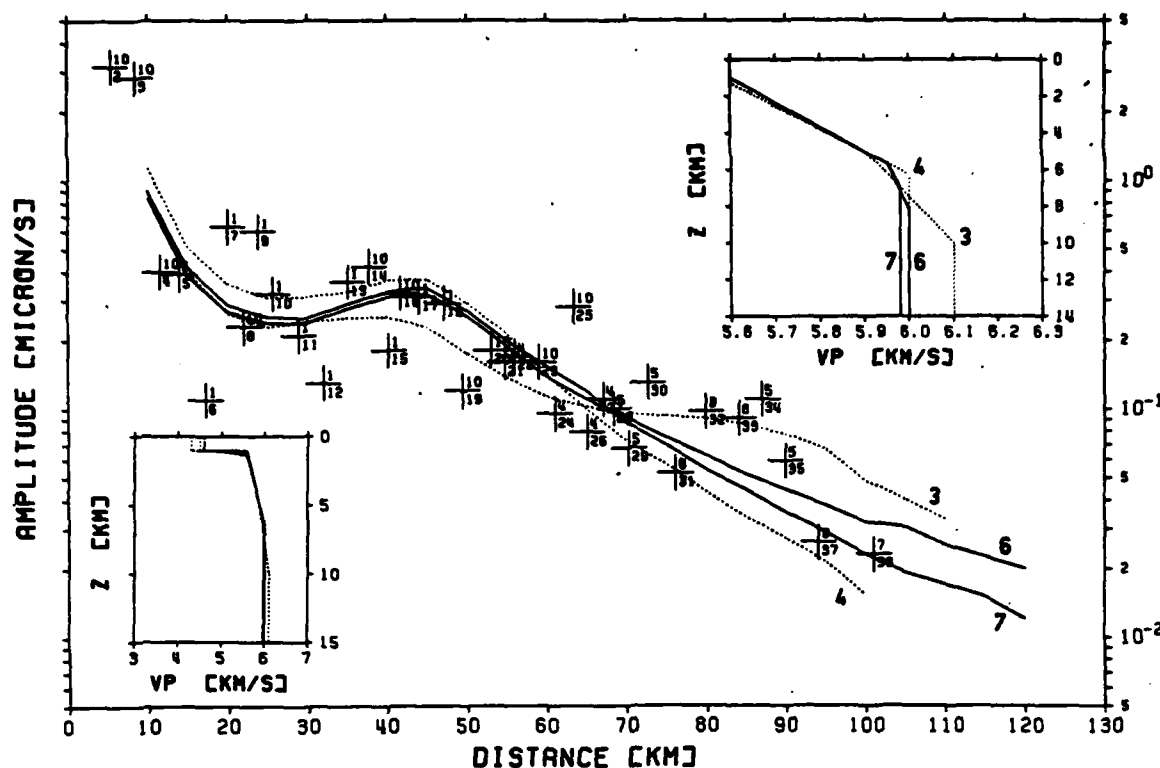


Fig. 14. Amplitude data of Sulz-South record section (Fig. 13) (crosses with shot and station numbers) and amplitude-distance curves for the four models shown in the lower inset and listed in Table 1. Top inset shows an enlarged view of the gradient zones of the four models

number 7 (insets in Fig. 14 and Table 1) and the sediments were simplified to a single layer. The resulting synthetic record section (vertical ground velocity with a dominant frequency of 8 Hz) is reproduced at the top of Fig. 13. The offset of the calculated amplitude-distance curve as a whole was adjusted to the experimental data by a least-squares method (Fig. 14, curve 7). For three other ray-trace models which satisfy the travel-time data equally well, amplitude-distance curves were calculated in the same way and plotted in Fig. 15 together with their velocity-depth functions. This illustrates some of the possible model variations. A comparison between models 3 and 4 shows how a second gradient zone of sufficient strength and extent can significantly increase the distance at which the amplitude decay occurs. Models 6 and 7 illustrate the effect of small changes in the extent of a second zone with slight gradient. The logarithmic standard deviations of data points from these curves range between 0.23 and 0.27, which correspond to amplitude factors of 1.7 and 1.9 respectively. The amplitude-distance behaviour of the models presented here do not differ from each other sufficiently to be able to discriminate between them on the basis of this data alone. However, as the insets in Fig. 14 show, the velocity-depth variations of these models are very small, so that the results are good evidence for a strong gradient (0.07–0.08 km/s/km) in the upper 5–6 km of the basement.

It should be noted that computational techniques restrict us to consideration of flat-layered models for the amplitude modelling even though small lateral variations are evident in the travel-time model for the Sulz data as shown

in Fig. 13. Shooting up-dip over the first 50 km and down-dip beyond that distance will have a slight focusing effect on the rays, thus contributing somewhat to the observed relative amplitude maximum at that distance. However, because the lateral changes in velocity structure indicated in Fig. 13 are small (note that the model is plotted with  $2 \times$  vertical exaggeration) and because the positive velocity gradients in the flat-layered models which satisfy the amplitude data also fit the travel-time data modelled with a curved sediment-basement boundary, we anticipate that the amplitude-distance effects of the two-dimensional structure will be negligible.

A very different amplitude-distance character of the  $P_g$  phase is observed for the Basin and Range province of the tectonically active western North American continent. A  $P_g$  data-set from this region was analyzed for this study. The seismic records are from the northern Basin and Range (NBR) (shotpoints Mountain City, Eureka and Elko) in Western United States and were originally studied by Hill and Pakiser (1966) and presented by Prodehl (1970, 1979).

Partial record sections emphasizing the  $P_g$  arrivals for the NBR data are shown in Fig. 15. The record sections are from Prodehl (1979) and the travel-time curves shown are the results of ray-trace modelling by Fauria (1981). Amplitudes of the  $P_g$  phase were read from the sections shown in Fig. 15 and corrected for plot scaling factors using the calibration signals presented on the original sections (Prodehl, 1979). The  $P_g$  amplitudes were adjusted to account for the differing shotpoints and plotted as a function of distance in Fig. 16. Although there is considerable

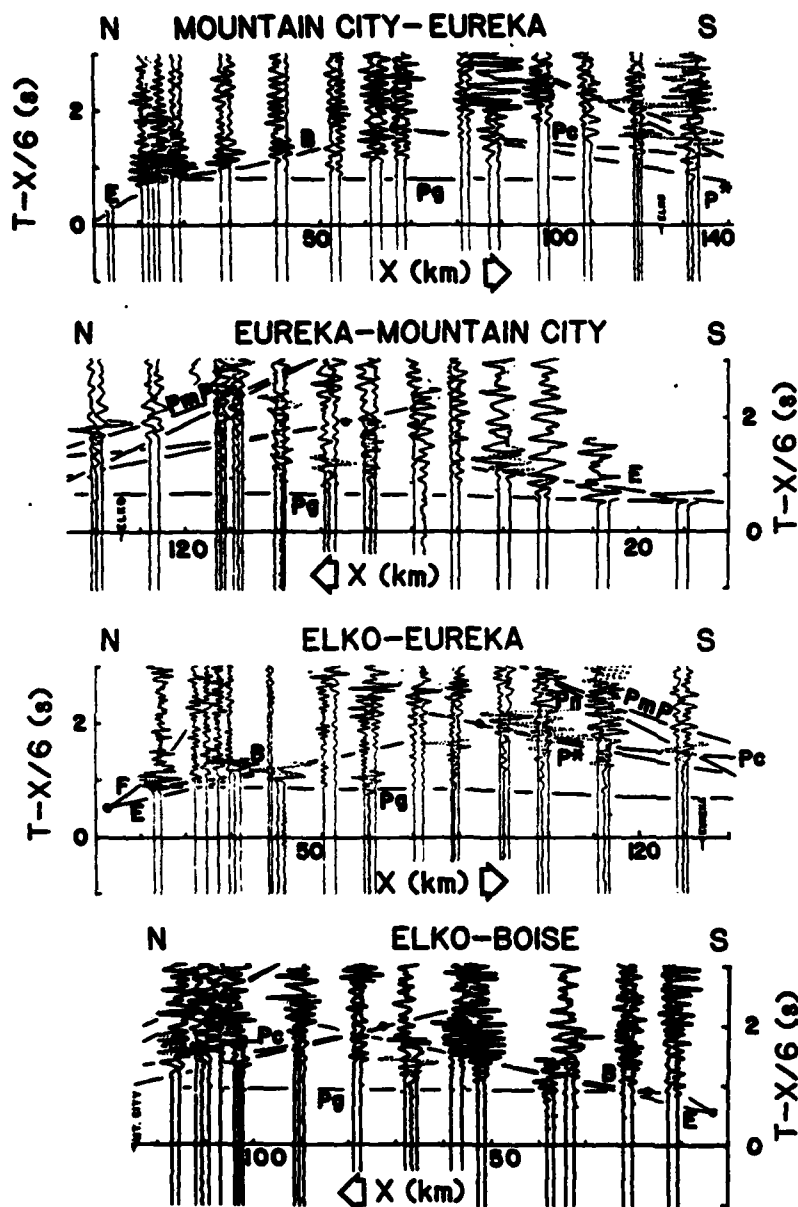


Fig. 15. Partial record sections of the  $P_g$  phase for the northern Basin and Range province. Travel-time curves shown are the result of ray-trace modelling by Fauria (1981)

scatter in these data (the range is illustrated by the shaded area of the plot) it appears that  $P_g$  amplitudes for the NBR decay rapidly with distance and do not display the local maximum which was characteristic of the Sulz data and which indicated a velocity gradient. In fact, the NBR  $P_g$  amplitude data are fitted best by the PG1 model consisting of homogeneous upper crust. The scatter in the data shown in Fig. 16 and the fact that the data represent a compilation from several different refraction lines preclude more detailed analysis. Note that the very small positive or negative gradients (less than that for model PG3) and virtually any  $Q$  value could be present in the upper crust of the NBR based on these data alone. However, because no strong gradient or low-velocity effects are observed in the amplitude distance data, the upper crust in the NBR appears to be nearly a homogeneous velocity layer.

#### Conclusions

The fine structure of the continental basement, i.e. the distribution of physical parameters with depth, can reveal significant aspects of the crustal evolution and the interaction of different crustal units as well as its thermal and compositional history. Very often the upper part of the crust does not show pronounced interfaces with discontinuities in velocity and density. Vertical incidence reflection cannot resolve velocity structure in the absence of distinct impedance boundaries. On the other hand, combined travel-time and amplitude analysis of refraction data can give more detailed insight into the velocity structure. Therefore combined reflection and refraction surveys should be carried out in crustal investigations.

A representative velocity-depth structure requires either

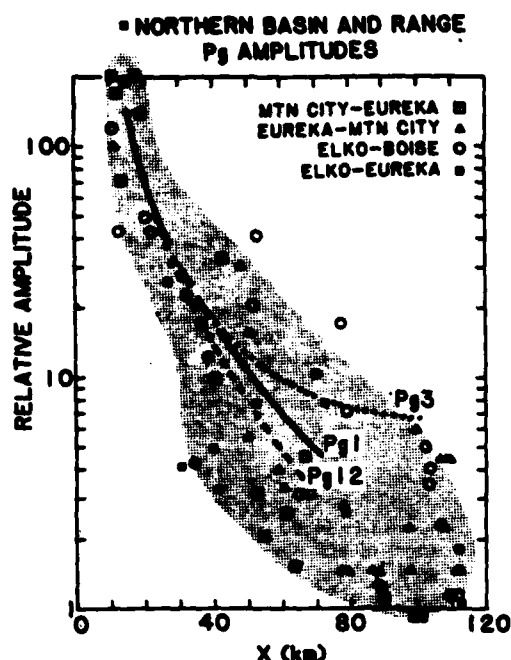


Fig. 16. Amplitude-distance data for the  $P_g$  phase for the NBR data shown in Fig. 15. The shaded region represents the range of scatter of the data points. Theoretical amplitude-distance curves calculated by the reflectivity method are shown for models PG1, PG3 and PG12 (Table 1)

detailed and highly accurate travel-time data, i.e. a spacing of observation points on the order of a few hundred meters, or a combination of travel-time and reliable amplitude data obtained from an average record spacing of a few kilometers. The following conclusions drawn from this study can help to achieve a better interpretation of the amplitude data and hence lead to a more reliable estimate of velocity-depth structure of the upper continental crust.

1. The frequency content of the source is a critical parameter when gradient zones and/or discontinuities of velocity are present. Higher frequencies produce more pronounced variations of amplitudes with distance. The amplitude variations are likely to be resolvable within the scatter of the data and thus high frequency source signals lead to better resolution.

2. A low-velocity cover of the basement accentuates relative maxima in the amplitude-distance curve when velocity gradients are present in the crystalline upper crust. Layer thicknesses of only 0.2 km, i.e. even weathered layers, can cause this effect. In addition, multiple reflections, refractions and conversions in the low-velocity cover contribute considerably to a complicated wave field following the initial  $P_g$  arrival and probably make later arrivals from deeper parts of the crust undetectable.

3. Reflections from the top of a low-velocity layer within the upper crust will affect the  $P_g$  amplitudes by interference only if they are strong enough. This requires low gradients in the basement above, a first order discontinuity at the bottom of the upper crust and a high frequency source signal.

4. The increasing thickness of the gradient zone in the basement reduces the amplitude decay with distance and broadens the width of the relative amplitude maximum.

5. The  $P_g$  amplitudes decay with distance much faster in the presence of a low-velocity layer than would be expected from geometrical ray theory.

6. Reliable  $P_g$  amplitude data, characterized by a continuous decrease, or a steady value over some distance or even a local maximum, allows us to distinguish between homogeneous constant velocity layers and various gradient zones in the upper crust.

7. Apparent  $Q$  values cannot be extracted from the amplitude distance behaviour of  $P_g$  data alone.

8. Synthetic seismogram calculations based on asymptotic ray theory can be used only as a first approximation to determine detailed velocity depth structures.

These results, of course, apply only to a crust which can be approximated by laterally homogeneous models. Focusing effects due to lateral heterogeneities may completely mask the amplitude-distance behaviour due to vertical structures and must be studied by other methods.

**Acknowledgements.** This work was initiated when one of us (LWB) was on sabbatical leave at the Institute of Geophysics, ETH-Zürich, Switzerland. We thank Rainer Kind for providing a copy of his modified reflectivity programme. Claus Prodehl provided original copies of some of the seismic record sections. Partial support for LWB was provided by Office of Naval Research Earth Physics Program contracts N00014-75-C-0972 and N00014-82-K-033 and by the U.S. Geological Survey Geothermal Exploration Program grant No. 14-08-0001-G-674. The help of Dieter Emter in organizing the quarry blasts at the shotpoint Sulz is gratefully acknowledged. We are also grateful to Erhard Wielandt for helpful discussions regarding the Fresnel-zone effect and to Walter Mooney for his contribution to the phase identifications in Fig. 1. Agustin Udias, Walter Mooney, Robert B. Smith and Josep Gallart critically read the manuscript.

## References

- Banda, E.: *Perfiles Sísmicos Profundos en Corteza Continental. Estructura de la Corteza y Manto Superior en las Cordilleras Béticas*. Ph.D. Thesis, University of Barcelona 1979
- Banda, E., Ansorge, J.: Crustal structure under the central and eastern part of the Betic Cordillera. *Geophys. J. R. Astron. Soc.* 63, 515-532, 1980
- Báth, M.: *Spectral Analysis in Geophysics*. Amsterdam: Elsevier 1974
- Boigk, H., Schoeneich, H.: Die Tiefenlage der Permabasis im nördlichen Teil des Oberrheingrabens. In: *Graben Problems*, J. H. Illies and St. Mueller, eds.: pp 45-55. Stuttgart: Schweizerbart'sche Verlagsbuchhandlung 1968
- Born, M.: *Optik*. Berlin: Springer 1933
- Braile, L.W., Smith, R.B.: Guide to the interpretation of crustal refraction profiles. *Geophys. J. R. Astron. Soc.* 48, 145-176, 1975
- Braile, L.W.: Interpretation of crustal velocity gradients and  $Q$  structure using amplitude-corrected seismograms. In: *The earth's crust*. Am. Geophys. Union Monogr. 20, 427-439, 1977
- Braile, L.W., Smith, R.B., Ansorge, J., Baker, M.R., Spartin, M.A., Prodehl, C., Schilly, M.M., Healy, J.H., Mueller, St., Olsen, K.H.: The Yellowstone-Snake River Plain seismic profiling experiment: Crustal structure of the Eastern Snake River Plain. *J. Geophys. Res.* 87, 2597-2610, 1982
- Buechi, U.P., Lemcke, K., Wiener, G., Zimdars, J.: *Geologische Ergebnisse der Erdexploration auf das Mesozoikum im Un-*

- tergrund des schweizerischen Molassebeckens. *Bull. Ver. Schweiz. Petrol. Geol. Ing.* 32, 82, 7-38, 1965
- Chapman, C.H.: A new method for computing synthetic seismograms. *Geophys. J. R. Astron. Soc.* 54, 481-518, 1978
- Cervený, V.: On dynamic properties of reflected and head waves in a-layered earth's crust. *Geophys. J. R. Astron. Soc.* 11, 139-147, 1966
- Cervený, V.: Accuracy of ray theoretical seismograms. *J. Geophys.* 46, 135-149, 1979
- Cervený, V., Molotkov, I.A., Pleník, I.: Ray method in seismology. Prague: Charles University Press 1977
- Fauria, T.J.: Crustal structure of the Northern Basin and Range and Snake River Plain: A ray-trace travel-time interpretation of the Eureka, Nevada, to Boise, Idaho, seismic refraction profile. M.S. Thesis, Purdue University 1981
- Fuchs, K.: The reflection of spherical waves from transition zones with arbitrary depth-dependent elastic moduli and density. *J. Phys. Earth* 16 (Spec. Issue), 27-41, 1968
- Fuchs, K., Müller, G.: Computation of synthetic seismograms with the reflectivity method and comparison with observations. *Geophys. J. R. Astron. Soc.* 23, 417-433, 1971
- Gebrande, H.: A seismic-ray tracing method for two-dimensional inhomogeneous media. In: *Explosion seismology in central Europe*, P. Giese, C. Prodehl and A. Stein, eds.: pp. 162-167. Heidelberg: Springer 1976
- Healy, J.H.: Crustal structure along the coast of California from seismic-refraction measurements. *J. Geophys. Res.* 68, 5777-5787, 1963
- Hill, D.P.: Velocity gradients and anelasticity from crustal body wave amplitudes. *J. Geophys. Res.* 80, 3309-3325, 1971
- Hill, D.P., Pakiser, L.C.: Crustal structure between the Nevada test site and Boise, Idaho, from seismic-refraction measurements. In: *The Earth beneath the continents*, Am. Geophys. Union Monogr. 10, 391-419, 1966
- Kind, R.: The reflectivity method for a buried source. *J. Geophys.* 44, 603-612, 1978
- Lemcke, K., Buechi, U.P., Wiener, G.: Einige Ergebnisse der Erdbelexploration auf die mittellaendische Molasse der Zentralschweiz. *Bull. Ver. Schweiz. Petrol. Geol. Ing.* 35, 87, 15-34, 1968
- Müller, G., Fuchs, K.: Inversion of seismic records with the aid of synthetic seismograms. In: *Explosion seismology in Central Europe*, P. Giese, C. Prodehl and A. Stein, eds.: pp. 178-188. Heidelberg: Springer 1976
- Müller, G., Mueller, S.: Travel-time and amplitude interpretation of crustal phases on the refraction profile Delta-W, Utah. *Bull. Seismol. Soc. Am.* 69, 1121-1132, 1979
- Olsen, K.H., Keller, G.R., Stewart, J.N.: Crustal structure along the Rio Grande Rift from seismic refraction profiles. In: *Rio Grande Rift: Tectonics and magmatism*, R.E. Riecker, ed.: pp. 127-143. Washington: Am. Geophys. Union 1979
- Prodehl, C.: Seismic refraction study of crustal structure in the Western United States. *Geol. Soc. Am. Bull.* 81, 2629-2646, 1970
- Prodehl, C.: Crustal structure of the Western United States. *U.S. Geol. Surv. Professional Paper* 1034, 18-23, 1979
- Smith, R.B., Braille, L.W., Keller, G.R.: Upper crustal low-velocity layer: a possible effect of high temperatures over a mantle upward at the Basin and Range-Colorado Plateau transition. *Earth Planet. Sci. Lett.* 28, 197-204, 1975
- Spudich, P., Orcutt, J.: A new look at the seismic velocity structure of the Oceanic Crust. *Rev. Geophys. Space Phys.* 18, 3, 627-645, 1980
- Wiggins, R.A.: Body wave amplitude calculation-II. *Geophys. J. R. Astron. Soc.* 46, 1-10, 1976

Received May 6, 1982; Revised version July 9, 1982  
Accepted July 12, 1982

## ABSTRACT

Espindola, Juan Manuel. Ph.D., Purdue University, August 1979. Finite Difference Synthetic Seismograms for Kinematic Models of the Earthquake Source. Major Professor: Lawrence W. Braile.

The dynamic displacement field of kinematic dislocation in two dimensions is modeled by a finite-difference technique in skew coordinates. The scheme involves the solution of the heterogeneous, elastic vector wave equation subjected to dislocation conditions. Algorithms are included to model the free surface and absorbing artificial boundaries which simulate an infinite half-space.

Specification of faults with arbitrary dip is implemented by means of the skew-coordinate system. Other source parameters such as time-history, slip-function, and rupture velocity are user selected.

Near-field synthetic seismograms were calculated by this procedure for selected source parameters for two cases of geologic interest (i.e., buried basin and layer over a half space). These examples illustrate the influence of fault parameters and local geology on ground motion. Significant effects due to the heterogeneous media and various fault and source parameters suggest that the method can provide a new realistic modelling tool for the study of the interaction between the earthquake source and the local geology in the near-field for long period ground motion.

## ABSTRACT

Mazzella, Frederick Elwood. Ph.D., Purdue University. August 1979. The Generation of Synthetic Seismograms for Laterally Heterogeneous Models Using the Finite Difference Technique. Major Professor: Lawrence W. Braille.

A method for the generation of synthetic seismograms for two-dimensional heterogeneous models specified only by P-wave (dilatation) velocity has been developed. The finite difference approximation technique is applied to the two-dimensional vector wave equation for an elastic and isotropic model. The finite difference calculations are applied to a designated portion of the model at any particular time step during the lifetime of the approximation. This portion of the model is referred to as the window and is prescribed to include the waves of interest which propagate through the model. A suite of models are evaluated with various window parameters which provides insight into the limitations and capabilities of the method. The computational efficiency of the windowing technique allows evaluation of models which are approximately twice as large as those which can be evaluated by other numerical approximation techniques not employing a

windowing scheme for the same computing resources (time and memory).

Two types of boundary conditions are employed on the walls of the window. The upper horizontal surface is treated with a second order heterogeneous free surface boundary condition developed during this study. All other surfaces of the window are treated with a nonreflecting boundary condition to minimize false reflections and mode conversions. Seismograms can be obtained for any location inside or on the boundaries of the model.

Synthetic seismograms are calculated for seven heterogeneous (both vertical and horizontal) geologically realistic models. Each model is described graphically and is accompanied by a displacement seismogram record section for the vertical and horizontal components. These record sections reveal significant amplitude and time effects which result from the velocity structure.

ND  
ATE  
LMED